The transonic compressor with non-uniform tip clearance: Effects on aerodynamics and aeroelasticity

Der Transsonikverdichter mit ungleichmäßigem Spitzenspalt: Auswirkungen auf Aerodynamik und Aeroelastizität

Zur Erlangung des akademischen Grades Doktor-Ingenieur (Dr.-Ing.) genehmigte Dissertation von Maximilian Jüngst aus Frankfurt am Main

Tag der Einreichung: 01.11.2018, Tag der Prüfung: 26.02.2019
Darmstadt — D 17

1. Gutachten: Prof. Dr.-Ing. H.-P. Schiffer
2. Gutachten: Prof. Tekn. Dr. D. Vogt

TECHNISCHE UNIVERSITÄT DARMSTADT

Fachbereich Maschinenbau
Fachgebiet Gasturbinen, Luft- und Raumfahrtantriebe

The transonic compressor with non-uniform tip clearance:
Effects on aerodynamics and aeroelasticity
Der Transsonikverdichter mit ungleichmäßigem Spitzenspalt:
Auswirkungen auf Aerodynamik und Aeroelastizität

Genehmigte Dissertation von Maximilian Jüngst aus Frankfurt am Main

1. Gutachten: Prof. Dr.-Ing. H.-P. Schiffer
2. Gutachten: Prof. Tekn. Dr. D. Vogt

Tag der Einreichung: 01.11.2018
Tag der Prüfung: 26.02.2019

Darmstadt — D 17

Don't stop believing.
- Journey

Vorwort des Herausgebers

Die Reihe Forschungsberichte aus dem Institut für Gasturbinen, Luft- und Raumfahrtantriebe gibt die Forschungs- und Entwicklungsfortschritte im Bereich der Turbomaschine an der Technischen Universität Darmstadt wieder. Aufgrund der starken Anwendungsorientierung in diesem Bereich der Forschung sind universitäre Fragestellungen Spiegelbild industrieller Entwicklungstrends.

Wechselnde politische, ökonomische und ökologische Rahmenbedingungen bestimmen hierbei aktuelle Entwicklungsschwerpunkte und bringen die Turbomaschine immer wieder an den Rand des technisch Realisierbaren. Dadurch werden neue Erkenntnisse aus der Forschung nicht selten unmittelbar industriell umgesetzt.

In diesem Umfeld entstehen die industrie- und anwendungsnahen, wissenschaftlichen Arbeiten dieser Reihe. Sie beschreiben aktuelle Erkenntnisse aus experimentellen Untersuchungen und numerischen Simulationen, die am Fachgebiet für Gasturbinen, Luft- und Raumfahrtantriebe an der Technischen Universität Darmstadt gewonnen werden konnten.

Heinz-Peter Schiffer

Darmstadt, 2015

Vorwort des Autors

Diese Dissertation ist während meiner Tätigkeit als wissenschaftlicher Mitarbeiter am Institut für Gasturbinen, Luft- und Raumfahrtantriebe entstanden. Die Arbeit wurde im Rahmen der Forschungsprogramme der Europäischen Kommission FP7-Transport mit der Projekt-ID 314366 sowie durch Rolls-Royce Deutschland Ltd & Co KG finanziert. Rolls-Royce Deutschland möchte ich an dieser Stelle für die Einwilligung zur Publikation der Arbeit danken. Insbesondere Thomas Giersch, Frank Heinichen, Bernd Becker und Henner Schrapp gebührt Dank für ihre Unterstützung und die hilfreichen fachlichen Diskussionen.

Wenn ich auf mein Studium und die Zeit am Fachgebiet zurückschaue, empfinde ich Glück, Zufriedenheit, große Dankbarkeit und etwas Wehmut. Große Dankbarkeit empfinde ich, weil ich die Möglichkeit hatte, 4 Jahre mit viel Freude und Freiheit an immer neuen Herausforderungen arbeiten zu können. Die Zeit hat mich geprägt und ich konnte mich enorm weiterentwickeln. Die Möglichkeit dazu hat mir Prof. Dr.-Ing. Schiffer gegeben, wofür ich mich in diesem Rahmen herzlich bedanken möchte.

Am Anfang meiner Zeit am Institut habe ich in einem Team arbeiten dürfen, von dem ich fachlich lernen konnte und mit dem ich auch in der Freizeit viel Spaß hatte. Christoph, Felix und Fabian, danke für die großartige Zeit, eure Unterstützung und Inspiration.

Wie das an einer Universität üblich ist, hat sich die Zusammensetzung der Arbeitsgruppe innerhalb der letzten 4 Jahre auch verändert. Gekommen sind großartige Kollegen, mit denen ich bis heute sehr gerne zusammenarbeite, von und mit denen ich lernen kann und die mir täglich große Freude an der Arbeit bereiten. Danke an die Daniels, Jonas, Steffen, Christian, Jan und das ganze Fachgebiet für starkes Teamwork und den Spaß den wir auf und außerhalb der Arbeit haben.

Ohne die kontinuierliche Unterstützung durch Hiwis und studentische Abschlussarbeiten wäre die Arbeit in dieser Form nicht möglich gewesen. Ich möchte daher auch meinen Studenten Samuel, Christian, Valentina, Timo, Julius und Jonas danken, die mit ihrer Arbeit zum Gelingen dieser Dissertation beigetragen haben.

Zu guter Letzt, aber allen voran möchte ich meiner Familie danken. Ihr habt mir den Weg zur Promotion ermöglicht, ihr habt mich unterstützt und mich aufgefangen, wenn es mal schwer war. Danke Mama, danke Papa für eure bedingungslose Unterstützung und Liebe. Danke Kati für jeden Tag mit dir, ganz viel Herz, dass wir alle Freude und alles Leid teilen können und uns grenzenlos stützen - this [is] the drug that doesn't bite.

Maximilian Jüngst

Frankfurt am Main, 2018

Kurzfassung

In der vorliegenden Arbeit wird das aerodynamische und aeroelastische Verhalten eines transsonischen Verdichters mit ungleichmäßigem Spitzenspalt experimentell untersucht. Aktuelle Trends in der Triebwerksentwicklung erfordern effizientere Verdichter mit hohem Druckverhältnis und geringerem Gewicht. Ein erhöhtes Gesamtdruckverhältnis ermöglicht es, das Kerntriebwerk bei gleicher Leistung kleiner zu bauen. Dadurch wird die für Lärm und Triebwerkseffizienz entscheidende Stellgröße, das Nebenstromverhältnis, erhöht.

Ein kompakteres Kerntriebwerk führt allerdings zu größeren relativen Spaltweiten zwischen Rotor und Gehäuse, da diese nicht entsprechend mitskaliert werden können. Aus dem gleichen Grund spielen auch Gehäuseasymmetrien zukünftig eine größere Rolle.

Ziel der Arbeit ist zum einen eine aerodynamische Analyse, die dem Bereich der Spaltsensitivität und damit der Triebwerksalterung zuzuordnen ist. Zum anderen erfolgt eine Analyse des aeroelastischen Verhaltens, da transsonische Verdichter in Frontstufen des Kerntriebwerks zum Einsatz kommen, die im Teillastbereich zu strömungsinduzierten Schwingungen neigen. Diese Schwingungen können zu Rissen oder sogar einem Versagen der Schaufeln führen. Stabilisierende Maßnahmen, wie etwa Gehäusestrukturen im Bereich der Rotorspitze sind bekannt. Ihr Einfluss auf Schaufelschwingungen, speziell einer ungleichmäßigen Umfangsverteilung, ist allerdings weitgehend unerforscht.

Die Ergebnisse der Arbeit entkräften aerodynamische und mechanische Bedenken beim Einsatz von Axialverdichtern in zukünftig kleineren Kerntriebwerken. Der destabilisierende Einfluss einer Gehäuseexzentrizität ist geringer als bisher vermutet, weshalb vorgesehene Sicherheiten in diesem Zusammenhang potenziell reduziert werden können. Bezüglich strömungsinduzierter Schwingungen, die mit konzentrischem Gehäuse im gesamten Drehzahlbereich auftreten, zeigt diese Dissertation erstmals, dass nichtachsensymmetrische Rotorspitzenspalte einen neuartigen Ansatz im Bereich der aerodynamischen Verstimmung des vorliegenden Schwingungssystems darstellen. Die durch Gehäuseasymmetrie erzeugte Massenstromumverteilung vor dem Verdichter, führt zu einer Umfangsvariation der Rotorinzidenz, die wiederum die aerodynamische Kraft auf die Schaufeln in Umfangsrichtung variiert. Demzufolge stabilisiert sich die Rotor-Relativströmung während einer Umdrehung, was letztlich zu einer Reduktion der Schaufelschwingungen führt.

Leichte Asymmetrien im Triebwerk haben somit einen stabilisierenden Einfluss auf Schaufelschwingungen. Im untersuchten Fall, reduziert z.B. ein exzentrischer Rotorspalt die Amplituden nicht-synchroner Schwingungen um -25% der am Prüfstand definierten Betriebsgrenze, verglichen mit einem symmetrischen Gehäuse, welches einen identischen mittleren Laufspalt besitzt.

Segmentweise gestaltete Gehäusestrukturen profitieren vom gleichen Effekt und sind daher zukünftig ein wirksames Werkzeug zur Vermeidung nicht-synchroner Schwingungen. Im Gegensatz zu einer in Umfangsrichtung gleichmäßigen Gehäusestrukturierung, die Schwingungsprobleme verstärken kann, sind ungleichmäßige Bauformen eine nun experimentell erprobte Lösung für das Problem nicht-synchroner Schwingungen in Frontstufen im Off-Designbetrieb.

Abstract

This study experimentally investigates the aerodynamic and aeroelastic behaviour of a transonic compressor with non-uniform tip clearance. Current design trends for aero engines require more efficient compressors with high pressure ratio and reduced weight. An increased overall pressure ratio permits a downsized core engine while its power output is maintained. This increases the bypass ratio, which is crucial for engine noise and efficiency.

However, a more compact core engine leads to larger relative gaps between rotor and casing, as the clearance cannot be scaled accordingly. For the same reason, casing asymmetry has become more important for future engines.

On the one hand, the aim of the work is an aerodynamic analysis in the field of clearance sensitivity and thus engine deterioration. On the other hand, an analysis of the aeroelastic behaviour is carried out, since transonic compressors are used in front stages of the core engine, which tend to flow-induced vibrations at part speed. These vibrations can result in cracks or even blade failure. Stabilizing measures, such as casing treatments at the rotor tip, are common knowledge. However, their influence on blade vibration, especially of a non-uniform circumferential distribution, is largely unexplored.

The results of the work relieve aerodynamic and mechanical concerns regarding the application of axial compressors in future small core engines. The destabilizing influence of casing eccentricity is less than previously assumed, which is why the intended safety margins can potentially be reduced. With regard to flow-induced vibrations that occur in concentric casings across the entire speed range, this dissertation shows for the first time that non-uniform rotor tip clearances represent a novel approach in the field of aerodynamic mistuning.

The mass flow redistribution upstream of the compressor with a non-uniform clearance causes a circumferential variation of the rotor incidence, which in turn varies the aerodynamic force on the blades circumferentially. As a result, the rotor-relative flow recovers during one turn of the rotor, which ultimately leads to a reduction of the blade vibration amplitudes.

Slight asymmetries in an engine have a stabilizing influence on blade vibrations. For the given case, e.g. an eccentric rotor clearance reduces the amplitudes of non-synchronous vibrations by -25% of the rig operating limit, compared to a concentric casing with the same average clearance.

Partial casing treatments benefit from the same effect and will hence be a powerful tool to avoid non-synchronous vibrations in the future. In contrast to a circumferentially uniform casing treatment that can amplify blade vibrations, non-uniform designs are now a smart solution for the problem of non-synchronous vibrations in front stages during off-design operation.

Contents

List of Figures

List of Tables

Nomenclature

Latin Symbols

A	m^2	Area
c	m/s	Absolute velocity
C	m	Circumference
c_L	-	Lift coefficient
c_p	$J/kg\,K$	Specific heat capacity at constant pressure
F	-	Exit flow function
f_{blade}	Hz	Natural frequency of a blade
h	J/kg	Specific enthalpie
k	-	Propagation speed constant
K	-	Reduced frequency
l	m	Rotor tip chord length
$\dot{m}$	kg/s	Mass flow
Ma	-	Mach number
n	-	Counter
n_{aero}	-	Aerodynamic cell count
N	-	Count
N_{blade}	-	Blade count
N_r	rpm	Rotational speed
m	-	Counter
p	Pa	Pressure
r	m	Radius
R	$J/kg\,K$	Specific gas constant
s	$J/kg\,K$	Specific entropy
t	m	Tip clearance
T	K	Temperature
u	m/s	Tangential speed
v	m/s	Propagation speed
w	m/s	Relative speed
x	m	Axial coordinate

Greek Symbols

α	K^{-1}	Linear thermal expansion coefficient
α	-	Angle of attack
β	°	Tangential flow angle (whirl angle)
γ	-	Flow rate coefficient
Δ	-	Difference
ϵ	-	Expansion coefficient
ε	m	Rotor offset
η	% p	Efficiency (in percent points)
κ	-	Heat capacity ratio
λ	m	Wavelength
ξ	%	Eccentricity (in percent)
π	-	Pi (Archimedes' constant)
Π	-	Pressure ratio
ρ	kg/m^3	Density
(ρu)	$kg/m^2\,s$	Mass flow density
σ	-	Standard deviation
φ	rad	Inter blade phase angle
Ψ_{t-s}	-	Total-to-static pressure rise coefficient

Subscripts and Superscripts

$\overline{\square}$	Average
$\square^{04}$	Measurement station settling chamber
$\square^{10}$	Measurement station inlet duct
$\square^{20}$	Measurement station rotor inlet
$\square^{21}$	Measurement station rotor exit
$\square^{30}$	Measurement station stator exit
$\square_{abs}$	Absolute
$\square_{ax}$	In axial direction
$\square_{baro}$	Barometric
$\square_{corr}$	Corrected
$\square_{design}$	At design point or speed
$\square_{dyn}$	Dynamic
$\square_{hub}$	Hub section
$\square_{is}$	Isentropic
$\square_{m}$	At midspan
$\square_{max}$	Maximum
$\square_{mech}$	Mechanical
$\square_{min}$	Minimum
$\square_{r}$	Rotational
$\square_{ref}$	Reference value
$\square_{rel}$	Relative to reference
$\square_{rot}$	In the rotating frame of reference
$\square_{s}$	Static
$\square_{stat}$	In the stationary frame of reference
$\square_{t}$	Total
$\square_{t-s}$	Total-to-static
$\square_{t-t}$	Total-to-total
$\square_{tip}$	Tip Section
$\square_{var}$	Variation

Abbreviations for Compressor Setting

CON	Configuration with uniform clearance
CON-MAX	Configuration with uniform clearance of 2.5% tip chord
CON-MIN	Configuration with uniform clearance of 0.9% tip chord
CON-NOM	Configuration with uniform clearance of 1.25% tip chord
CT	Casing treatment
CT180	Configuration with partial casing treatment in segment of 180°
CT360	Configuration with full circumference casing treatment
ECC	Configuration with non-uniform clearance
ECC-MAX	Configuration with large eccentricity of 96% and average clearance of 1.7% tip chord
ECC-MIN	Configuration with small eccentricity of 60% and average clearance of 1.25% tip chord
IGV	Inlet guide vane
IGVA	Inlet guide vane angle
NS	Near stall
IM	Intermediate operating point
DP	Design point
NC	Near choke
N45	45% Aerodynamic design speed
N63	63% Aerodynamic design speed
N80	80% Aerodynamic design speed
N95	95% Aerodynamic design speed
N100	100% Aerodynamic design speed

General Abbreviations

1F	First flap blade mode
1T	First torsion blade mode
3D	Three dimensional
ACARE	Advisory Council for Aeronautic Research in Europe
Al	Aluminium
Blisk	Bladed integrated disc design
CFD	Computational fluid dynamics
CO_2	Carbon dioxide
CWB	Chord wise bending blade mode
DR 1	Slow exit throttle speed
DR 3	Fast exit throttle speed
E-BREAK	Engine BREAKthrough components
ENOVAL	ENgine mOdule VALidators

EO	Engine order
FHP	Five hole probe
GE	General Electric
HCF	High cycle fatigue
HPC	High pressure compressor
IPCC	Intergovernmental Panel on Climate Change
ISA	International standard atmosphere
KHP	Kiel head probe
LCF	Low cycle fatigue
LE	Leading edge
LEMCOTEC	Low EMissions COre-Engine TECHnologies
MTU	ger.: Motoren und Turbinen Union; MTU Aero Engines AG
NACA	National Advisory Committee for Aeronautics
NASA	National Aeronautics and Space Administration
ND	Nodal diameter
Ni	Nickel
NO_x	Nitrogen oxides
NSV	Non-synchronous vibrations
OL	Operating Limit (dependent on rotor blade HCF)
PIV	Particle image velocimetry
R1	First rotor of multistage compressor
RI	Rotating Instability
SFC	Specific fuel consumption
SM	Stability margin
TE	Trailing edge
THP	Three hole probe
Ti	Titanium
TRL	Technology readiness level
UPP	Unsteady pressure probe
w/o	Without
WPT	Wall pressure tapping

1 Introduction

Global challenges are forcing aero engine research to constantly introduce innovations and to develop new technologies. Industry, research institutes and universities work closely together to achieve future goals. The objectives of the entire engine projects can be divided into requirements for subsystems, which are investigated primarily in academic research. In this context, the research contribution of this thesis is outlined below.

1.1 Development Goals for Future Aero Engines

Aviation has become an elementary part of our globalised civilization. The transport of goods and passengers from all over the world is indispensable for the global economy and the social life of people.

According to the current market analyses of major players in the aircraft industry, Boing (2018) and Airbus (2018), the demand for transport via air will continue to grow during the next decades. Recently, they estimated an averaged market growth of 4.2% to 4.4% per year until 2037.

Back in 1999, the Intergovernmental Panel on Climate Change (IPCC) analysed the effects of aircraft on climate and predicted the emissions from aviation for the future (until 2050). They warned economic decision-makers to reduce the impact and requested that they should consider new aircraft and engine technologies, innovative fuels, operational issues and many other options (Penner et al., 1999). Aware of future challenges, strategic key players in Europe were encouraged to establish the "Advisory Council for Aviation Research and Innovation in Europe" (ACARE). As a result, the European Commission (2001) published the "*Vision for 2020*" as a roadmap for the aviation industry. Moreover, in 2011 the guideline until 2050 has been formulated in the "*Flightpath2050*" (European Commission, 2011). The specified targets for the aircraft industry in terms of reducing carbon dioxide emissions per passenger kilometre, nitrogen oxide emissions and perceived noise average levels (relative to an

	CO_2	NO_x	
2020	-50%	-80%	-50%
2050	-75%	-90%	-65%

Figure 1.1: Reduction of emissions and noise, relative to an aircraft from the year 2000.[a]

[a] Icons made by Freepik from www.flaticon.com.

aircraft from year 2000) are quantified in Figure 1.1. To achieve these goals, the aviation industry must develop improved aircraft, efficient and lightweight aero engines and fundamentally new design concepts.

It was also outlined by the European Commission that work is needed to establish new safety standards, improvements of air traffic management, higher quality and comfort, lower costs and other. As these aims are very challenging for the aviation industry as a whole, there was a need for pooling the risks. Co-funded framework programs were set up by the European Commission to establish interdisciplinary research and technological progress. To name a few, the projects ENOVAL, LEMCOTEC and E-BREAK have been funded within these frameworks. All of them are collaborative projects with partners from industry, universities and research institutes. The objectives of the mentioned projects are briefly outlined below, as they reflect the current development trends of modern engines.

Modern engines are typically built as turbofan engines. A large front rotor (fan) charges a high amount of air and is driven by a smaller core engine, which mainly generates power to drive the fan. As outlined by Vollmuth (2013), the EU project ENOVAL was set up to enable new engine designs with ultra high bypass ratios. The bypass ratio describes the relation of the bypass stream compared to the amount that is guided through the core (the sum of both is passing the fan). Increasing the bypass ratio is attracting interest due to the possibility to effectively reduce noise and the fuel consumption of an aero engine (Rolls-Royce plc, 2007).

The main objective of the E-BREAK project was the improvement of the engine's subsystems to enable high bypass ratios and higher pressure ratios of the compression system (Hoeveler, 2015). As reported by von der Bank et al. (2015), the advantage of high pressure ratios is that the core engine produces more power (for the equivalent size) and can thus be scaled down.

The projects E-BREAK and LEMCOTEC are closely related. LEMCOTEC also focuses on core engine technologies, but adds e.g. research in the area of revolutionary burning systems as well as improved combustion to contribute to the reduction of NOx, carbon oxides, unburned hydrocarbons and smoke emissions (Hoeveler, 2014).

For instance, the engine manufacturer Rolls Royce plc. is involved in all of the mentioned projects and aims to translate the results in new engine designs with approximate entry into service by 2020 and 2025. The Advance engine (market entry by 2020) has a new core architecture, a bypass ratio of 11+ and higher overall pressure ratio (60+). The UltraFan will be designed with a gearbox to permit even larger fan designs, which will lead to an estimated fuel burn saving of 25% compared to an engine from the year 2000, the Trent700 (Haselbach et al., 2015).

These examples outline that engine manufactures are working on *comprehensive design concepts* (e.g. geared fans), but also try to improve the efficiency and weight of each component, i.e. an *optimisation of the subsystems*. This thesis contributes to the improvement of one of these subsystems: the compression system of the core engine.

1.2 Targets Regarding the Compression System

The compressor has a significant influence on the engine as it represents 40-50% of the weight, 35-40% of the manufacturing and 30% of the maintenance costs (Steffens, 2001). This was also highlighted by von der Bank et al. (2015). Referring to the ACARE Vision for 2020, they derived specific objectives regarding the compression system. The stated goals are summarized in Figure 1.2 and shortly addressed in the following.

The essential aerodynamic quantities of the compression system are its efficiency, pressure rise and stability margin. The *pressure rise* and the component *efficiency* contribute to the efficiency of the whole engine that transfers to its specific fuel consumption (SFC). According to Domercq and Escuret (2007), a one percent drop of the high pressure compressor (HPC) efficiency translates to 0.5% to 0.8% SFC penalty. In addition to the environmental issues, this is critical from an operators perspective as the cost of fuel is typically 15 to 25% of the aircraft operating costs (Rolls-Royce plc, 2007).

Besides the increase of the pressure ratio and the component efficiency, an increase of the system's robustness in terms of performance deterioration and tip clearance effects as well as weight savings are of importance.

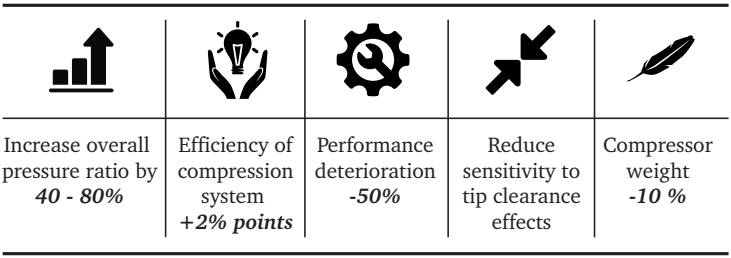

Figure 1.2: Specific targets regarding the compression system, developed from von der Bank et al. (2015). Values are given relative to an engine from the year 2000.[a]

[a] Icons made by Freepik from www.flaticon.com.

With regard to the *deterioration* of engines due to wear and enlarged tip clearance, Wisler (1985) stated that a typical high bypass ratio engine has an SFC increase of about 1 to 1.5% per year. He pointed out that periodic overhauls do not fully recover the problem, which results in SFCs that are 3 to 10% larger compared to a completely new engine.

The importance of *size effects and rotor tip clearance* in future research was also emphasized by Day (2016) in his recent review. His work is endorsed by experience of 11 years in industry and 30 years in compressor research. He pointed out the need for engine scale investigations in high speed facilities and stated that "the recent trend toward engines with smaller cores and larger gap-to-span ratios gives rise to a need for more work on clearance and eccentricity. The loss of stability, pressure rise and efficiency which accompany a shift to larger tip gaps needs to be quantified. So do the effects of casing eccentricity."

With regard to the service life and deterioration of the engine, Day (2016) mentioned "factors which control the loss of stall margin in older compressors [,] most importantly, tip clearance and eccentricity (due to rubbing) [as] these all have a detrimental effect on fuel burn."

The subject of rubbing is illustrated further in Figure 1.3. Axial compressor front stages of modern aero engines consist of variable inlet and outlet guide vanes and abradable coatings, generally referred to as liner, which ensure minimal rotor tip gaps in service. These liners also prevent the blade tips from being damaged if the rotor hits the casing. Figure 1.3a reveals four abradable liners, which were exposed

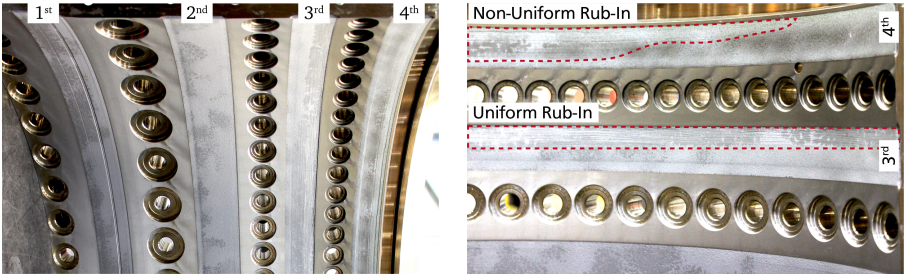

(a) Split casing of a high pressure compressor with abradable liners in stage one to four

(b) Zoom to third and fourth stage - Non-uniform (fourth stage) and uniform (third stage) rub-in

Figure 1.3: Liner segments in a modern aero engine (Published with permission, courtesy of Rolls-Royce Deutschland Ltd & Co KG)

to rotor contact in service of an engine. If the rotor is in contact with the casing, the rotor tips remove material from the abradable casing. A variety of wear mechanisms can occur, which is a field of research of its own (Borel et al., 1989).

In the given example (Figure 1.3a), the rotor of the first stage scraped a short pit off the casing. The liner of the second stage is intact. In the third stage, the casing is skimmed uniformly, which leads to a concentrically enlarged clearance during engine operation. Figure 1.3b outlines that the contact between rotor and casing can also lead to circumferentially non-uniform tip clearance and eccentricity (refer to fourth stage). This shows that altered and non-uniform gaps are likely. As there is a direct correlation between rotor gap width and the fuel consumption (Domercq and Escuret, 2007) on the one hand and the compression system's stability on the other (Freeman, 1985), there is a need to address this by current research.

Besides the motivation to investigate the effects from an aerodynamic point of view, there is also a structural-mechanical challenge. As *weight savings* of the compression system are essential for new engine designs, the possibility of unwanted vibration problems is increased. Light-weight structures are more vulnerable to vibration. If the source of the vibration is understood and modelling of the underlying mechanism is possible, amplitudes of the vibration can be controlled and do not lead to acoustical problems or structural failures. Several examples from various fields of engineering were presented by Verein Deutscher Ingenieure (1992). In the particular case of high pressure compressors, engineers still struggle to thoroughly understand and model the observed blade vibrations that result from flow separation at high angles of attack. As a result, these vibrations still occur in engines or full size compressor rigs (Kielb et al., 2003, Dodds and Vahdati, 2014). The influencing factors that control the vibration amplitudes of the blades have not been fully clarified, e.g. enlarged tip clearance and tip clearance non-uniformity.

In practice, engineers observed that breaking symmetry of a mechanical system can lead to a stabilization of the component in case of vibration problems. Automotive brake squeal for example, is a self-excited vibration, which results in acoustical problems that many know. The topic is still widespread, but it has been shown by Spelsberg-Korspeter (2013) that the system can be stabilized, if symmetry is avoided. This creates an optimization problem to evenly cool the brake disc while at the same time designing asymmetry to maximally detune the system. In the HPC, similar approaches exist for the rotating components - the rotors. It is well known that mistuning of the rotor can lower the amplitudes of the vibrations at high angles of attack (Castanier and Pierre, 2002). So, considering that the effect of uniform and non-uniform tip clearance on vibrations in HPCs are not fully understood, investigating these influencing factors is a promising research goal for this thesis.

To investigate all of the aforementioned aspects from both an aerodynamic and aeroelastic[1] point of view, a high speed facility is needed. Within the framework project E-BREAK, a 1.5 stage setup[2] of an engine compressor was investigated in the Darmstadt Transonic Compressor facility in collaboration with Rolls-Royce Deutschland Ltd & Co KG.

1.3 Outline of the Thesis

Increased rotor tip clearance, tip clearance eccentricity and a general non-uniformity of the gap between the rotor and the casing are essential aspects to be considered in the development process of axial compressors for modern aircraft engines. This thesis explores associated effects experimentally. The Darmstadt Transonic Compressor is used to investigate the 1.5 stage axial compressor at TRL 4[3]. The advantage of tests like this is the access for instrumentation to derive maximum understanding of the phenomena within the technical system. To validate technologies for higher TRLs, the complexity increases (e.g. multi-stage compressors), which lowers access for instrumentation and possible insight. A modern front stage compressor design is used for this investigation and the rotor is studied at engine representative speed. The aim of the current work is to reveal the effects of non-uniform tip clearance in the HPC with a detail unattained so far at transonic speed.

Chapter 2: Fundamentals and State of the Art presents the fundamentals of axial compressors in the context of this work. Current knowledge of tip clearance effects in the scope of state-of-the-art compressor research is introduced. At the end of this chapter, specific research questions are derived and the structure of the data analysis is outlined.

Chapter 3: Methods describes the measurement techniques and the compressor setup used for the investigation. This chapter contains descriptions of the test program, test design and application of the measurement technology. Possibilities and restrictions regarding the measurement task are highlighted.

[1] The term aeroelasticity refers to the field of study that deals with the interactions between the inertial, elastic, and aerodynamic forces that occur when a structure is exposed to a fluid flow.

[2] Single stage with variable inlet guide vanes.

[3] TRL 4 components/models are technologies that have been tested in a laboratory on rig scale to validate their functionality as independent component (DIN Deutsches Institut für Normung e. V., 2016).

Chapter 4: Results is the main part of the document. Within this chapter, the outcomes of this thesis are presented. The findings are divided into aerodynamic and aeroelastic results, both for configurations with uniform and non-uniform rotor tip clearance. At the end of each section, the findings are discussed and compared to the literature. The closing section depicts the results in an extended scope to show their significance for future aero engines and research.

Chapter 5: Conclusion summarizes the results of the current work and closes with recommendations for further research.

2 Fundamentals and State of the Art

In this chapter, the field of research is introduced. As tests are carried out in a single stage test facility, the transferability of rig tests to an engine application is shown. Design aspects for axial compressors are presented and the development of transonic compressors is motivated. Because the investigated setup is representative of a front stage, specific development goals are derived by considering effects in multi-stage compressors. These considerations trigger the investigation of the compressor's stability from both, an aerodynamic and aeroelastic perspective. Finally, the effects of uniform as well as non-uniform rotor tip clearance are discussed and specific research questions are derived for this thesis.

2.1 Compressor Testing and Scaling

To transfer the results of the experiments described in this work to an engine, similar flow conditions are needed. For tests in such a facility, engine compressors are scaled to fit to the geometrical constraints as well as the maximum power of the rig.

In order to achieve representative flow in the Darmstadt Transonic Compressor, the Mach number similarity, i.e. comparable fluid compressibility between engine and test rig is taken as a basis. This distinguishes high-speed tests from low-speed facilities, which operate at incompressible flow at the blade tips at any time. In terms of Mach number, exemplary values for the low speed Cambridge Facilities Deverson and Gibbons Rig are in the order of 0.1 to 0.22. These rigs are engine-scaled in terms of Reynolds number, i.e. similar ratio of inertia and viscosity of the fluid.

According to Schäffler (1979b) engine scale Reynolds numbers typically range in the order of 10^5 to 10^6 for civil applications. The lower the Reynolds number, the larger the regions of separated flow. This leads to a lower pressure coefficient and a lower efficiency than what might be achieved with a more turbulent flow (Cumpsty, 2004).

The influence of the Reynolds number is transferred from rig tests to engines by empirical corrections, which was experimentally investigated by Schäffler (1979b). He found a severe influence for Reynolds numbers below 10^5. In that order of magnitude, laminar blade boundary layers start to evolve. Today, Reynolds numbers below that value are only reached in military application at high altitude and in the rear stages of multi-stage compressors.

In the Darmstadt Transonic Compressor, the Reynolds numbers at stage inlet[1] range above 10^6, which is why Reynolds number effects are considered to be constant during the tests. The test compressor is scaled with respect to Mach number of the engine compressor to ensure similar aerodynamic flow conditions at the blade tip. This is achieved via equal axial and tangential Mach numbers according to

$$\mathrm{Ma}_{\mathrm{ax}} = \frac{c_{\mathrm{ax}}}{\sqrt{\kappa R T}} = \text{const.} \qquad \text{and} \qquad \mathrm{Ma}_{\mathrm{tip}} = \frac{u_{\mathrm{tip}}}{\sqrt{\kappa R T}} = \text{const.} \tag{2.1}$$

where κ is the heat capacity ratio, R the specific gas constant and T a reference temperature[2]. The axial velocity c_{ax} and the blade tip speed u_{tip} can be expressed as

$$c_{\mathrm{ax}} = \frac{\dot{m}}{\rho A} = \frac{\dot{m} R T}{p A} \qquad \text{and} \qquad u_{\mathrm{tip}} = 2\pi \frac{N_{\mathrm{r}}}{60} r_{\mathrm{tip}} \tag{2.2}$$

where $\dot{m}$ is the mass flow, p is a reference pressure, A the area of the compressor annulus, N_{r} the compressor's rotational speed in rpm and r_{tip} the tip radius of the compressor.

We assume that both compressors, the engine compressor and the test rig compressor, are operated with the same fluid at the same conditions. It is common that the compressor diameters in engines are larger than those in the test rig. So, in order to maintain a constant tip speed, the compressor must rotate faster under test conditions. Since the absolute axial velocity at inlet c_{ax} must be kept constant while having a smaller annulus, the mass flow through the test rig is reduced. As a side effect, the required input power of the facility decreases because it scales with the amount of mass flow passing the compressor. However, the test setup cannot be scaled to any arbitrary size as the required rotational speeds would otherwise become too high in respect of the blade stresses and mechanics of the drive train and bearings. Also, the application of instrumentation might be complicated. If these ideas are used, a test compressor can be designed that fits to the maximum power and geometrical constraints of the rig.

Throughout the tests, the same machine is used. However, as the facility is built as an open cycle, i.e. air is sucked in from the outside, ambient conditions vary.

[1] This value is calculated using the blade chord as characteristic length and relative inlet velocity at mean radius as characteristic speed. It is a reasonable choice to consider blade boundary layer effects.

[2] I.e. mostly the total temperature as the static temperature depends on the local speed of the fluid, which remains unknown in most cases.

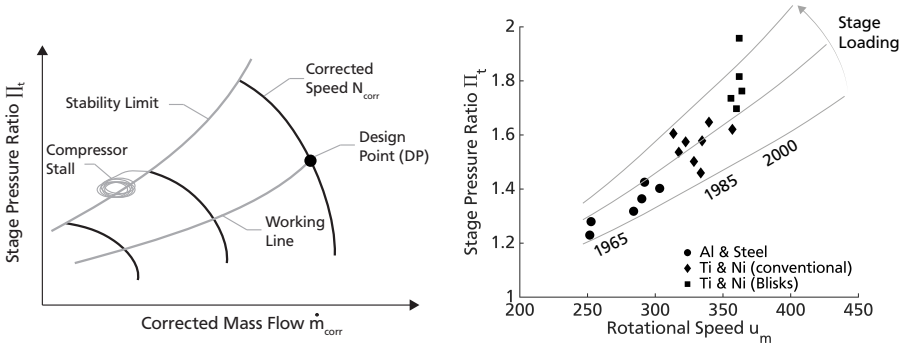

(a) Axial compressor map with stage pressure ratio as a function of corrected mass flow and speed

(b) Evolution of stage pressure ratio dependent on rotor design, developed from Steffens (2001)

Figure 2.1: Axial compressor performance and typical design parameters

Using Equations 2.1, this is addressed by correcting the mass flow and rotational speed according to

$$\dot{m}_{\mathrm{corr}} = \dot{m}\,\frac{p_{\mathrm{ref}}}{p^{04}}\sqrt{\frac{\kappa_{\mathrm{ref}} R\, T^{04}}{\kappa\, R_{\mathrm{ref}}\, T_{\mathrm{ref}}}} \tag{2.3}$$

$$N_{\mathrm{corr}} = N\sqrt{\frac{\kappa_{\mathrm{ref}} R_{\mathrm{ref}}\, T_{\mathrm{ref}}}{\kappa\, R\, T^{04}}} \tag{2.4}$$

where p^{04} and T^{04} refer to the inlet conditions to the compressor stage. All measurement stations besides ⑭ will be introduced later on in detail (Figure 3.4). The tests are referenced according to International Standard Atmosphere (ISA) at sea level ($p_{\mathrm{ref}} = p_{\mathrm{ISA}} = 1013.25\,\mathrm{mbar}$, $T_{\mathrm{ref}} = T_{\mathrm{ISA}} = 15°\mathrm{C}$, $\kappa_{\mathrm{ref}} = \kappa_{\mathrm{ISA}} = 1.4$ and $R_{\mathrm{ref}} = R_{\mathrm{ISA}} = 287.058\,\mathrm{J/kg\,K}$).

For a compressor with no variable geometry and where the dependence on Reynolds number can be neglected, the pressure ratio is a function of corrected mass flow and corrected speed. This is shown in Figure 2.1a. In a multi-stage assembly, all compressor stages are designed with regard to one particular condition, commonly referred to as design point (DP). This means that the stages are matched for a specific mass flow rate and pressure ratio.

In an engine, the working line of the compressor is (mostly) defined by the choking high pressure turbine. At rig scale, this line is defined by the losses of the duct from inlet to outlet. If the compressor is throttled by reducing the exit area, the pressure loss in the outlet of the compressor rises.

For constant corrected speed and increased degree of throttling, the compressor must deliver higher exit pressure at a lower mass flow. At the aerodynamic stability limit, the pressure cannot be increased any further, the operation becomes unstable and compressor blades start to stall alternately. This manifests itself in regions with reduced (or even reversed) flow and results in mass flow and pressure fluctuations. These and further design aspects are explained in more detail in the following sections.

2.2 Axial Compressor Design Considerations

The pressure ratio of the compression system is a major factor to improve the efficiency of an aero engine (Bräunling, 2009). It can be expressed as

$$\Pi_\mathrm{t} = \left[\frac{\eta_\mathrm{is}}{c_\mathrm{p}} \frac{\Delta h_\mathrm{t}}{u_\mathrm{m}^2} \left(\frac{u_\mathrm{m}}{\sqrt{T^{04}}} \right)^2 + 1 \right]^{\kappa/(\kappa-1)} \tag{2.5}$$

where the essential parameters to increase the pressure ratio are highlighted. These are

- stage isentropic efficiency η_is
- stage loading $\Delta h_\mathrm{t}/u_m^2$
- rotational speed $u_\mathrm{m}/\sqrt{T^{04}}$

Over the last century, efficiency, stage loading and rotational speed of axial compressors have been continuously improved. The development trends of rotational speed and stage loading are highlighted in Figure 2.1b. Until the late 60s, low speed compressors with rotational Mach numbers between 0.8 and 0.85 were in service. In order to further increase the pressure rise and mass flow capacity of axial compressors, the rotational speed had to be increased continuously. As a result, the development of the first transonic rotors began in 1953, mainly forced by NACA (later referred to as NASA). The rotor relative flow in these compressor rotors is partly supersonic, which is why they are called transonic compressors. The static pressure rise is mainly achieved via compression shocks in the blade passages. Or in other words, the deflection in the absolute system does not take place via a cambered profile but via the deceleration across the shock in the relative frame of reference. This next generation of compressor rotors entered service approximately by 1970.

A step change in compressor design was enabled by the use of titanium and nickel alloys, which allowed higher mechanical stresses and consequently increased rotational speeds. These rotors were built as discs with mounted blades (Rolls-Royce plc, 2007).

For even higher speeds, the resulting forces at the joints in the disk were too high and new rotor designs were needed. As described by Steffens (2001), "Blade integrated disc designs" (Blisks) enabled a further increase of the compressor rotational speeds and stage loadings. Such a state-of-the-art transonic compressor rotor in Blisk design will be used for the current investigation.

2.2.1 Transonic Compressors

The supersonic speed at the blade tips of modern high pressure compressors results in aerodynamic shocks that occur in the vicinity of the blades. The flow field and the occurring shocks are influenced by the rotor inlet Mach number, the stage exit pressure, the blade geometry, the endwall geometry and the inlet flow angle. Shocks are generally irreversible that means they lead to loss and can decrease the efficiency of the compression system. In order to efficiently use the static pressure rise of a shock in a transonic machine, its pressure rise has to outweigh the coherent shock loss. Shock losses rise approximately by $(\mathrm{Ma}_{\mathrm{rot}}^2 - 1)^3$, so a small increase in Mach number in the relative frame of reference may substantially increase the shock loss (Denton, 1993). Consequently, typical inlet Mach numbers to compressor rotors in core engines do not exceed 1.4.

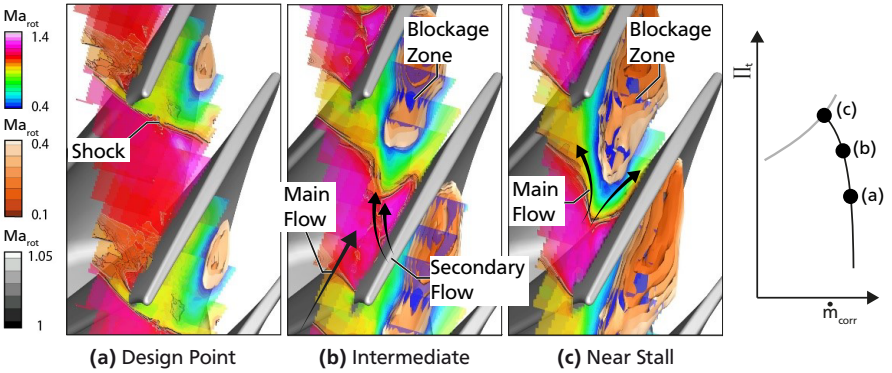

Figure 2.2: Blade-to-blade flow in a axial compressor with supersonic inflow at about 93% channel height. Dependency on throttling condition is illustrated, developed from Brandstetter and Schiffer (2018)

Figure 2.2 illustrates the flow field in a rotor at transonic speed, measured in the Darmstadt Transonic Compressor facility. At the design point, the inlet Mach number and the stage exit pressure lead to a shock close to the leading edge of the blade. The shock intensity is high, which results in subsonic relative flow velocity downstream of the shock.

Further throttling of the compressor (Figure 2.2a to Figure 2.2c) decreases the rotor inlet Mach number and increases the stage exit pressure and the rotor incidence, i.e. inlet flow angle. As a consequence, the shock moves upstream and detaches from the leading edge of the blades. Due to the increased interaction of main flow with *secondary flow*, the shock is bent. Downstream of the shock, this interaction results in an enlarged region of fluid with low axial momentum. This is commonly referred to as *blockage*, as it reduces the effective passage area and forces the main flow to redistribute radially and circumferentially.

2.2.2 Secondary Flow in Axial Compressors

In turbomachinery, the term secondary flow is generally applied to all flows that occur across the main flow. For this thesis, the flow at the rotor blade tips is of special interest. Research has shown that secondary flow within this area is particularly characterised by two vortex structures. A tip clearance vortex and a radial vortex (see Figure 2.3).

The tip clearance vortex develops from tip leakage flow that passes through the gap between the rotor and the casing. It has been addressed by many researchers in the last century. Early surveys were already published by McNair (1960) and Reeder (1966). The following introduction to the topic cannot be all-governing. Instead, a brief overview reflecting the main aspects relevant to this thesis, is given.

The occurrence of radial vortices close to the stability limit has been revealed by recently published studies. Its origin and evolution is the subject of ongoing research.

Tip Clearance Vortex. As a result of the pressure gradient between the suction and pressure side of the rotor blades, tip clearance flow is passing the gap between the rotor and the casing. In the blade passage, the tip leakage flow interacts with the main flow and roles up to a vortex. Throttling of a compressor rises the pressure difference between pressure and suction side, which increases the overall mass flow in the tip gap. This was used by Denton (1993) to model tip clearance loss in an axial compressor. The loss is generated, when the tip clearance flow mixes out with the main flow in the blade passage and downstream of the blade row (Wisler, 1985).

With increased tip clearance flow, the amount of flow with low axial momentum is raised, which leads to blockage effects in the tip region. Conceptionally, this blockage can be seen equivalently to the displacement thickness of a boundary layer,

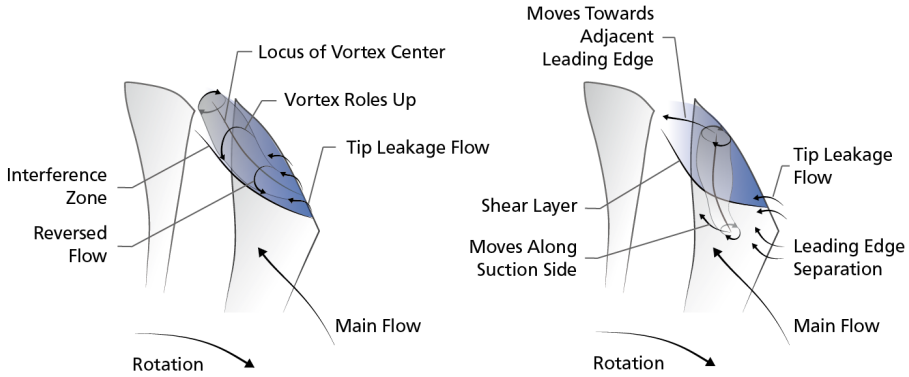

(a) Topology of tip clearance vortex

(b) Topology of radial vortex

Figure 2.3: Secondary flow at the blade tip in an axial compressor, developed from Inoue and Kuroumaru (1989), Pullan et al. (2015), Eck et al. (2017)

i.e. it reduces the effective flow area in the tip region. As a result, less main flow is passing this section of the compressor annulus, which increases the incidence at the blade tip. Several attempts were made to model and quantify blockage generation that results from the tip clearance flow (Storer and Cumpsty, 1993, Khalid, 1995, Suder, 1998).

The blockage is even more severe, if the formed tip clearance vortex breaks down and expands further. In a low speed compressor, the breakdown of a bubble-like recirculation region was found close to the stability limit by Furukawa et al. (1999). Earlier, the relevance of such an expanding blockage area by shock-vortex interaction in transonic compressors was pointed out by Adamczyk et al. (1993). At high rotor speeds, the vortex breakdown is caused by the sudden deceleration across the passage shock. Schlechtriem and Lötzerich (1997) concluded that the accompanied growth of blockage in the tip region has a large impact on the stability of axial compressors, which is in agreement with the findings of Furukawa et al. (1999) in the low speed machine.

For the rotor used in the current work, the destabilizing influence of vortex breakdown and its accompanied blockage were highlighted for both subsonic and transonic speeds by Brandstetter et al. (2018) just recently.

Various numerical studies of shock-vortex interaction showed that its intensity is very complex (Thomer et al., 2001, Hofmann, 2006, Yamada et al., 2007). It depends on the angle of interaction, the ratio of tangential vortex velocity to the

axial velocity of the vortex core, the free stream Mach number and the pressure ratio across the shock. For simplicity, these interrelations are not illustrated in Figure 2.3a.

Radial Vortex. Radial vortices were first observed by Inoue et al. (2000) in a low speed research compressor. They occurred above a critical value of rotor incidence. The origin of this radial vortex is currently widely discussed. Its topology is shown in Figure 2.3b.

According to Pullan et al. (2015), radial vortices can develop from a leading edge separation, role up and propagate from the leading edge of the original blade to the pressure side of the adjacent blade. They found that the lower end of the vortex stays attached to the suction side of the blade, whereas the upper end is attached to the casing wall at the tip. In their compressor, the continuous growth of the vortex structures leads to an unstable behaviour of the machine.

The radial vortices found by Eck et al. (2017) occur at stable operating points of the compressor. These vortices develop at the interface of the main flow and the blockage zone in the blade passage. Eck et al. (2017) stated that the origin of the vortices might be connected to shear layer instabilities. They found no direct connection to tip clearance flow.

However, earlier findings indicated that fluid transported with radial vortices might be connected to the blade tip clearance flow (Yamada et al., 2013). Currently, it cannot be entirely excluded that there is a tip gap dependency. Hah (2016) noted that the formation of a radial vortex depends on tip clearance, as enlarged clearance alters blockage and the subsequent radial vortex formation.

So, the origins of radial vortices are still being investigated. However, the role of both the tip clearance vortex and the radial vortex are essential in terms of stability of axial compressors, which is further discussed in Section 2.3.

2.2.3 Multistage Designs and Aerodynamic Stage Matching

The compression system in an aero-engine consists of several stages that are rising the pressure continuously to achieve overall pressure ratios of larger than 40 in state-of-the-art aero engines. Increased density and higher temperature accompany this pressure rise. In modern compressors, the temperature rise per stage reaches up to 70°K (Steffens, 2001).

Due to the increased density from stage to stage, the channel height of multi-stage axial compressors is decreasing. In front stages, hub-to-tip ratios of about 0.5 are quite common. Middle stages are designed with a ratio of roughly 0.75 and the ratio increases further in the rear stages (Pampreen, 1993). As a result of increasing temperature and the decreasing tip radius, the rotor relative flow remains subsonic in the rear stages (reconsider Equations 2.1). Transonic flow conditions are restricted to the front stages in multi-stage compressors (Cumpsty, 2004). Both aspects are

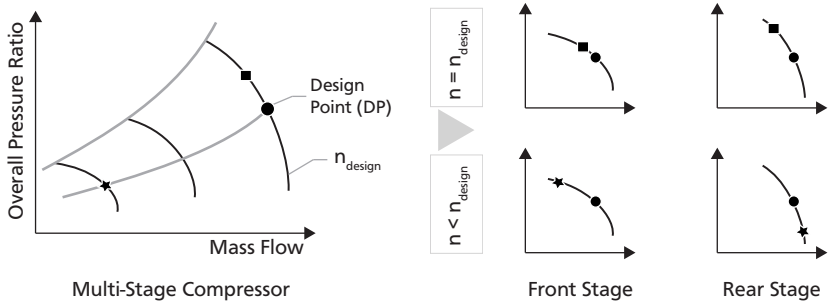

Figure 2.4: Off design operation of a multi-stage compressor - Part speed operation and throttling at design speed

relevant for the rotor used in this thesis. The stage design has an hub-to-tip ratio of about 0.5 and transonic rotor relative flow.

All compressor stages in a multi-stage assembly are designed with regard to one particular condition, the design point (DP). The stages are matched for a specific mass flow rate (compare Equation 2.3) and pressure ratio. The contraction of the annulus is adjusted with respect to the density change at design conditions. If the actual operation of the compressor differs from the DP, the density rise per stage varies accordingly and difficulties arise. Two common examples are outlined in the following.

At design speed, increased throttling of a multi-stage compressor will reduce the overall through flow compared to the DP. If all stages operate at lower mass flow, the pressure ratio and the resulting density rise per stage increases. This intensifies from the first to the last stage whereby the inlet density to the last stage is higher compared to the DP. The design of the annulus contraction is not large enough to yield the originally intended axial inlet velocity. This lowers the inlet velocity in the rear stages and shifts the operation further to the stability limit (compare Figure 2.4).

Vice versa, the front stages operate at higher incidence compared to the originally intended design at low speeds. In extreme cases, the last stage of the multi-stage assembly chokes due to the insufficient density rise from stage to stage. The result is a problem in the front stages, which appear to work on the unstable side of the characteristic.

2.3 Stability of Axial Compressors

The stability of axial compressors is essential for the safe operation of the entire engine. If the flow breaks down in the rear stages, surge can occur, which means

that hot gas from the combustion chamber can pulsate upstream and lead to the destruction of the compression system and the whole engine.

In the front stages of a multi-stage compressor, the problem of rotating stall can also be problematic, if it leads to blade vibrations with high amplitude. Early studies of Huppert et al. (1954) already considered vibrations in the rotor of a first stage that were excited by a multi-cell rotating stall. Their investigations were terminated by a fatigue failure of a rotor blade. The development of rotors in Blisk design contributes to the susceptibility to vibration as it reduces mechanical friction damping of today's compressor blades. A recent study by Dodds and Vahdati (2014) of a modern multi-stage aero engine compressor highlights that the problem is absolutely relevant.

From a pure aerodynamic perspective, a multi-stage compressor can still be operated if stages are present downstream of an unstable front stage. For single-stage compressors, the ultimate operating limit is their aerodynamic stability. Blade vibrations are a matter of concern in front stages of aero engines and high speed rigs, which are designed with thin and flexible blades.

In this thesis, the investigation is carried out on such a stage, where further throttling is either terminated by rotating stall or blade vibrations occurring before. In the following, the compressor's stability is thus studied from both, an aerodynamic and also an aeroelastic viewpoint.

2.3.1 Aerodynamic Stability

If the angle of attack of an airfoil is constantly raised, the lifting force acting on it is increased. The maximum lift coefficient is limited by the flow being attached to the suction side of the airfoil. Stall of an airfoil results in a sharp drop of that lift and is a consequence of boundary layer separation (see Figure 2.5a).

In an axial compressor rotor, the stalling of rotor blades leads to propagating stall or so called *rotating stall*. The naming originates from its characteristic to rotate relative to the compressor rotor and the casing. Figure 2.5b illustrates rotating stall in an axial compressor. If the incidence is high and leads to separated flow at a single blade, or - that is usually the case - at several rotor blades, blockage occurs in the affected blade passages. Considering the problem from a two-dimensional perspective, the aerodynamic loading of the neighbouring blades is altered. The local incidence of the leading blade is lowered and - in contrast - the loading of the adjacent blade is increased. As a result, leading blades will recover and adjacent blades will start to stall. This leads to the propagating characteristic of rotating stall cells against rotor direction.

After roughly half a decade of research on rotating stall and its inception, uncertainty still exists on several important aspects. For example, Pampreen (1993) concluded that the stall cell geometry is seldom stable, which similarly applies to

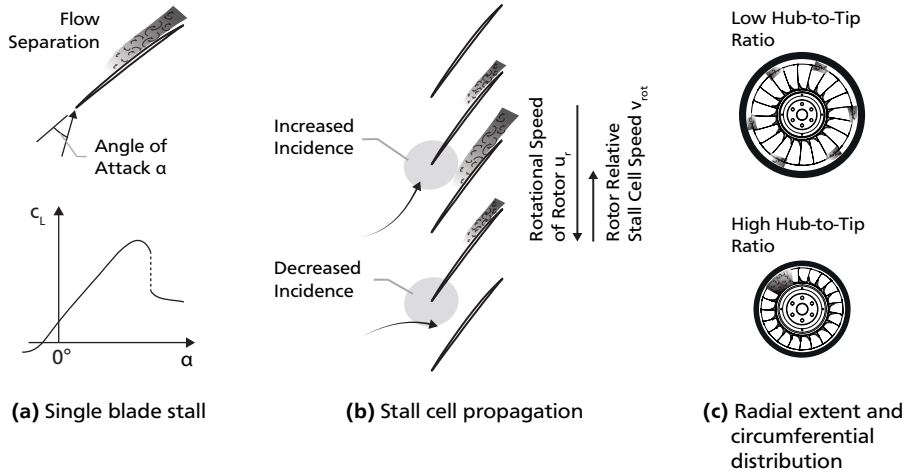

(a) Single blade stall **(b)** Stall cell propagation **(c)** Radial extent and circumferential distribution

Figure 2.5: Rotating stall in an axial compressor rotor, developed from Pampreen (1993), Cumpsty (2004)

the cell count. He stated that "four cells can break up into five cells and then rejoin to form four or three temporarily". The prediction of the cell count and their speed was also just recently pointed out as a key problem by Day (2016).

Besides unpredictability, some things are certain. The following aspects were stated by Pampreen (1993), Grieb (2007) and Day (2016), who reviewed research on stall inception:

- Compressors with short blades usually develop a *single full-span stall* cell. For long blades (high aspect ratio, low hub-to-tip ratio, e.g. aero engine front stage designs) the initial pattern is mostly a *multiple part-span stall* at the blade tips (compare Figure 2.5c).

- The development of a single stall cell is accompanied with an *abrupt pressure drop* of the characteristic. If a compressor develops several part-span stall cells, the *pressure loss* is rather *progressive*. These part-span stall cells are usually equally distributed.

- The initiation of rotating stall may be *spike-* (short circumferential extent, high initial speed) or *modal-type* (long length-scale, less abruptly). Stall inception was also observed to be a superposition of both extreme cases.

- Modal waves represent sinusoidal modulations of the mass flow and blockage in circumferential direction. Their length-scale exceeds the magnitude of

several blade pitches. In most cases, they propagate relative to the rotor, but not necessarily.

- As the mass flow decreases, the cell number may increase or decrease, but the percentage of annulus blocked by the total cell area constantly increases.
- The absolute propagation velocity increases with rotor speed. It may vary with cell count and changes during the transition from part-span to full-span stall.
- At steady operation near stall, the development of *pre-stall disturbances* or so called *rotating instabilities* has been observed. The distinction between these disturbances and mild forms of part-span stall is not ultimately clear in the literature.

The rotor under investigation is known to initiate stall spike-type, i.e. by short length-scale disturbances (Biela, 2012, Streit, 2014, Brandstetter, 2015). Moreover, pre-stall disturbances were observed, which occurred at steady operating points near stall (Jüngst et al., 2015, Holzinger et al., 2015, Brandstetter et al., 2018).

Spike-Type Stall Inception. The nomenclature of spikes originally referred to the steep pressure drop and rise in wall pressure or hot wire signals that were observed prior to rotating stall (Camp and Day, 1998). It was found that these spikes are associated with a breakdown of the flow at the blade tip and are therefore more likely to occur in *tip critical* blade designs (also refer to Section 2.4.2). Vo et al. (2008) developed two criteria for the formation of spike-type stall, based on numerical studies. They stated that the spillage of tip clearance fluid around the leading edge of adjacent blades is needed, along with tip clearance flow that passes the blades' trailing edges. This was called leading edge spillage and trailing edge backflow. They argued that these criteria explain the short circumferential length-scale of spikes. However, cause and effect of the forward spillage of tip clearance fluid and the formation of spikes was later on questioned (Weichert and Day, 2014).

In a way, the past decade has renewed the view on spike-type stall inception. Recent findings show that besides the classical two-dimensional explanation of rotating stall, three-dimensional vortex structures are involved in stall inception, which propagate from blade to blade. The findings by Pullan et al. (2015) indicated that the static pressure drop of spikes originates from the vortex core of radial vortices and that the pressure rise is linked to blockage in the vicinity of the vortex. Experimentally, it was shown by Brandstetter et al. (2018) that this evolution of radial vortices occurs similarly in high-speed machines at transonic speed. The vortices were measured via particle image velocimetry at 93% span and identified as low pressure regions that occurred in the static wall pressure between the leading

edges of the compressor blades. In the transonic compressor, these vortex structures occur near the stability limit, can cause blade vibrations, but instead of growing rapidly they instantly lead to rotating stall.

Pre-Stall Disturbances and Rotating Instability. The generation of pre-stall disturbances was first described by Mathioudakis and Breugelmans (1985) as a form of *small stall*. The authors stated that the observed form of rotating stall is attributed to boundary layer separation of the blades. Their measurements suggested the simultaneous existence of disturbances of different wavelengths, i.e. cell counts. They proposed to replace the classical way of referring to a certain number of stall cells by a compilation of several dominant wavelengths.

Later on, Mailach et al. (2001) found tip clearance vortex oscillations and März et al. (2002) found radial vortices that propagate between the leading edges of the rotor blades prior to stall. Both found certain characteristics in the frequency spectra of the wall pressure signals and referred to this mechanism by the name rotating instability (RI), which started large discussions on the nomenclature and the underlying mechanism. Since then, the phrases pre-stall disturbances and rotating instabilities co-exist. The name RI has rather been used in the German-speaking community. In the context of this work, the more generally accepted term pre-stall disturbances is used.

Hah et al. (2008) found vortices that form at both the leading edge and the trailing edge, comparable to von Kármán-Vortex-Shedding. Their results highlighted that the passage shock and the tip clearance vortex oscillate with the same frequency as the vortices are shed. Cause and effect remained questionable.

It was later on observed that the characteristics of pre-stall disturbances emerge even with a shrouded rotor, i.e. without any tip clearance flow at all (Pardowitz et al., 2015).

Recent studies by Eck et al. (2017) indicated similarities to the radial vortices observed by Pullan et al. (2015). In both cases, a radial vortex is investigated with its lower end attached to the suction surface of the blade and the upper end attached to the casing. In contrast to Pullan et al. (2015), the vortices observed by Eck et al. (2017) are not part of a spike-type stall inception process, but instead propagate in a stable manner. In addition, the vortices that Pullan et al. (2015) observed are created by a leading edge separation, whereas Eck et al. (2017) found that they develop along the shear layer between main flow and the blockage zone in the passage.

The origin and evolution of these pre-stall disturbances is subject of current research. However, it is known that they are a source of compressor noise and blade vibration. Due to their propagating characteristic with cells of high count, stationary observer pick up high frequent tones in the far field of compressors (Kameier and

Neise, 1997). Baumgartner et al. (1995) analysed that pre-stall disturbances can excite blade vibrations in compressor front stages.

The cause for both effects are periodic pressure fluctuations as a result of the unsteady aerodynamics of pre-stall disturbances and also rotating stall.

Periodic Pressure Fluctuations. Unsteady aerodynamics lead to periodic fluctuations of the static and also the dynamic pressure. The frequency of this fluctuation, measured in the stationary or rotating (rotor) frame of reference depends on the propagation speed and cell count (compare Rick (2013) and Dodds and Vahdati (2014)). A stationary observer, such as a wall pressure transducer in the casing or a person in the vicinity of the compressor, will pick up the frequency

$$f_{\mathrm{stat}} = \frac{v_{\mathrm{abs}}}{\lambda} \tag{2.6}$$

that depends on the absolute propagation speed v_{abs} and the wavelength λ of the disturbance. By expressing aerodynamic waves as discrete stall cells in the compressor annulus and expressing the measured frequency relative to the rotational frequency of the rotor f_{r}, this term can be written as

$$\frac{f_{\mathrm{stat}}}{f_{\mathrm{r}}} = \frac{v_{\mathrm{abs}}}{f_{\mathrm{r}}} \frac{n_{\mathrm{aero}}}{C}, \tag{2.7}$$

with the aerodynamic cell count n_{aero} and the circumference C of the casing. This formulation simplifies to

$$\mathrm{EO}_{\mathrm{stat}} = \frac{v_{\mathrm{abs}}}{u_{\mathrm{r}}} n_{\mathrm{aero}}, \tag{2.8}$$

with the engine order $\mathrm{EO}_{\mathrm{stat}}$, measured in the stationary frame of reference. Its value depends on the cell count and the absolute speed of the disturbance relative to the rotational speed u_{r} of the rotor. The formulation can be equally expressed for the rotating frame of reference, which would apply for measurements with rotor mounted strain gauges and which is relevant regarding to blade vibration:

$$\mathrm{EO}_{\mathrm{rot}} = \frac{v_{\mathrm{rot}}}{u_{\mathrm{r}}} n_{\mathrm{aero}} \tag{2.9}$$

The propagation speed v_{rot} is the stall speed relative to the rotor speed that can be expressed as

$$v_{\mathrm{rot}} = u_{\mathrm{r}} - v_{\mathrm{abs}}. \tag{2.10}$$

By using this expression in Equation 2.9 and by addition of Equation 2.8 and Equation 2.9, a simple relation for the stall cell count is:

$$n_{\text{aero}} = \text{EO}_{\text{stat}} + \text{EO}_{\text{rot}} \tag{2.11}$$

This expression is very helpful regarding data analysis if measurements exist in both the stationary and rotating frame of reference. To be of any physical sense, n_{aero} is always an integer. In the case of acoustic phenomena, Equation 2.10 must be adapted, if the propagation speed v_{rot} is above rotor speed u_{r} or below zero. In these cases, the differences $\text{EO}_{\text{rot}} - \text{EO}_{\text{stat}}$ or $\text{EO}_{\text{stat}} - \text{EO}_{\text{rot}}$ must be considered for the determination of the circumferential wavelength, respectively.

2.3.2 Aeroelastic Stability

The mechanical integrity of compressor blades must be maintained throughout the service life of an engine. In order to achieve this, the amplitudes of the vibrations have to be controlled and underlying excitation mechanisms need to be understood. The field of engineering that deals with this topic in axial compressors is the branch of aeroelasticity.

If structures are exposed to cyclic forces, their failure depends on the amplitude and the number of cycles of the vibration (as well as the static load). Below a certain amplitude, it is likely that the material withstands more than ten million cycles. If the amplitudes are above this critical value, it takes less time for the material to crack and fail. Commonly this is referred to as high cycle fatigue (HCF). A simple example highlights the severity of this problem. Assuming a blade vibrates at 5000 Hz. If the amplitudes exceed the HCF limit only during 30 minutes (time to accumulate about 10^7 cycles), a crack of the structure is likely to occur. These 30 minutes represent very little time in relation to the service life of an engine. In case of higher amplitudes, the structure will withstand less cycles. A failure in the range below 10^4 to 10^5 cycles is commonly referred to as low cycle fatigue (LCF).

There are two main kinds of blade excitation mechanisms that lead to HCF and LCF. The mechanisms differ fundamentally and are called *synchronous* and *non-synchronous vibrations*.

Clarification of Nomenclature. Synchronous vibrations typically result from the relative motion between the rotor and its neighbouring stationary blade rows and struts. The most common example are wakes of upstream stator rows or the potential fields of downstream stators, which a rotor will pass during one turn. In these cases, the resulting force on the rotor blades is a multiple of the rotor speed, dependent on the number of stationary bodies. Such simplicity does not apply to non-synchronous vibrations, which are the subject of this thesis. Even the name itself requires discussion.

Besides the general term non-synchronous vibration, a historically well know term is *flutter*. This term is often used universally by engineers, if aeroelastic problems occur at non-multiples of the rotor speed. Historically, it describes the oscillation of an airfoil that is self-sustaining. No external oscillator or forcing is required to cause the vibration, so the force on the blade is entirely a result of the blade motion and the induced aerodynamic response. Flutter occurs, if the speed of the flow relative to the airfoil is above a critical value. In that case, small disturbances can initiate a vibration that leads to the destruction of the structure (Fung, 2002). If during some time of the vibration cycle the fluid is (partially) separated, the phenomenon is often referred to as *stall flutter*. This is used by several authors to be more precise. A recent interpretation by Clark et al. (2005) uses this term for an aeroelastic interaction between fluid and structure via vortex shedding of the blades. The vortices are propagating from blade to blade and lead to reduced and reversed flow in the vicinity of the blades. The authors refer to a similar observation by Sisto et al. (1989), who found propagating vortices in stalling cascades.

Over the years, the use of the terms *flutter*, *stall flutter* and the more general expression *non-synchronous vibration* (NSV) has become blurred and is not always perfect (Holzinger et al., 2015). This is amplified if the cause and mechanism of the vibration is not completely clear. Clark et al. (2005) distinguishes the blade instability (flutter) and the flow instability (rotating stall), which both contribute to a non-synchronous vibration. The transition between both extremes is smooth. If the fluid dynamic instability is dominating, it has been suggested by Kielb et al. (2003) to refer to the observed phenomenon by the term NSV. He also defined that in case of flutter, all self-sustaining pressure forces are caused by the motion of the blades itself (Kielb, 2018).

During recent work at the Darmstadt Transonic Compressor, blade vibrations occurred at high incidence and (partially) separated flow (Jüngst et al., 2015, Holzinger, 2017, Brandstetter et al., 2018). Some aspects would consequently allow the term *stall flutter*, which was used by Holzinger (2017). However, the commonly accepted term NSV is used throughout this thesis, which is in accordance with the aforementioned proposal (Kielb et al., 2003, Kielb, 2018).

Vibration of Blades and Blisks. To achieve the target of 10% compressor weight reduction in case of current development engines, structures are built increasingly lightweight (von der Bank et al., 2015). This amplifies their susceptibility to vibration. For example, rotors in Blisk design have low mechanical damping due to missing joints and no friction between the disc and the blades.

The fundamental blade modes consist of flap (equivalent to bending of a beam) and torsional motions (equivalent to torsion of a flat plate). Due to aerodynamic

design considerations, the rotor blades are twisted from hub to tip. As the natural frequencies of the modes increase, the chord-wise motion (i.e. torsion) is increasingly coupled with the flap motion (Srinivasan, 1997). The bending mode at the lowest natural frequency is commonly referred to as first flap. For this thesis, three eigenmodes of the blades are introduced, *first flap* (1F), *first torsion* (1T) and *chord-wise bending* (CWB) (compare Figure 2.6a).

Considering the entire rotor, the individual blades cannot be taken into account independently. The relative movement of the blades needs assessment at every time step (compare Figure 2.6b). By definition, a wavelength is the minimal distance of two points with the same phase. In a circular system, such as a compressor rotor, the wavelength can be expressed as a fraction of the circumference, using the expression nodal diameter (ND):

$$\lambda = \frac{2\pi r}{\mathrm{ND}} \tag{2.12}$$

where λ is the wavelength and r the radius. The minimum structural wavelength is restricted as there exists a finite number of rotor blades N_{blade}. Therefore, the maximum ND can be expressed as

$$\mathrm{ND}_{\mathrm{max}} = \pm\frac{\mathrm{N}_{\mathrm{blade}} - 1}{2}, \qquad \text{if} \qquad N_{\mathrm{blade}} = \{2n+1 : n \in \mathbb{Z}\} \tag{2.13}$$

and

$$\mathrm{ND}_{\mathrm{max}} = \pm\frac{\mathrm{N}_{\mathrm{blade}}}{2}, \qquad \text{if} \qquad N_{\mathrm{blade}} = \{2n : n \in \mathbb{Z}\} \tag{2.14}$$

and its value is always integer.

The relative movement of the blades can be expressed, using the inter-blade phase angle φ, which is calculated in radians by

$$\varphi = \pm 2\pi \frac{\mathrm{ND}}{N_{\mathrm{blade}}}. \tag{2.15}$$

By using Equation 2.14, the possible quantities of the inter-blade phase angle translate to $\pm\pi$ in Equation 2.15. As a consequence of the constant phase lag of neighbouring blades, the blade motion seems to propagate circumferentially for subsequent time steps, just as a wave pattern. According to this, the general equation for the propagation velocity of waves

$$v = \lambda f, \tag{2.16}$$

can be expressed as

$$v_{\mathrm{rot}} = \frac{2\pi r f_{\mathrm{blade}}}{\mathrm{ND}} \tag{2.17}$$

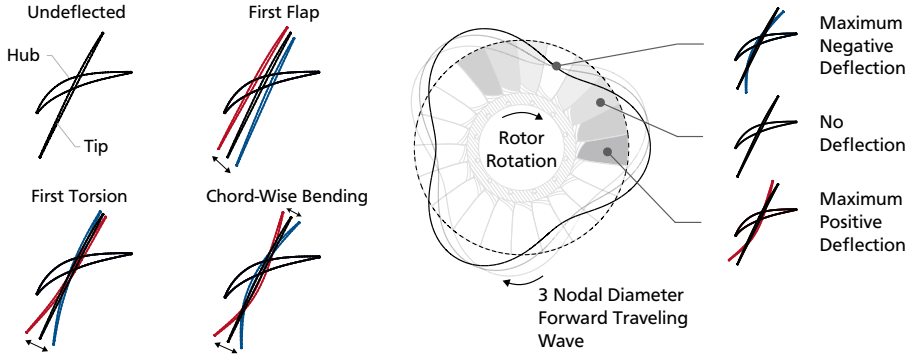

(a) Deflection of tip section for first flap, first torsion and chord-wise bending mode

(b) Phase lag of blade motion, shown for +3 ND forward travelling wave

Figure 2.6: Eigenmodes of single rotor blades and travelling waves in a compressor rotor, developed from Holzinger (2017)

where f_{blade} is the natural frequency of a rotor blade. Every Blisk vibration can be expressed as a superposition of several NDs. This is analogous to the idea of Fourier-decomposition. An example of a +3 ND forward travelling wave is given in Figure 2.6b.

A special case is 0 ND, which is sometimes referred to as *umbrella mode*. In that case, all blades vibrate in phase and the wave is not propagating. Otherwise, dependent on inter-blade phase angle, the waves travel in rotor direction or against. In this thesis, positive NDs refer to forward travelling waves (in rotor direction) and negative NDs to backward travelling waves in the rotor frame of reference.

The aerodynamic waves occur similarly in the annulus. They are not restricted to the number of blades or blade passages and can occur with independent wavelength. In the literature, it is not common to refer to aerodynamic waves by nodal diameter. Throughout this thesis, the cell count n_{aero} is used as aerodynamic equivalent (compare Equation 2.11).

Non-Synchronous Vibrations. The following aspects on NSV are not meant to be all-embracing. They highlight the underlying interactions between fluid and structure and provide a general overview of the topic. In the past, three mechanisms have been considered in the context of NSV: *Vortex shedding, convective transport* and *acoustic resonances*.

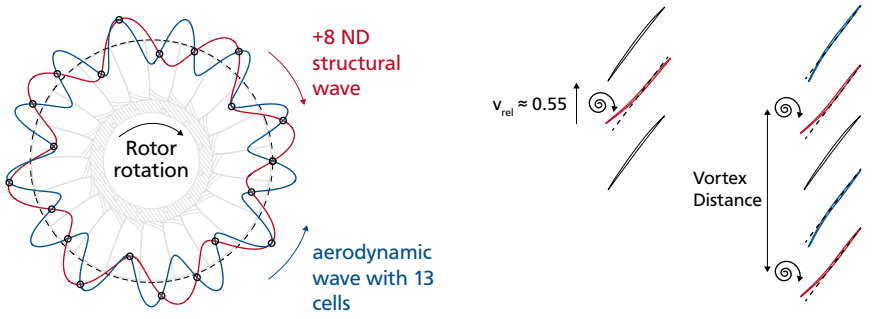

(a) Coherent wave pair, developed from Holzinger (2017)

(b) Vortex propagation between leading edges of the blades, developed from Brandstetter et. al (2018)

Figure 2.7: Mechanism of NSV in a transonic compressor rotor

Vo (2006) indicated the involvement of tangential convection of tip clearance flow and its impingement on adjacent blades. His investigation was purely numeric and motivated subsequent analytical and experimental work by Thomassin et al. (2009). They found an acoustic wave, triggered by the convective transport of fluid via tip clearance flow and its impingement on adjacent blades. This acoustic feedback wave can be thought of as an echo reflected on the solid wall of the adjacent blades' pressure side. Thomassin et al. (2009) found a resonance condition in which the acoustic wave was reinforcing the blade vibration and the associated tip clearance flow fluctuation.

This strong involvement of tip leakage fluid with regard to the mechanism of NSV was also considered by Holzinger (2017). He further showed that the propagation of waves in rotor direction (acoustic waves above rotor speed) are not a critical feature of the observed blade vibrations, but simply a result of the synchronization between fluid and structure (see Figure 2.7a). During NSV, a coherent pair of waves propagates in the compressor annulus. He found that the convective speed of the aerodynamic waves that propagate against rotor rotation are a key feature of the observed phenomenon. The propagation speed of the aerodynamic disturbances was about half of the rotor speed. Holzinger (2017) attributes the propagation of the aerodynamic wave largely to fluctuations of the tip clearance vortex that synchronises with the dominating blade motion. Because of the characteristic speed he also assumed a strong connection to rotating stall.

Earlier, Kielb et al. (2003) also identified a convective mechanism that drives NSV. Using computational fluid dynamics (CFD), they found vortices that were propagating from blade to blade and that were shed at the leading edge of the

blades. The intent of a subsequent analysis by Besem et al. (2014) was to more accurately describe the flow conditions in which this instability of the flow coincides with that of the blades. This is called *lock-in*. They analysed the vortex shedding of an airfoil at high angles of attack, its vibration amplitude and the vortex separation frequency. It was found that the range of the lock-in is extended by large vibration amplitudes.

Just recently, Brandstetter et al. (2018), measured radial vortices at the blades' leading edges via PIV and wall pressure transducers at transonic speed. The measurements indicated the propagation of these vortices from blade to blade with an approximate constant speed (compare Figure 2.7b). Constantly reinforced blade vibration and pre-stall disturbances triggered large blade vibration amplitudes. Their findings indicated that large blade tip deflections lead to a self-enhancing mechanism whereby the blade vibration forces a dominant vortex distance in the compressor annulus and a lock-in of the propagation speed.

Referring to the same condition, Holzinger (2017) formulates that "the blades filter the random excitation and yield the strongest vibratory response in their eigenmodes". Exactly this condition has a strong connection to the lock-in phenomenon that Kielb et al. (2003) and Besem et al. (2014) describe. It is a period of the vibration in which it is controversial whether structure or aerodynamics dominate the mechanism.

Table 2.1 sums up publicly available data on NSV. The shown publications range from the mid-1990s to the present day. NSV are still challenging and demand deeper understanding. Multi-stage investigations show that the problem occurs in front stages. So far, the influence of the tip clearance has not been investigated in detail, but it seems that the problem can occur for small and large clearance settings. A comparison of the individual publications reveals that the convective propagation speed of the phenomenon is in the range of 0.4 to 0.6 times rotor tip speed. Particularly critical is that NSV can obviously occur over wide speed ranges.

Large progress has been made in understanding NSV. However, predictions are yet not possible and the influencing factors that control the amplitudes of the observed vibrations are yet not fully understood. A variety of geometric variations and imperfections occur in aero engines. Holzinger (2017) highlighted the impact of bent leading edges and rotor orbiting. He observed higher unsteadiness in the vicinity of blades with bent leading edges, as a result of locally higher incidence. He further showed that orbiting of the rotor leads to increased vibration amplitudes of particular blades.

Still, considerable uncertainty exists regarding the amplitudes of the blade vibrations during engine development. In practice, engineers stabilize the front stages aerodynamically to avoid flow separation and by that avoid unsteady harmonic

Table 2.1: Publicly available data on NSV

Publication	Setup	Hub-to-Tip Ratio r_{hub}/r_{tip}	Tip Gap t/l	Convection Speed v_{abs}/u_{tip}	Shaft Speed Range
Baumgartner et al. (1995)	Multistage	0.5	-	0.62	90% ...95%
Kameier and Neise (1997)	Low-Speed	0.62	5.6%	0.4 ...0.45	-
Kielb et al. (2003)	Multistage	R1[a]	1.1%	0.48	≈80%[b]
Thomassin et al. (2011)	Single Stage[c]	0.5	1 and 2%	0.4 ...0.57	≈70%
Dodds and Vahdati (2014)	Multistage	R1	-	0.55	80% ...90%

[a] R1 suffered NSV. Front stages typically have hub-to-tip ratios of approx. 0.5.
[b] Assumed that max. speed is 16,000 rpm, which is typical for the high speed shaft.
[c] R1 suffered NSV in a multistage assembly and was rerun as single stage on a rig.

forces. In addition, a well established method is the application of rotor mistuning to lower the blade vibration amplitudes. An overview of these stabilizing measures is given in the following.

2.3.3 Stabilizing Measures

The transient operation of aero engines demands features to ensure their operability at all times. Countermeasures are needed to increase the part speed stability of compressor front stages. With respect to future engines with higher pressure ratios, von der Bank et al. (2016) and Day (2016) pointed out that these new systems will require more stability improvement features, such as *variable inlet guide vanes*, *compressor bleed* (i.e. inter-stage air extraction) and *rotor tip treatments*. They also concluded that more work is needed on the scheduling of variable vanes and bleed valves, particularly when operating at part speed.

Active Methods. At part speed, the front stages work with too less volume flow. By opening bleed valves in mid stages of the compressor, the through flow can be abruptly increased. This shifts the working line to higher mass flow and is a fast option to stabilize the front stages (compare Figure 2.8a).

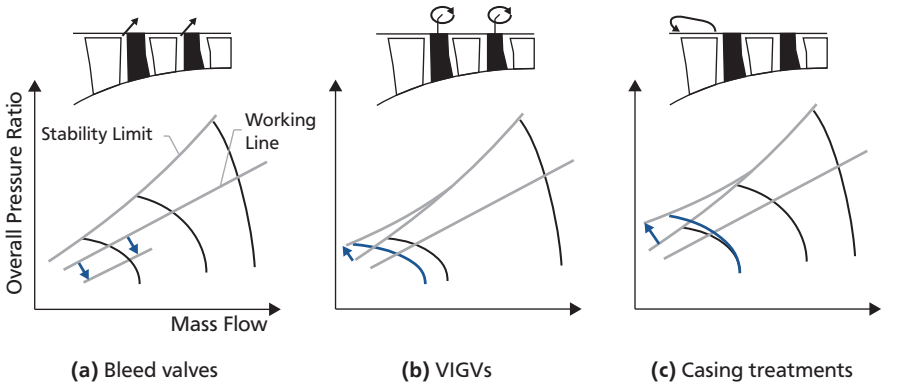

Figure 2.8: Stabilizing measures for front stages at part speed operation

By use of variable inlet guide vanes (variable IGVs), the inlet flow angles to the rotors can be adjusted individually. Altered rotor inlet angles vary the pressure rise per blade row and enable stable operation at lower mass flow (compare Figure 2.8b).

Both options are very flexible, but bleed, as well as variable guide vanes increase work on the engineering design and the effort during engine assembly.

Casing Treatments. In an engine, passive structures in the casing can increase stability and at the same time decrease the complexity compared to a smooth casing design that can not be operated without the use of active methods. These modifications of the casing geometry are called casing treatment (CT, compare Figure 2.8c). Broichhausen and Ziegler (2005) stated that by implementation of a casing treatment, engineers were able to get rid of variable guide vanes, to reduce the cost of the compressor by 3% and the compressor weight by 6%. Also a reduction of synchronous blade vibration amplitudes by a factor of 3-4 was indicated.

The idea to improve a compressor's stability by extracting air in the rear and to re-inject it in the front, was stated by Wilde (1953). This is usually referenced as the earliest record of CTs. The idea gave a push to extensive research on stall margin improvement, the cost of efficiency and understanding of the working mechanisms for numerous designs. The potential is high, but mostly, the stability improvement is accompanied by a loss of efficiency (Day, 2016).

The literature review by Hathaway (2007) emphasized the potential of this endwall technology, but highlighted that more work is needed in the field of stall inception to clearly and accurately understand the flow mechanisms with and without casing treatments.

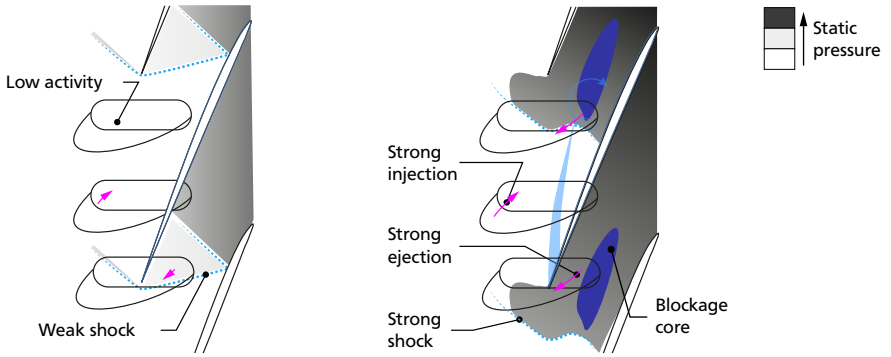

(a) Near choke **(b)** Near stability limit

Figure 2.9: Casing treatment working mechanism as a function of operating point, developed from Brandstetter (2015) and Holzinger (2017)

The geometry variations of CTs are limitless, which makes their design troublesome. Until today, there is no common base how to achieve stall margin improvement without the cost of efficiency (Rick, 2013). CFD and experimental studies are still deemed to be needed. The problem for CFD is the complex interaction of the stationary endwall with the moving rotor. The complexity of CFD meshes and the transfer of variables between different frames of reference demand new code developments.

The experimental task is equally challenging, because all blade rows (IGV, Rotor and Stator) can interact with a CT. High effort is needed to investigate the efficiency and working mechanisms of CTs as those measurements must resolve clocking effects that result from this interaction.

During his work at the Darmstadt Transonic Compressor, Brandstetter (2015) analysed the working mechanisms of modern recirculating half-heart CTs. The basic design intention of axial grooves is the removal of fluid from the blockage zone in the blade tip region. Due to the static pressure variation per blade pitch, fluid is harmonically circulated upstream and reinjected in front of the rotor leading edge. To minimize mixing loss, the reinjection of the recirculated fluid is angled. The geometry is patented by Johann and Hembera (2015).

In transonic machines there is an increased complexity, created by the interaction with shocks that occur in the vicinity of the blades. The intensity of the recirculation depends on the shock position, which is a function of the operating point (see Figure 2.9). During operation with weak upstream shocks and a strong downstream

shock, there exists only a small static pressure difference in the area of the cavities. This changes with increased back-pressure. At a certain flow topology (shock and blockage configuration), the maximum recirculation will occur. Consequently, the axial position of the cavity has a strong influence on the impact at individual operating points from choke to stall. For the design used in this work, Brandstetter (2015) showed that there is no loss of efficiency at the design point compared to the smooth casing configuration.

And there are more aerodynamic benefits. First, by reinjecting fluid upstream of the rotor, the CT compensates the total pressure deficit in the inlet boundary layer. Second, as a result of the reduced blockage relative to a smooth casing, the tip clearance vortex is stabilized by an increased mixing distance before interacting with the shock. Third, the fragmentation of tip clearance flow allows an improved mixing with the main flow.

Recent research has also revealed that the blockage reduction lowers tip flow fluctuations, which is in turn beneficial from an aeroelastic viewpoint (Möller et al., 2017, Holzinger, 2017).

However, there are known disadvantages of the half-heart CT design. For design speed, the observations of Brandstetter et al. (2016) and Holzinger (2017) highlighted difficulties at the stability limit. Resonance effects lead to large blade vibration and great concern in terms of an engine application. Yet, the part speed operation of the half-heart CT is still to discover. This is of particular interest, as the whole purpose of a CT is the increase of the front stage stability at part speed. This will be investigated as part of the current work.

Rotor Designs with Increased Stability. The measures described so far focus on compressor casing components and stator technologies. There are also numerous ideas for a rotor optimization in case of aerodynamic and aeroelastic stability.

To increase the stable operating range, the aerodynamic design trend of axial compressor rotors since the 1970s was towards *wide chord blades*. That means the blades have comparably low aspect ratio (Schäffler, 1979a, Rick, 2013).

Between 1994 and 2004, MTU aero engines continuously developed a modern transonic compressor stage at the Darmstadt Transonic Compressor. The original design, commonly referred to as Darmstadt Rotor 1, is a compressor rotor in Blisk design with transonic wide chord blading. The stage was improved, using 3D features, such as *lean*, *sweep* and *twist*. For brevity, the topic is only discussed shortly and the reader is pointed to reviews of these properties (Rick, 2013, Holzinger, 2017).

In short, it was found that forward sweep optimizes the shock position relative to the leading edge of the blade. The distance between the tip leakage vortex formation and the region of its interaction with the shock is extended. The increased gain

of main flow momentum stabilizes the vortex before it passes the shock (Kablitz, 2003). Vortex breakdown, which contributes significantly to the blockage in the tip region is delayed (compare Section 2.2.2). Aerodynamically, forward sweep was validated as a major stabilizing feature for transonic rotor designs and is current state of the art in aero engines.

To reduce the susceptibility of rotors in terms of non-synchronous blade vibration, a common tool to increase the robustness is *structural* or *aerodynamic mistuning*. The term mistuning is used for non-uniform rotor designs with blade-to-blade variations due to imperfections or disorders.

Already Whitehead (1965) stated that structural mistuning can reduce vibration amplitudes. This originally addressed imperfections and was later on understood as a suppression technique for unwanted vibration, also distinguished as random and intended mistuning (Castanier and Pierre, 2002). Random imperfections result from e.g. manufacturing or in-service damage and blade repair (Keller et al., 2017). Intended structural blade-to-blade variations address variations of the natural frequencies or mode shapes of the blades. The problem with structural mistuning is that forced response amplitudes of individual blades increase (Bendiksen, 1988). This results in an optimization task with respect to modern rotor designs (Figaschewsky et al., 2017).

Just to name a few ideas regarding aerodynamic mistuning, Hoyniak and Fleeter (1986) investigated a rotor with non-uniform spacing. They were the first to address this topic. Later on, Sladojević et al. (2007) analysed non-uniformly staggered rotor blades. The rotor used in the current work is neither aerodynamically nor structurally mistuned by intent.

In the past, the topic of mistuning has received much attention in connection with flutter, as analytical models are available that describe flutter reasonably well (Clark et al., 2005). For the mechanism leading to NSV, it remains to be specifically demonstrated that rotor mistuning can similarly contribute to the reduction of blade amplitudes.

Imperfections of the casing geometry have not been considered in research of mistuning so far, neither in the context of flutter nor in the context of NSV. The analysis of such stationary non-uniformity within the research field of mistuning in connection with NSV is one major goal of the current work.

2.4 Effect of Varying Rotor Tip Clearance

Another possibility to increase stability and efficiency of an axial compressor that appears rather simple, is to reduce blade tip clearance. However, this task is becoming increasingly difficult due to downsizing of the core in modern engines.

The application of small tip clearance is limited as thermal and centrifugal loads appear during engine operation.

2.4.1 Tip Clearance in Aero Engine Compressors

The tip clearance of aero engine compressors varies during one flight cycle and over engine life time.

The rotor speed and gas temperature of the fluid in the gas path varies, as a result of transient acceleration and deceleration of an engine. This is illustrated in Figure 2.10a. During rapid acceleration of an engine, the tip clearance varies approximately by 1 to 3% rotor chord (Cumpsty, 2004). The cause can be explained as follows.

Increased rotor speed lengthens the blades immediately and decreases the rotor tip gap. The side effect of the high speed is the heating of the rotor blades, disc and the casing. Due to the higher temperature, these parts expand. As the blades are very thin and directly exposed to the warmer fluid, they are heated up quite fast. Also, the compressor casing is thin, because of weight savings. So it takes the longest time for the rotor disc to adjust to the increased temperature. As a result, the tip clearance is largest just after the engine is accelerated to high speed.

The biggest challenge regarding the tip gap design arises during deceleration of the engine. The cooler air stream enforces a shrinkage of the casing, which is faster than the shrinkage of the rotor disc. This is the most critical time for contacts between the rotor blades and casing, i.e. *rub-ins* to occur. For that reason, abradable liner materials are used in the casing. They ensure minimal gaps, which is optimal in terms of efficiency and they prevent serious damage to the rotor.

In service, the contact of the rotor with the casing can also result from e.g. manoeuvres, non-uniform casing temperatures and blade vibration. These in-service rubs can result in an average tip clearance increase from 1.25% to 2.5% chord (see Figure 2.10b). Further examples of rub-ins were given in Chapter 1, which highlighted that the rotor tip clearance is never perfectly uniform in an engine.

For subsequent sections, it is appropriate to distinguish the effects of uniform and non-uniform rotor tip clearance.

2.4.2 Effect of Uniform Tip Clearance

Numerous attempts to quantify the influence of increased rotor tip clearance have been made in the past. Three fundamental aspects must be taken into account before further reviewing the literature.

First, the tip gap shape determines the severity of a tip clearance variation on compressor aerodynamics. For example, Freeman (1985) showed that increasing the

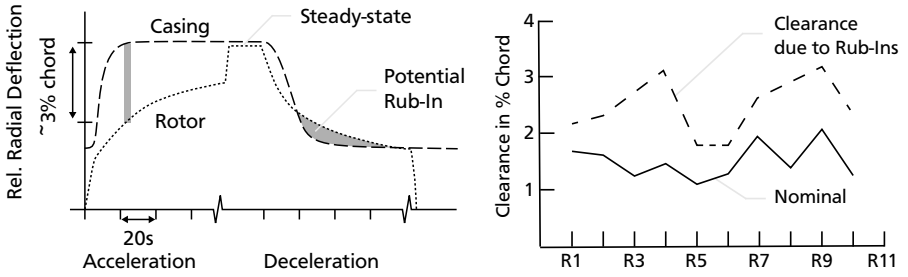

(a) Tip clearance variation in an engine compressor due to transients, developed from Hennecke (1985)

(b) Pratt & Whitney 10-stage HPC tip clearance, developed from Baghdadi (1995)

Figure 2.10: Tip clearance variation in aero engines

casing diameter is not equivalent to cropping the blades, because an increased annulus increases the capacity of the compressor. In engines, the annulus normally grows, blade crops are rather seldom (Cumpsty, 2004). Richardson et al. (1979) analysed wear mechanisms in aged engines. The efficiency penalty due to HPC liners with sharp trench dugs on the one hand and eroded trench dugs with axially smoother tip clearance transition on the other hand is different. According to Richardson et al. (1979), a sharp trench dug is only half as severe as a smoothly increased casing diameter. Research in this area is still ongoing (Thompson et al., 1998, John et al., 2017). The clearance variation of the current work is attributable to aged compressors. The axial position of the tip gap transition is representative for rub-ins. However, its edges are ground, which is only achieved by further accumulation of cycles and associated erosion in an engine (compare Figure A.1a).

Second, in literature different definitions regarding the stability limit of a compressor exist. Sometimes, this complicates comparison. For a multi-stage compressor at design speed, the stable operating range will most likely be defined by its surge margin. Also, stage-to-stage interactions are determinant (Baghdadi, 1995). A single stage compressor will most likely not surge, which is why the stable range is usually defined by its stall margin. In that case, the extension of the operating range to lower flow coefficient is sometimes stated for low speed compressors. In contrast, for high speed compressors the stall margin is defined by the relative reduction of the pressure rise and/or the mass flow (Rick, 2013).

Regarding the pressure and mass flow reduction, Cumpsty (2004) suggested the use of exit flow function to account for the loss of stability. Enlarging the tip gap

reduces the efficiency to some extend, which affects both the pressure ratio and temperature ratio of the compressor. The exit flow function

$$\mathrm{F}^{30} = \dot{m} \frac{\sqrt{c_p T_\mathrm{t}^{30}}}{p_\mathrm{t}^{30} A} \tag{2.18}$$

considers this impact, by correcting the mass flow by total pressure and temperature at stage exit. Its value is appropriate to compare the identical throttling conditions of a stage. The reduction of F^{30} is a direct indicator of the throttle area, necessary to enforce compressor stall:

$$\Delta \mathrm{SM} = \frac{\mathrm{F}_\mathrm{ref}^{30} - \mathrm{F}_\mathrm{min}^{30}}{\mathrm{F}_\mathrm{ref}^{30}} \tag{2.19}$$

This definition will be used for the current investigation in Chapter 4.

Third, it has been shown that the development of correlations for peak pressure, efficiency and stability margin - from data in open literature - is a challenging task (Reeder, 1966, McNair, 1960, Freeman, 1985, Liedtke, 2017). If data from different machines are compared with various uncontrolled parameters and influencing factors, the results scatter widely. Nevertheless, some general trends will be stated in the following.

Design Considerations. The essential aerodynamic quantities of a compressor stage are its efficiency, pressure rise and stability margin.

Regarding the *efficiency* of a compressor, Schäffler (1979a) illustrated that the sensitivity is about constant at very tight clearance (below 1% span). For that range, Sakulkaew et al. (2013) found an optimum for the sum of mixing loss due to tip leakage flow on the one hand and shear losses between the rotor tips and the casing on the other. For a low hub-to-tip ratio compressor stage, the experimental findings by Wennerstrom (1984) revealed the existence of an ideal clearance at 0.64% chord. He investigated a transonic compressor in the range between 0.42% and 0.94% chord. At larger clearance, Sakulkaew et al. (2013) observed a linear trend. For very large clearance, the sensitivity decreased (compare Figure 2.11a).

Above the unaffected values at tight clearance, different levels regarding the reduction of a compressor's efficiency exist. A huge amount of experimental data is available for low speed compressors, but data for high speed machines is limited. Moore (1982) investigated a transonic fan with a tip gap between 0.5 to 2.6% chord. The loss of efficiency depended approximately quadratic on relative clearance to chord. Hence, his findings suggested high sensitivity at tight clearance and lowered

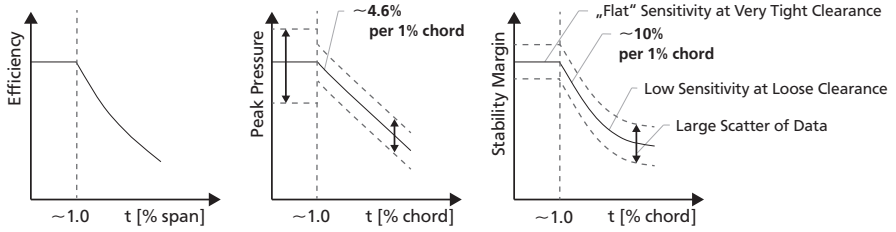

(a) Efficiency, from (Schaeffler, 1979a, Sakulkaev et al., 2013)

(b) Peak Pressure, from (Smith, 1958)

(c) Stability Margin, from (Baghdadi, 1995)

Figure 2.11: Dependency of performance and stability on rotor tip clearance

sensitivity at large clearance. The reduction was in the order of 2% points per 1% chord increase of the clearance. Freeman (1985) investigated a high speed six-stage compressor. He indicated that a 1% increase in casing diameter will give a 1.4% decrease in efficiency. In case of a three stage axial compressor, representative of HPC rear stages, the findings by Berdanier and Key (2015) suggest a linear efficiency loss in the order of 2%.

Consequently, common values for the reduction of efficiency are in the order of 1.5 to 2% per 1% chord increase in gap width.

Regarding the *peak pressure rise* of a compressor, first reviews and data correlations date back to the middle of the last century. For a clearance above 1% chord, Smith (1958) noted a correlation of the peak pressure sensitivity by 4.6% for each 1% chord. Below, the data were uncorrelated (compare Figure 2.11b). The spread of values in recent studies is large. The transonic fan investigation by Moore (1982) revealed a decrease of about 8%, whereas the multi-stage study by Berdanier and Key (2015) indicates a quite robust sensitivity of 1% reduction per 1% chord. Note that the stated compressor designs are considerably different (e.g. hub-to-tip ratio, low and high speed, single and multi-stage).

Regarding the *stability margin* of a compressor, it is evenly difficult to derive rules of thumb from the values given in literature. A convincing correlation for HPCs is presented by Baghdadi (1995). As a database, he used single stage compressors by Pratt & Whittney, GE and also low speed research compressors. The data comparison revealed that a region of zero sensitivity exists at very tight clearance. For moderate clearance in the range of 1 to 3% chord, his findings indicated an approximately linear sensitivity. A 1% chord increase, gives a decrease of the stability margin by about 10%. In case of a clearance larger than 3% chord, the tip gap sensitivity is reduced (see Figure 2.11c). Similarly, Young et al. (2016) observed a more sensi-

tive stall margin reduction at small clearance in a single stage low speed research compressor. The findings by Hewkin-Smith et al. (2017) indicated an optimum for 0.5% chord. They stated that this results from the opposing trend of casing corner separation at the blade trailing edge at tight clearance and tip leakage blockage followed by spill forward at large clearance.

The compilation shown is a striking picture of a large set of aerodynamic compressor designs and publications. It must be considered with caution, as some unrestrained design parameters (e.g. forward sweep in state-of-the-art designs) have been ignored. However, the results show that the absolute value of tip clearance is fundamental. Publications that do not state the investigated range of clearance, lack informative value.

For some machines, increasing the tip clearance led to a - at first sight - surprising increase of the stability margin. This was shown to depend on varying stall inception mechanisms at very tight clearance (McDougall et al., 1990). So also the initial radial loading distribution at a tight clearance determines the tip clearance sensitivity of a rotor design. This is discussed next.

Effect on Stall Inception. The effect of a larger tip clearance on the radial mass flow distribution and aerodynamic loading is shown in Figure 2.12. An increase of secondary flow and its associated blockage decreases the main flow in the tip region and results in a higher mass flow at the hub. Assuming constant integral inlet mass flow, this results in an increased rotor tip incidence and a lowered incidence at the hub. Consequently, the aerodynamic loading is altered radially.

If the initial radial loading of the rotor is *hub critical*, an increased clearance has a balancing effect. The design, investigated by McDougall et al. (1990) was of that type. When approaching stall, they found flow separation that at first developed at the rotor hub. By increasing the tip clearance, a rise of the blockage at the tip concentrated mass flow at the hub. This mass flow redistribution helped to prevent the rotor hub separation due to the lowered incidence in that region. The radial shift of the critical section led to a largely unaffected stability margin at medium clearance.

Front stage rotor designs are usually not hub critical. Instead, these rotors initiate stall at the tip and are consequently called *tip critical*. Stators are mostly prone to flow separation at the hub (Cumpsty, 2004). So a reduced gap in the rotor can lead to an increased risk of stator hub separation. However, this separation can be tolerated mostly. In a multi-stage assembly it can even have stabilizing effects on downstream and upstream rotors, because it discharges the rotor tip sections by shifting mass flow back from hub to tip.

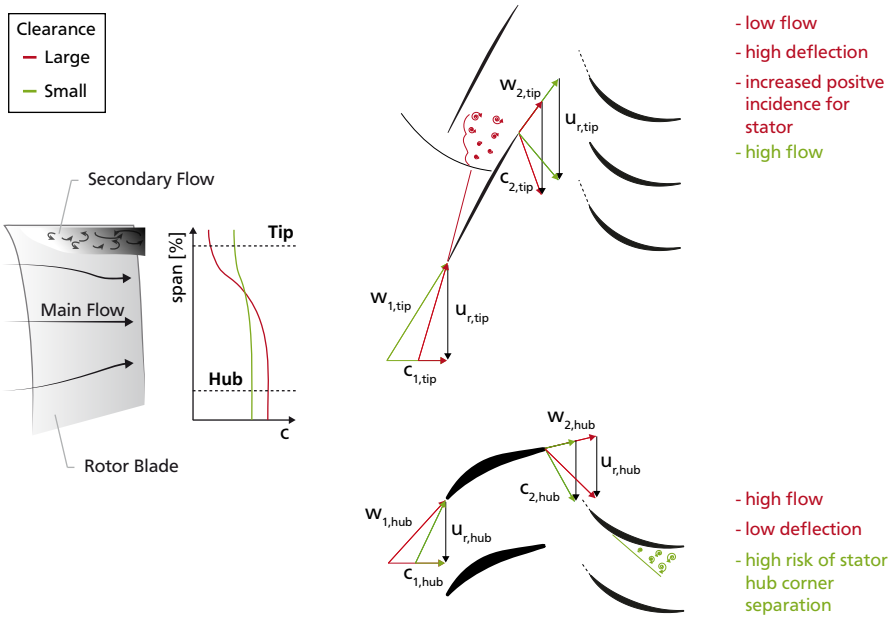

Figure 2.12: Velocity triangles at hub and tip depending on rotor clearance

Brandstetter (2015) showed that the effect of the casing treatment used for the current investigation is comparable to a tip clearance reduction. His work revealed that the lower secondary flow and blockage in the rotor tip section results in an extended compressor stability margin and increased near stall pressure rise. This and other examples point out that tip critical designs are a basic requirement for the use of the full potential of casing treatments (Greitzer et al., 1979).

Some publications on increased clearance indicate a transition from spike to modal-type stall inception. Day (1993) varied the tip clearance of a low-speed compressor with an initially tip critical blade design. He observed that the length-scale of pre-stall disturbances was long (several passages) for compressors with relatively large clearance (3% chord), whereas at 1.2% clearance, the length-scale of the cells was much shorter and restricted to the dimension of a blade passage.

Similarly, the numerical investigation by Yamada et al. (2013) revealed that the stall inception of a compressor with a clearance of 1% chord was spike-type. With increased clearance (3% chord), a rotating disturbance developed. This rotating disturbance originated from vortex breakdown and the consequently fluctuating blade

tip blockage. It led to a continuous variation of the local mass flow and incidence, which propagated in circumferential direction relative to the rotor. These disturbances were of long length-scale and occurred at the tip. At operating points that accompanied the vortex breakdown, high fluctuations were measured downstream of the rotor.

Until today, a lively discussion exists if the shift from small to large clearance alters stall inception from spike- to modal-type. Berdanier et al. (2018) questioned this general rule because their measurements, which they conducted in a low speed multi-stage compressor, indicated the opposing trend. They concluded that varying tip clearance altered the stage matching and consequently the stall inception mechanism of distinct stages.

Effect on Aeroelasticity. As tip clearance influences the stall inception process aerodynamically, associated blade vibrations, the mechanisms and their amplitudes may also change. Vo (2006) emphasized the role of tip leakage flow regarding the mechanism of NSV and triggered a subsequent study by Drolet et al. (2013). The study was carried out to correlate the convection speed of tip leakage fluid and the propagation velocity of NSV. Their findings suggested that the influence of tip clearance on NSV is significantly larger compared to other parameters such as local blade tip temperature.

The dependency of NSV on tip clearance was later confirmed by Leichtfuss (2015) in numerical studies. His work motivated experiments with varying tip clearance at the Darmstadt Transonic Compressor. Jüngst et al. (2015) and Holzinger (2017) conducted those measurements, using the rotor that is currently investigated. They analysed the stall inception process of the rotor with a concentric clearance of 1.25% as well as 2.5% tip chord. They found that pre-stall disturbances propagate largely unaffected by clearance with a speed of about 0.5 times rotor speed. However, the disturbances tended to evolve with a higher count if the clearance was large. This resulted in altered blade vibrations that switched from 1T vibrations in case of a small clearance to vibrations of the CWB mode in case of a large clearance.

Thus, the limiting phenomena of modern blade designs, which are prone to vibration, can vary from both an aerodynamic and aeroelastic perspective. For these designs, it is appropriate to use the general term *stability margin* rather than referring to the *stall margin* of these rotors. Stall margin would imply a pure aerodynamic viewpoint.

2.4.3 Effect of Non-Uniform Tip Clearance

Any non-uniformity may consist of a rotating and stationary non-uniformity (see Figure 2.13). Rotor whirl is a movement of the rotor centre around the centre of the casing. This movement can arise e.g. by a radial and tangential force on the rotor as

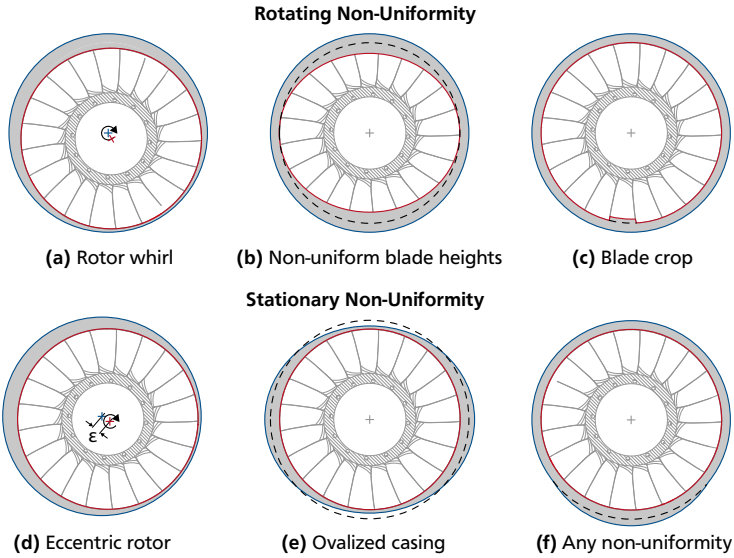

Figure 2.13: Tip clearance non-uniformity, developed from Graf et al. (1998) and Holzinger (2017)

a result of eccentricity. These destabilizing forces are called Thomas-Alford Forces, named after the first researchers who addressed this topic in Germany (Thomas, 1958) and the USA (Alford, 1965). The phenomenon was recently examined further by Gordan (1999) and Storace et al. (2001).

Manufacturing tolerances can lead to non-uniform blade heights, which vary the tip clearance of the rotor. Associated effects were elaborated by Holzinger (2017). Quite common are blade crops of one or several rotor blades. Wear mechanisms in older compressors crop the blades non-uniformly (Richardson et al., 1979). Also, blade crop can be a result of conscious trimming of the rotor blades to achieve rotor mistuning and reduce blade vibrations (Keller et al., 2017).

This thesis addresses the problem of stationary non-uniformity. Rub-ins lead to irregularities that are not necessarily eccentric or oval. Instead, any variation, which consists of higher harmonics may occur (reconsider Figure 1.3). A quantification of this non-uniformity is not easy. Ziller (2014) guessed that oval geometry variations occur in the magnitude of 0.2 to 0.3 mm, as a result of non-uniform temperature distribution of thin engine casings. Very few data is available in open literature. Young et al. (2016) stated that eccentricity in the range of 50 to 75% is quite

common for aero engines. It is common that eccentricity is expressed in percentage, defined as

$$\xi = \frac{t_{max} - t_{min}}{\bar{t}} \cdot 100\% = \frac{2\Delta\varepsilon}{\bar{t}} \cdot 100\%, \tag{2.20}$$

where t is the tip clearance and ε the rotor offset. According to this definition, the contact between the rotor and the casing would correspond to a value of 200%. In this Section, all subsequent ideas on the influence of tip clearance non-uniformity concentrate on the influence of eccentricity.

Design Considerations. Freeman (1985) established widely accepted rules of thumb for a compressor with an eccentric casing. In case of efficiency and pressure ratio, he concluded that an eccentric compressor works equivalent to a concentric one with the same average clearance. Furthermore, he stated that the largest clearance is defining the stall margin penalty. Similarly, Graf et al. (1998) stated that the stall margin of an eccentric compressor is defined by its largest tip clearance. This assumption is also mentioned in textbooks (Cumpsty, 2004, Grieb, 2009). The approach is quite simple, but was later questioned by Young et al. (2016). They found the stall margin penalty to be not as severe as described before by Freeman (1985) and Graf et al. (1998), instead about 40% smaller.

The findings by Graf et al. (1998) highlighted that the most severe aerodynamic effect - regarding a circumferential variation of pressure, efficiency and mass flow - due to non-uniform gaps was observed for eccentric tip gaps, compared to higher harmonic tip gap variations, such as ovality.

Parallel Compressor Theory and Mass Flow Redistribution. In previous studies, non-axisymmetric tip clearance has been analytically modelled. Graf et al. (1998) applied the parallel compressor theory to machines with non-uniform tip gaps. The parallel compressor model originally addressed inlet distortions and was proposed for the first time 60 years ago. Pearson and McKenzie (1959) divided a *compressor with distorted inflow* into two segments, a distorted and an undistorted sector. They assumed that no crossflow occurs between the segments and neglected inlet and exit swirl. Assuming that both sectors discharge to a large plenum with uniform static pressure, the pressure rise is non-uniform due to the reduced inlet total pressure in the distorted segment. This is illustrated in Figure 2.14a. As a result of the pressure rise non-uniformity, which determines the flow through the compressor, the mass flow must redistribute and varies circumferentially.

Plourde and Stenning (1968) found that the amount of redistribution depends on the slope of the characteristic. Compressors with a steep pressure rise redistribute less mass flow. Cumpsty (2004) noted that these compressors are advantageous in avoiding stall as they work more strongly to smooth out the flow.

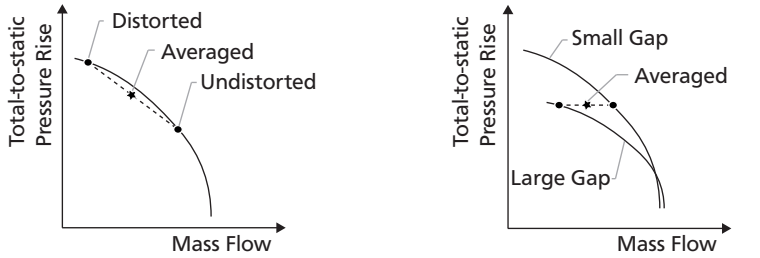

(a) Total pressure distortion **(b)** Tip clearance non-uniformity

Figure 2.14: Parallel compressor model for distorted inflow and non-uniform tip clearance, developed from Pearson and McKenzie (1959) and Graf et al. (1998)

Mazzawy (1977) revised the parallel compressor model by the application of multiple segments instead of just a distorted and an undistorted sector. At about the same time, the theory of compressors in parallel was also used to predict the characteristic of stalled compressors analytically (Day et al., 1978). This pointed towards a wide range of application for this theory.

For compressors with a *non-uniform tip clearance*, Graf et al. (1998) assumed uniform total pressure at the inlet, static pressure uniformity at the stage outlet and low Mach numbers to neglect compressibility effects (see Figure 2.14b). Depending on local tip gap, different characteristics apply for the compressor segments. As a result of the uniform total-to-static pressure rise constraint, mass flow is redistributed circumferentially.

To predict the circumferential flow redistribution of the investigated compressor, Graf et al. (1998) introduced a fluid inertia term. The expression models a circumferential offset of the maximum mass flow amplitude relative to the smallest clearance, which occurs because the fluid in the passage must adapt to the local gap. This offset was also investigated by Di Mare et al. (2009), but there is still uncertainty about the extent of this delay for different compressors and speeds. Another approach to predict mass flow redistribution was carried out by Young et al. (2016). They used a model developed by Cao et al. (2017) to investigate both, radial and circumferential flow redistribution, and thus extended the modelling of eccentric compressors to a three dimensional perspective. They were able to analyse the flow redistribution at rotor inlet and outlet over span, using a combined experimental and analytical approach in a low speed compressor. Experimental investigations of the radial and circumferential redistribution of the flow are rare. Morris et al. (2008) analysed a high hub-to-tip ratio transonic compressor. The findings sup-

ported the parallel compressor approximation, but measurements were taken at 70% corrected speed, which was subsonic at the blade tip. At transonic speed, there is no available data in open literature so far. One goal of the current study is to fill this gap.

Effect on Stall Inception. The influence of non-axisymmetric tip clearance on stall inception has been the subject of several publications. Graf et al. (1998) found that the region of maximum flow unsteadiness is consistent with the end of the large clearance sector. Morris et al. (2008) and Bennington et al. (2010) observed spike-type disturbances in the region with a large tip gap and observed their decay in the annulus when the tip gap decreased. The axial position of these disturbances was upstream of the rotor leading edge. Young et al. (2011) located the largest pre-stall disturbances shortly after the rotor leaves the largest tip gap during its rotation. The disturbances were found to propagate with about 50% of blade tip speed. They stated that similar trends apply at high speed, however, due to missing instrumentation accurate data analysis was not possible.

That the rise and decay of aerodynamic disturbances is essential for the stable operation of a compressor with a non-uniform gap was also shown by Cumpsty (1989), who applied casing treatments over some part of the circumference. It was remarkable that a configuration with two opposite quarters with casing treatments had almost the same stability limit as a setup with three quarters of the circumference treated. He concluded that the untreated sector - in both cases 90 degree smooth casing - determines stall.

From an aeroelastic point of view, the topic of non-uniform clearance has not been examined yet.

2.5 Conclusions and Scope for Present Research

Modern high-pressure compressor front stages of an aero engine work at transonic speed and are built in Blisk design with blades swept forward at the tip.

In today's engine development, there are two major challenges regarding front stages. *First*, downsizing of the core engine forces ever larger relative gaps and an increased relevance of clearance non-uniformity. *Second*, the aerodynamic and aeroelastic stability of the front stages must be ensured at part speed. To ensure this stability, casing treatments are part of the state-of-the-art design process and front stages are equipped with variable inlet guide vanes.

A rotor tip clearance between 1 and 3% chord is quite common for compressors in service. Experimental work at this level of clearance is mainly available for low speed compressors. Investigations of single front stages at transonic speed are rare. High speed data are either available at lower levels of clearance or for geometries quite different from front stages. In addition, the literature survey on eccentricity

outlined the demand for investigations in this field of research. Rough rules of thumb are used for guidance and basic models were developed at low speed only. Consequently, one aim of this study is to reveal the effects of eccentric tip clearance at transonic speed with a detail unattained so far.

There has been great progress in understanding the process of stall inception in recent years. However, since it is not yet possible to accurately predict the number of cells and their propagation speed, front stages are usually still at risk after the design phase of an engine. Additionally, stationary non-uniformity is unexplored from an aeroelastic point of view. The rotor under investigation is susceptible to NSV and can thus be used to investigate the effect of tip clearance non-uniformity on blade vibration.

Due to increased stage matching problems, future engines require more stability improvement features, such as rotor tip treatments. Recent observations at the Darmstadt Transonic Compressor highlighted difficulties at design speed with a full circumference half-heart geometry. Resonance effects led to large blade vibration and great concern in terms of an engine application. Yet, the part speed operation of the half-heart casing treatments is still to consider.

In addition to these measurements, a casing with grooves covering only 180 degree of the circumference are used as a test case. This investigation is a further case of stationary non-uniformity and closely related to the measurements with an eccentric gap. Using this application, the results of the tests with eccentric clearance can be transferred into an extended context.

The analysis of the data consists of two parts. The first part addresses design aspects due to large relative clearance and eccentricity. This section covers various issues related to the design of compressor front stages. The second part addresses aerodynamic and aeroelastic effects at the stability limit. Its aim is to analyse and quantify the effect of stationary non-uniformity on blade vibrations.

In particular, the following questions arise. They are discussed in Chapter 4 on the basis of measurement data:

I. Regarding the trend towards larger *uniform clearance*...

   i. How sensitive is a modern front stage with a common in-service clearance in terms of efficiency, pressure rise and stall margin at its design speed?

   ii. Tip clearance influences the radial loading that effects stall inception and the tip gap sensitivity of the rotor. Is the current rotor tip critical at a tight clearance?

   iii. NSV occur at several rotor speeds and for various tip gaps. There is still considerable uncertainty of the influencing factors. What are the trends at

part speed operation and how are NSV influenced by e.g. clearance, rotor speed and inlet guide vane angle?

II. Regarding the trend towards larger *eccentric clearance*...

i. How are efficiency, pressure rise and the stability margin affected by a casing offset? Do the commonly known assumptions apply to modern high speed machines?

ii. The compressor's pressure constraint at in- and outlet and the associated non-uniform blockage distribution enforce radial and circumferential flow redistribution. Previous work lacks detailed measurements at transonic speed. How is the mass flow distribution at these conditions? Is this comparable to low speed investigations?

iii. An eccentric front stage results in an inlet distortion for downstream stages in a multi-stage assembly. How much do the mass flow and pressure rise vary locally? How much do these effects decay due to mixing across a single stage?

iv. A non-uniform clearance affects stall inception. In which sectors do pre-stall disturbances occur during the stall inception process? What is their length-scale, count and speed? How is stall initiated?

v. If there is an effect on stall inception. How are NSV influenced by an eccentric clearance?

III. Regarding the future demand for *stability improving features* such as variable stationary vanes and casing treatments, particularly for part speed operation...

i. How does the scheduling of inlet guide vanes affect NSV in a 1.5 stage compressor?

ii. Casing treatments extend the aerodynamic stability of a compressor. However, do state-of-the-art casing treatments solve the problem of NSV?

iii. Are the aerodynamic effects caused by a non-uniform casing treatment similar to casing eccentricity? How is the flow redistributed?

iv. How does a non-uniform casing treatment affect stall inception and NSV?

3 Methods

This chapter describes the measurement techniques and the compressor setup used for the investigation. It contains descriptions of the test program, test design and application of the measurement technology. Possibilities and restrictions regarding the measurement task are highlighted.

3.1 The Darmstadt Transonic Compressor

Tests were carried out at the Darmstadt Transonic Compressor. The rig infrastructure was built by Schulze (1996) and has been continuously expanded and developed since then. Figure 3.1 illustrates the laboratory. The facility comprises an inlet throttle in the intake (not used for the current dataset). By adjusting the pressure level, it enables Reynolds number variations and also a reduction of the power consumption that can be necessary on hot days if the maximum capacity of 800 kW electrical power is exceeded. The rig is operated in an open cycle. The flow is sucked in from ambience, is guided through the inlet throttle and settling chamber and accelerated through a nozzle in the intake. The nozzle is calibrated and used for mass flow measurements. Afterwards, the air enters the test compressor and is then guided back into ambience. A gearbox transmits the DC-Drive outlet shaft speed up to a maximum speed of 20,500 rpm. As a result, blade tip speeds above

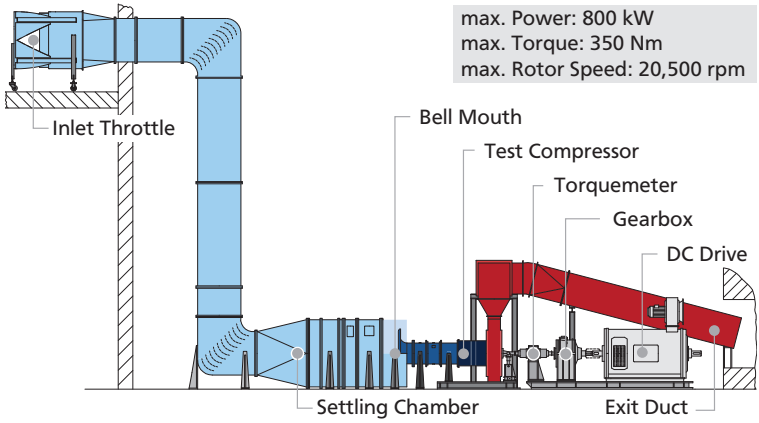

Figure 3.1: Darmstadt Transonic Compressor test rig, developed from Wartzek (2017)

the speed of sound can be reached. The rotor speed and shaft torque are measured via a torquemeter and determine the input power to the rig.

3.2 Tested Compressor Stage

For the current investigation a stage design was used, which was first commissioned by Biela (2012). It is illustrated in Figure 3.2. The inlet guide vanes and the rotor have remained unchanged since then, only the stator geometry separates the current from previous investigations with this setup (Biela, 2012, Brandstetter, 2015, Holzinger, 2017).

The rotor design is suitable for achieving the objectives developed in Chapter 2. Recent investigations have revealed that the design intent of Rotor 5 is tip critical (Streit, 2014). Its stable operating range was extended by application of a half-heart casing treatment (Brandstetter, 2015) and previous studies showed that the rotor is vulnerable in terms of NSV (Jüngst et al., 2015, Holzinger, 2017, Brandstetter et al., 2018).

The stage is representative of a front stage. At the blade tip, the inlet Mach number at design speed is above speed of sound (compare Figure 2.2). Also the Blisk design of the rotor, its hub-to-tip ratio of about 0.5 and the implementation of IGVs is typical for front stages of aero engines. The variable IGV allows operating point adjustments in accordance to typical schedules of modern aero engines.

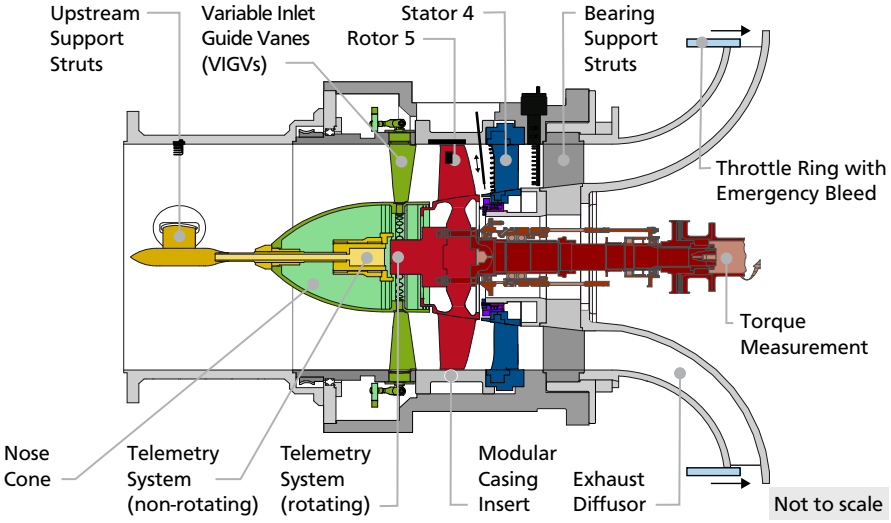

Figure 3.2: Cross section of test compressor, developed from Biela (2012), Holzinger (2017)

To achieve a typical stator flow, stator hub leakage must be set exactly. For that purpose, a labyrinth seal at the stator hub permits a defined leakage flow comparable to that in an engine. For the current work, a gap width of 0.35 mm is applied.

Three support struts in the intake are used for the cable bushing of the telemetry signal, which transfers data from the rotor blades to the non-rotating system.

Five support struts in the outlet pass the bearing force and the aerodynamic forces, which work on the radial exhaust diffuser, to the test bed.

For experiments at the stability limit of the compressor stage, a throttle ring with emergency bleed is used. The ring is adjusted in axial direction to open and close the exit flow area of the compressor. Just as bleed valves in aero engines, the emergency bleed can be opened immediately to shift the working line of the compressor to higher mass flow if the stage is operating unstable.

The compressor casing is designed to allow the integration of different casing diameters and treatments via modular inserts.

3.3 Tested Casing Settings

With regard to the resources available, an acceptable number of configurations is chosen. At the same time, a minimum number is required to answer the questions

Table 3.1: Tested casing settings

	Concentric (CON)			Eccentric (ECC)		Casing Treatment (CT)	
	MIN	NOM	MAX	MIN	MAX	360	180
Average Clearance[a] t/l	0.90%	**1.25%**	2.50%	**1.25%**	1.70%	**1.25%**	**1.25%**
Min. Clearance t_{min}/l	**0.90%**	1.25%	2.50%	**0.90%**	**0.90%**		
Max. Clearance t_{max}/l	0.90%	1.25%	**2.50%**	1.60%	**2.50%**		
Eccentricity ξ				60%	96%		
Circ. Extent of CTs		0°				360°	180°
Color Code							
Pictogram							

[a] For settings with casing treatment, the average clearance indicates the smooth casing reference without half-heart grooves.

stated in Chapter 2. Table 3.1 provides an overview of the tested settings. Equal properties are indicated in bold and highlight possible cross-comparison.

In an aero engine, the level of tip clearance is typically between 1% to 3% chord (Baghdadi, 1995, Cumpsty, 2004). Below 1% chord, efficiency and stability margin remain about constant (compare Figure 2.11). The concentric configurations cover the range that is relevant to an engine (CON = 0.9% to 2.5% clearance). In this range - according to the literature study - the influence of a gap width variation is greatest and approximately linear.

Eccentricity of up to 100% is quite common (200% correspond to a contact of the blades with the casing). Two settings with small and large eccentric clearance are designed (ECC = 60% and 96% eccentricity). They match certain geometric commonalities with the concentric setups.

For both eccentric configurations, the rotor passes CON-MIN in the sector with a small clearance. In case of ECC-MIN, the average clearance (1.25% chord) is similar to the nominal reference CON-NOM. This allows statements on the influence of eccentricity at constant average clearance. In case of ECC-MAX, the maximum and minimum clearance are equal to CON-MIN and CON-MAX, with the average clearance increased compared to CON-NOM.

Future engines will require more stability improving features, such as rotor tip treatments. Brandstetter et al. (2015) and Holzinger (2017) already investigated a half-heart casing treatment on the current rotor. Within the present work, this setting is named CT360. The current work examines its applicability for various part speeds and IGV settings. In a second step, a non-uniform casing treatment that consists of 180° smooth casing and 180° treated with axial grooves is analysed. This partial casing treatment is named CT180. As the wavelength of the variation is equal to the compressor circumference, this geometry is comparable to a tip clearance variation by eccentricity. Using this special application the results of the eccentric designs can be transferred into an extended context.

Real depictions of the implementation of the non-uniform casing designs can be found in the Appendix in Figure A.1.

The behaviour of the compressor stage changes due to the use of different casing inserts. Aerodynamically, altered tip clearance flow influences the pressure rise and efficiency of the stage. In addition, circumferential non-uniformity can cause synchronous vibrations of fundamental blade modes. At the stability limit, the limiting phenomena for all measurement speeds must be analysed, since the behaviour with respect to non-synchronous vibrations can also differ considerably. Therefore, the compressor was re-commissioned for each configuration. Only after completion

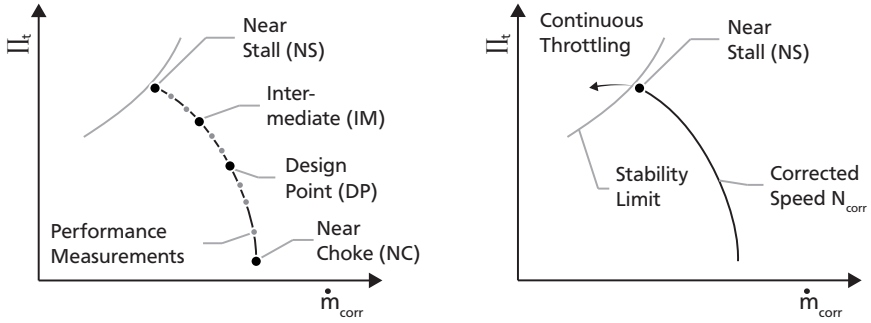

(a) Steady Compressor Operation **(b)** Unsteady Compressor Operation

Figure 3.3: Measurement procedures at the compressor rig

of these analyses the compressor stage was approved and further investigated via performance and probe measurements.

3.4 Measurement Procedures and Technology

The measurement procedures are subdivided into two major categories according to the operating behaviour of the compressor.

For performance and probe measurements, the compressor is stabilized at constant corrected speed (see Figure 3.3a). Various throttling conditions are adjusted using the exit throttle introduced in Figure 3.2. In terms of the measurement accuracy, stationary conditions must prevail during these tests. This is achieved by taking the measurements from choke to stall (cold to hot) and by measuring the casing temperature to ensure its uniformity. Before the tests, the compressor is operated for at least half an hour at steady-state to allow the entire rig to heat up completely.

A compressor characteristic is typically resolved by about 10 performance measurements from near choke (NC) to near stall (NS). In case of measurements with traversable probes, the time required for a single measurement is higher. As a result, probe measurements are taken at three conditions of the characteristic, at the design point (DP), an intermediate throttling point (IM) and near stall (NS). Similarly, configurations with non-uniform clearance increase the time effort per measurement. Therefore, a compromise between the resolution of the characteristic and the total measurement time is needed.

During commissioning and in order to analyse the stall inception process of the compressor, the stage is continuously throttled while rotor speed is kept constant. At the beginning of these measurements, the compressor is operating stable at NS (see Figure 3.3b). If rotating stall occurs or blade vibration limits are exceeded

during the throttling process, the emergency bleed of the throttle ring is opened immediately. Because the outlet area is abruptly increased, the rotor inlet mass flow increases, which helps the blades to recover from stall and lowers blade vibration amplitudes.

In the following, the term *near stall* will refer to steady operating conditions, which are stable to enable performance or probe measurements. The term *stall inception* will be used for the transient process during which the compressor is shifting from stable to unstable operation. The term *rotating stall* is used for unstable conditions, which accompany an abrupt pressure drop of the characteristic and demand an opening of the outlet throttle.

For the sake of brevity, not all details regarding the measurement techniques can be presented in the following. Instead, the information is organized in a way that allows the interpretation of the results presented in Chapter 4. In order to carry out the measurements in the same way presented, further literature regarding probe calibration, data acquisition and post-processing is needed. For this purpose, students' work in the framework of the current thesis is cited[1].

3.4.1 Measurement Techniques for Steady Compressor Operation

The aerodynamic steady-state quantities are recorded at several stations in the in- and outlet. Figure 3.4 illustrates the assigned labels.

Assignment of Measurement Stations. Station ⓪⓪ denotes the measurement of ambient conditions, such as the barometric pressure. At Station ⓪①, humidity measurements are taken in the inlet duct to correct the gas properties according to wet air. In the settling chamber, probes at Station ⓪③ monitor dirt contamination of the screens. This needs assessment at any time, as they condition the inflow and hence a need for monitoring.

Directly upstream of the inlet nozzle, at Station ⓪④, the inlet total pressure and temperature to the rig are measured. According to the nomenclature of this thesis, these quantities are denoted as p_{t}^{04} and T_{t}^{04}. Assuming negligible flow velocity in the settling chamber, these are also the static values upstream the nozzle. From Station ⓪④ to ⑩, the flow is accelerated through the calibrated nozzle in the intake. Accordingly, static wall pressure tappings at Station ⑩ allow mass flow measurements.

A boundary layer rake at Station ⑫, just upstream of the stage accounts for pressure losses in the inflow to the compressor. To determine the reference inlet pressure, a radial profile is calculated using this boundary layer rake and the total pressure in the settling chamber, which is assumed constant in the centre of the

[1] Cited students' work: Kunkel (2013), Jüngst (2014), Bopp (2015), Hormel (2015), Friedrich (2015), Liedtke (2016, 2017)

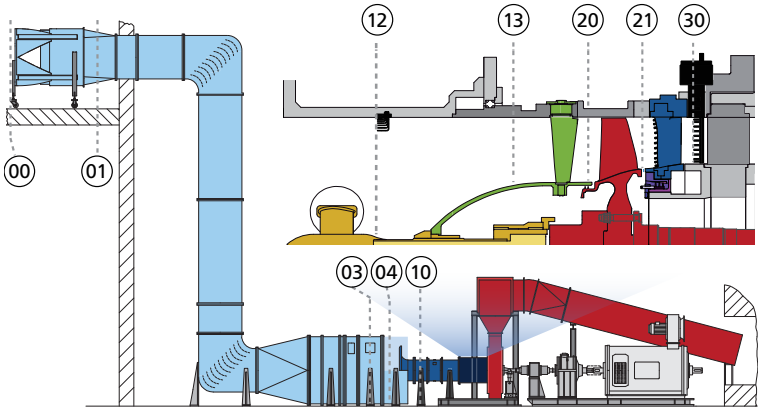

Figure 3.4: Assignment of measurement stations

duct (turbulent boundary layer in the inlet duct). The integral reference value is determined via area average. Measurements of the static pressure p_s^{13} at Station ⑬, directly upstream of the IGV, complement the measurements in the inlet. All measured and derived quantities at the inlet of the stage are summed up in Table A.1. The measurement stations are displayed via nomenclature, as exemplary shown above for Station 13.

The rakes and probes that are used for aerodynamic measurements are illustrated in Figure 3.5. The small size of the boundary layer rake reduces inlet disturbances to the stage to a minimum.

At the exit of the stage (i.e. Station ㉚), total temperature and total pressure rakes are equipped with Kiel heads. The Kiel heads increase the independence of the measurements in terms of the flow angle relative to the probe. The nominal configuration of the rakes was designed and calibrated by Kunkel (2013) at the Institute of Gas Turbines and Aerospace Propulsion. During the current work, they were further improved by Bopp (2015). He developed rakes to measure total temperature and pressure via a single Kiel head probe.

The closest probe position of the exit rakes to the wall is 3.5 mm. Hence, there is a need to extrapolate the measurements to the wall. Uncertainty can result from these assumptions (Cumpsty and Horlock, 2006). Therefore, the assumptions are noted shortly and are kept constant for all stated results. The total pressure is approximated via a turbulent boundary layer assumption in accordance with Spurk

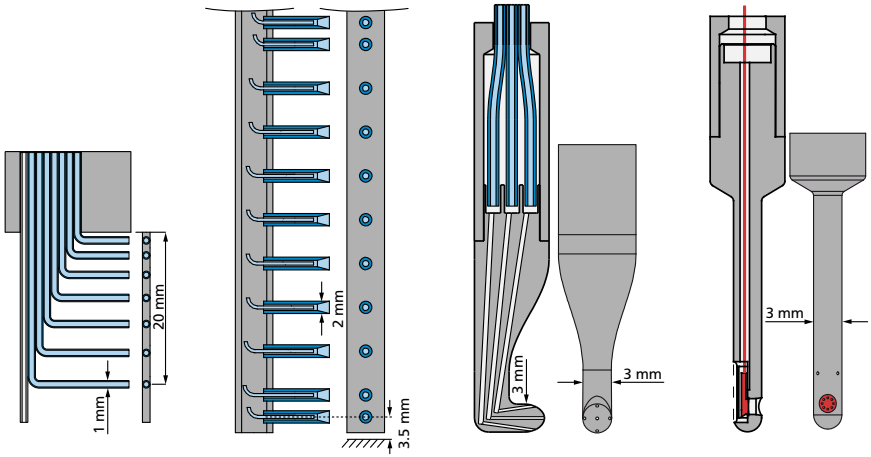

(a) Boundary Layer Rake **(b)** Kiel Head Rake **(c)** Five Hole Probe **(d)** Unsteady Pressure Probe

Figure 3.5: Rakes and probes for measurements at rotor and stator exit (scaling of probes varies), developed from Wartzek (2017)

and Aksel (2010)[2]. For this extrapolation, the dynamic pressure in the boundary layer is approximated, which is determined via static wall pressure measurements and the total pressure values obtained from the rakes. As the static wall temperature is not directly measured, the temperature boundary layer is neglected[3] and simply assumed constant from the probe position to the wall.

Instrumented stator leading edges measure total temperature and total pressure at the rotor exit (i.e. Station ㉑). In addition, a five hole probe and an unsteady pressure probe provide further insight. Their geometry is visualized in Figure 3.5c and d. Both probes were calibrated and aligned to zero flow angle in a calibration channel at the Institute of Gas Turbines and Aerospace Propulsion. During operation, the lateral holes of the five hole probe are continuously checked. According to their pressure difference, the probe is corrected to zero flow angle in order to minimize measurement errors.

[2] See pp. 475: Power law to the order of seven, valid in the range of Reynolds numbers present in the rig.

[3] For ideal gas, the Prandtl number is about one. So in fact, the thickness of the temperature boundary layer is similar to the fluid boundary layer (Spurk and Aksel, 2010).

Unsteady Pressure Probe. The unsteady pressure probe analyses rotor relative effects. It is equipped with an absolute pressure transducer LQ-062-25 from Kulite that is recorded with 500 kHz. At design speed, this results in about 75 values per blade passage. As a requirement for the frequency resolution, recording the 3rd harmonic blade passing frequency without interference is necessary. The maximum speed of the test rig is 20,500 rpm. Assuming a blade count of 20, the 3rd blade passing frequency is at maximum 20.5 kHz.

Using a shock tube, the natural frequency of the probe's inlet cavity and sensor was determined. The resonance of the cavity is broadband with a maximum at about 40 kHz. Therefore, a low-pass filter at 23 kHz clears the signal of the high frequent cavity resonance. The influence of the cavity on amplitudes below 20 kHz is compensated by an amplitude correction function. Accordingly, the dynamics of the sensor signal is sufficient to resolve the 3rd blade passing.

The unsteady pressure transducer is recorded over 2 seconds at each radial position. At maximum speed, this results in over 600 recorded revolutions. Thus, the data can be averaged in order to obtain independent values for the average pressure and standard deviation. The averaged pressure $\overline{p}$ at each rotor relative measurement position determined by angle θ and radius r, is calculated according to

$$\overline{p}(\theta, r) = \frac{1}{N} \sum_{n=1}^{N} p_n(\theta, r), \tag{3.1}$$

where p_n is the measured pressure during revolution n. N is the discrete number of measured revolutions. To derive a measure of the unsteadiness of the flow, the standard deviation of the pressure signal is used. This is generally referred to as the square root of the variance. If the standard deviation is related to the average value, the relative standard deviation is obtained. For a discrete number of measured values it is calculated via

$$\sigma_{\mathrm{rel}}(\theta, r) = \frac{1}{\overline{p}(\theta, r)} \sqrt{\frac{1}{N-1} \sum_{n=1}^{N} [p_n(\theta, r) - \overline{p}(\theta, r)]^2} \tag{3.2}$$

The circumferential distribution of all probes and rakes is illustrated in Figure A.3 in the Appendix. Accompanying, Table A.2 explains, which values are measured directly, which are derived and which assumptions are made for their calculation.

Averaging and Measurement of Flow Non-uniformity. All quantities at stator exit ㉚ are weighted according to the local mass flow. The only exceptions are static pressure and mass flow density, which are area related by laws of physics. Further guidance on the proper choice of averaging non-uniform flow are discussed in Cumpsty and Horlock (2006).

As static pressure measurements at Station ㉑ were not possible at the hub, quantities at rotor exit are area averaged. Five-hole probe measurements, which provide the static pressure values are carried out at limited operating points only.

The instrumentation at the stator exit and the probes at the rotor exit are circumferentially fixed in the casing. To account for the influence of stationary blade rows, these are traversable by one pitch and can be moved past the rakes. One passage is measured in ten steps. To calculate the averaged quantities for the concentric settings, the flow is assumed to be periodic by one pitch and thus representative for the entire exit surface.

For the measurements with a non-uniform casing, the assumption that the flow at the stator exit is periodic by one pitch and representative for the entire exit surface is not valid. Therefore, the rotor casing insert is traversable by 360°. This results in high effort and time consuming measurements that endured more than one hour per operating point. The measurement procedure is as follows.

First, the casing insert is positioned at a relative position to the stationary vanes. Both are traversed in ten steps by one pitch. Then the stator vanes are moved back to their original position. Afterwards, the casing and stationary vanes are traversed again. In this way, the relative positions of the casing to the probes is varied, while the relative position of the casing to the vanes is kept constant. As the insert is rotating stepwise one full turn, the non-uniformity is measured via all probes in a segment of 360 degree. Further illustration of the measurement procedure and post-processing routines regarding non-uniform rotor casings were documented by Liedtke (2017).

Probe measurements are taken at eight - evenly distributed - casing angles at the rotor exit. The dynamics of the five hole probe measurements is low. Rotor relative effects are averaged as a result of the measurement technique. The data therefore represent a rotor averaged radial distribution for a certain angle relative to the non-uniform casing. The data of the unsteady pressure probe are also measured at eight casing relative angles. The probe resolves rotor relative effects. For the purpose of visualization the eight rotor relative images are superimposed during post-processing (for further details refer to Liedtke (2017)). This permits a 360° illustration of the rotor exit flow in an eccentric casing.

The mounting of all probes, rakes and the traversable casing are documented in Figure A.1 and Figure A.2.

3.4.2 Measurement Techniques for Unsteady Compressor Operation

During stall inception, transient phenomena of time scales in the order of micro seconds do occur. Based on previous work, it is possible to select optimized sensor positions (Biela, 2012, Brandstetter, 2015, Holzinger, 2017). The rotor section is equipped with unsteady measurement technology to record all quantities that allow a full analysis of the stall inception mechanism. To do this, it is necessary to monitor both the flow conditions at the rotor blade tips and the blade vibrations. Unsteady wall pressure transducers, rotor mounted strain gauges and capacitive probes are used.

Unsteady Wall Pressure Transducers. The casing inserts are instrumented with up to 72 simultaneously recorded wall pressure transducers of type Kulite XCS-062. The natural frequency of the sensor membrane is above 100 kHz. Every single transducer is sampled with 500 kHz according to three reasons. First, the sampling rate must be set at least twice as high as the natural frequency of the sensor because no analog signal filter is used. Additionally, these sensors resolve up to the 4th harmonic of the blade passing frequency. A low-pass filter at 30 kHz clears the signal of noise. Despite the high rotational speeds, this sampling rate also allows to record about 75 values per blade passage at design conditions.

The wall pressure transducers are distributed in axial and circumferential arrays (see Figure 3.6). There are two types of axial distributions. The first one is a complete axial array and the second one consists of two sensors only. The full axial array analyses the complete pressure field at the blade tip as the rotor moves past the sensors. The axial separation is about 8% axial blade chord. The circumferentially distributed sensors evaluate aerodynamic phenomena that propagate in the duct. Based on previous knowledge, these transducers are located 8% downstream of the LE as well as the TE.

The sensor distribution shown in Figure 3.6 is exemplary and represents the reference configuration CON-NOM. For the sake of brevity, a detailed description of all sensor positions for all configurations is not shown. Put simply, for uniform tip clearance settings, the choice is one axial array and several very closely spaced circumferentially distributed sensors.

For settings with eccentric clearance, several evenly distributed axial arrays are used. In this case, a tight circumferential distribution is not used. As the axial design space is more limited due to the traversing unit for non-uniform designs, probes are not put into effect at the blade TE. Hence, for non-uniform settings, the axial pressure distribution is only resolved up to about 70% of the axial chord length.

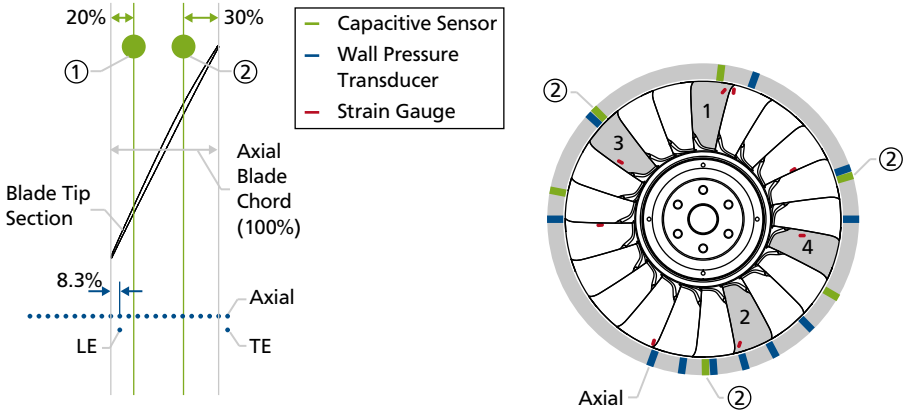

(a) Axial probe positioning

(b) Circumferential probe positioning

Figure 3.6: Axial and circumferential probe positioning of unsteady instrumentation, developed from Holzinger (2017)

In Chapter 4, the definition of the total-to-static pressure rise coefficient normalizes the wall pressure p_s:

$$\Psi_{\mathrm{t-s}} = \frac{p_s - p_t^{04}}{0.5\rho^{04}u_{\mathrm{tip}}^2} = \frac{p_s - p_t^{04}}{0.5\rho^{04}\left(2\pi r_{\mathrm{tip}}\frac{N_r}{60}\right)^2}, \tag{3.3}$$

In addition to the mechanical rotor speed N_r, the total pressure and temperature, measured in the settling chamber at Station ⑭ are used for the normalization. In this form, the pressure rise across the rotor and averaged wall pressure data are presented.

In order to illustrate non-synchronous pressure deviations from the average pressure signal, the ensemble average of 30 revolutions prior to revolution n is subtracted from the signal. So, the pressure variation during revolution n at axial coordinate x and pseudo-spatial angle θ (i.e. sample per revolution) is determined via

$$p_{\mathrm{s,var}}(x,\theta,n) = p_{\mathrm{s}}(x,\theta,n) - \frac{1}{30}\sum_{m=1}^{30} p_{\mathrm{s}}(x,\theta,n-m) \tag{3.4}$$

Similarly, this was used before by Young et al. (2011) and Brandstetter et al. (2018) because it achieves a higher resolution over time in comparison to Equation 3.2.

Strain Gauges. Blade vibrations are monitored via blade mounted strain gauges and additionally in the casing via capacitive tip timing probes. The strain gauges monitor different modes. For this purpose, they are placed mode optimized on various blade positions. Figure 3.6b illustrates the probe positions at midspan and at the LE and TE of the blade's tip. The vibration amplitudes vary between the blades, which is why it is necessary to monitor several blades simultaneously. For example, to monitor the 1T blade mode, four different strain gauges on four different blades are used. These blades are highlighted in Figure 3.6b. Via the presented distribution, a monitoring of modes up to an order of 25 is possible. Strain gauge data are recorded at 100 kHz. For post-processing of the strain gauge data, the spectra are calculated with a FFT block size of 12792. This is a compromise between time and frequency resolution. The choice of the window size influences the computation of the maximum amplitude in a time frame, which is called spectral leakage. This effect is reduced by using e.g. a Hanning window, but cannot be completely avoided. As a result, comparisons of different measurements can be affected by an additional post-processing error. To eliminate this error, the window size and window function for the strain gauge data is kept constant throughout this thesis.

Throughout this thesis, the measured strain of each mode is referred to the high cycle fatigue (HCF) limit of the rotor blades. Due to safety issues, the rig operating limit (OL) is 0.8 times the HCF limit.

Blade Tip Timing. A big advantage of the tip timing system compared to strain gauges is the contactless measurement of the blade tip deflection plus the supervision of all blades. Also, the data storage requirement is comparably small. On this account, tip timing data is always recorded for documentation purposes during critical operation and supplements the strain gauge instrumentation. The disadvantage of the capacitive measurement system is the limited frequency resolution given by the blade passing frequency[4]. This results in an aliasing of the measured frequencies that cannot be avoided. For further reading regarding the measurement system refer to Zielinski and Ziller (2000), Zielinski and Ziller (2005) and Jüngst (2014). The higher complexity during data analysis, compared to the strain gauges, is why the data evaluation routines can be programmed far less automated. So, in the scope of this work, the data of the strain gauges is used for post-processing. Still, the tip timing is of great value for online-monitoring. To monitor different modes, the capacitive probes must be positioned in several axial planes, because the sensors measure the blades' time of arrival, i.e. the blade tip deflection, which varies axially for different modes. The blade LE and TE are suitable, because the blade deflection of the fundamental modes is large (compare Figure 2.6a). As shown in Figure 3.6a,

[4] This is true for single blade spectra only. Via advanced methods, this disadvantage is outweighed.

two axial planes are used in the present case. In the future, the monitoring of higher modes can be improved by additional axial measurement positions.

Blade Tip Clearance. At axial position ②, the variation of the blade thickness in axial direction is smallest. In order to measure tip clearance with the capacitive probes, this is beneficial. During calibration, at each axial sensor position, the tip clearance is assigned to the measured voltage. A change in thickness changes the measured voltage. At position ②, an axial offset of the assembly does affect the tip clearance calibration least. Consequently, these sensors are separated by about 120° and analyse tip clearance and eccentricity.

For details on the tip clearance calibration and post-processing of the capacitive probes refer to Jüngst (2014), Friedrich (2015) and Liedtke (2016).

3.5 Adjustment Accuracy of the Tip Clearance

The individual configurations are designed with a tip clearance that varies in the order of 0.1 mm. Hence, the design and assembly must be adjusted precisely. Throughout the test, tip clearance was online-monitored to permanently check whether the design intent is maintained.

At design point, the level of tip clearance and eccentricity corresponded to the designed objective. As a result of varying temperature, the concentric tip gaps varied in small extent between NC and NS by about $\Delta t/l = 0.1\%$ (t is the tip clearance and l the rotor tip chord length). Assuming an uniform temperature distribution of the casing and the rotor, the variation of tip clearance can also be estimated based on the measured temperature difference between NC and NS and the thermal expansion of the modular casing insert (aluminium) and the rotor (titanium):

$$\Delta t/l = r_{\text{tip}}(\alpha_{\text{Al}} - \alpha_{\text{Ti}})\Delta T/l = 0.125\% \tag{3.5}$$

This calculation fits well to the measured data. The estimation is slightly higher.

For the concentric settings, the level of eccentricity ranged below 8% between the DP and NS. In case of the non-uniform designs (ECC-MIN, ECC-MAX and CT180), the level of eccentricity (60, 96% and 0%, respectively) did not vary more than ±2%. The deviations in eccentricity are most likely attributable to the temperature influence on the tolerances and bearings in the casing. Further illustration of the measured tip clearance and temperature variation can be found in Liedtke (2017).

3.6 Evaluation of Measurement Accuracy

The tip clearance of the individual configurations, varies between 0.90% and 2.50% rotor tip chord. For this tip clearance range, the expected variation of efficiency, pressure ratio and stability margin can be determined from literature (refer to

Table 3.2: Expected deviation compared to rig measurement accuracy

	Literature Values for t/l Variation between 0.9 and 2.5%	Pre-Test Error Analysis (Hormel, 2015)	Post-Test Error Analysis (Biela, 2012)
Efficiency	2 ... 3%	0.28%	0.75%
Pressure Ratio	7.2%	0.06%	0.1%
Stability Margin	16%		
Mass Flow		0.22%	0.12%

Section 2.4.2). The estimate is presented in Table 3.2. These values must be assessed regarding the measurement accuracy of the rig. The exact determination of the measurement error of a test rig such as the one used is demanding. However, there is a need to estimate the order of magnitude for which deviations are considered significant.

Measurement errors are divided into bias and precision errors. The bias error is the deviation of the measured value from the real value. The precision error is an additional random deviation. Measurements with a high precision error can indicate the correct value if a large number of measurements is averaged. The bias error can only be determined if the real value is known. As this real value is mostly unknown in practice, the bias error can only ever be defined in comparison to a standard reference.

For the current measurements, several configurations are compared *back-to-back*, so the precision error is decisive (assuming the bias to be constant). An uncertainty analysis for rigs like the Darmstadt Transonic Compressor consists of two steps. First, an estimation prior to the testing and second, a post-test evaluation (Saravanamuttoo, 1990).

Hormel (2015) ran a Monte Carlo Simulation prior to the current tests. This method uses the deviation of the measured quantities as input. Via a large number of computations, the expected deviation of the output variables is estimated. His predictions are stated in Table 3.2. A post-test evaluation was done by Biela (2012), who estimated the precision error from a large number of rig measurements at similar conditions. His results are also shown in Table 3.2.

In accordance to both estimates, the accuracy of the pressure ratio and the mass flow measurement, which is decisive to determine the stability margin, are more than one order of magnitude higher than the expected deviation, estimated from literature. However, the accuracy of the efficiency measurement is less than one order of magnitude compared to the expected values. Thus, the quality and reproducibility of the measurements must be addressed by repetitions of the measurements. The

procedure is advisable not only for performance measurements, but also for probe measurements and regarding the circumferential variations in mass flow, pressure and temperature, which occur during measurements with non-uniform tip clearance. The repeated measurements are indicated separately in the crucial sections of this thesis. For further reading on the error of probe measurements refer to Hormel (2015) and Liedtke (2017).

Inflow Homogeneity. In order to achieve a high measurement accuracy of the test rig, the homogeneity of the flow in the intake must be guaranteed. For this reason, inlet pressure and temperature were measured across the entire inlet surface via a traversed inlet rake.

Beyond the duct boundary layer, the circumferential pressure variation is less than ±1% of the dynamic inlet pressure. However, the total pressure decreases towards the centre of the channel and varies over the radial height by less than ±2.5%. Absolute values are in the order of 150 Pa.

Since the inlet traversing unit was not available until after the measurement campaign, the measurements check the homogeneity post-test. The above stated level of radial and circumferential homogeneity is sufficient. However, further improvements can be achieved by re-evaluating the integration of the screens in the settling chamber in the future. Total pressure deviations across the radial height could result from pressure losses across the screens, which are placed close to the inlet nozzle due to geometric constraints.

4 Results

This chapter presents the results of the experimental work and is divided into two parts.

The first part addresses design aspects due to large relative clearance and eccentricity. These sections cover issues related to the aerodynamics of axial compressor front stages. The analysis is carried out at design speed.

The second part addresses aerodynamic and aeroelastic aspects at the stability limit. Its aim is to analyse and quantify the effect of stationary non-uniformity on blade vibrations. The investigation is first carried out at design speed for two setups with the same average clearance and an operating point of equivalent mass flow and pressure rise. Then, the findings are continuously generalized via a segmental casing treatment that is examined at design conditions and for various conditions at part speed.

Some of the results that are discussed within this Chapter were published within the framework of two technical conferences (Jüngst et al., 2018a,b). In addition, the research into the application of a segmental casing treatment led to the filing of a patent application in cooperation with Rolls Royce Deutschland Ltd & Co KG (Giersch et al., 2018).

4.1 Effect of Tip Clearance and Eccentricity at Design Speed

4.1.1 Effect on Compressor Performance

First, the precision of the performance measurements is addressed. Also, the measurements reveal the impact of uniform tip clearance variation on the performance of the compressor stage.

Figure 4.1 illustrates three redundant measurements of the nominal setting (CON-NOM) in comparison to the settings with a large and small clearance. Mass flow, pressure rise and efficiency are referenced to the design point (DP) of the nominal clearance.

All configurations were measured within a period of one year. Measurements with the CON-NOM configuration were repeated before and after this period of time. The precision of the pressure rise and the efficiency measurements of the stage is high. The measured deviations are within the estimated errors stated in Chapter 3. The deviation is significantly smaller than the differences between the casing designs.

As the tip clearance is increased from CON-MIN to CON-MAX, peak pressure rise, stability margin and stage efficiency are continuously reduced. This indicates a tip critical design at tight clearance and is in contrast to compressors that were designed

hub critical in their initial configuration (compare Section 2.4.2). At near stall (NS), the slope of the characteristic is negative and the highest pressure rise is achieved.

The measurements at near choke (NC) indicate that the stage is choking in the rotor. A larger rotor tip clearance leads to higher mass flow. This is the result of an increased rotor capacity. The maximum mass flow rate of the nominal design CON-NOM is consistent for the repeated measurements. However, it appears that the NC pressure rise increases steadily with the progress of the tests. This is most likely the result of a contamination of the inlet screens that causes losses in the inlet to increase continuously.

A common measure of the stability margin of a compressor is based on exit flow function (reconsider Equation 2.19). This definition is used in Figure 4.2a to illustrate the circumferentially averaged operating points of the concentric and eccentric configurations. As above, all values are presented relative to design conditions. On average, ECC-MIN and CON-NOM have an equal tip clearance and deliver the same pressure rise. Efficiency is not shown, but the same applies in this case as well. The average gap of ECC-MAX is 1.7% chord, which is between

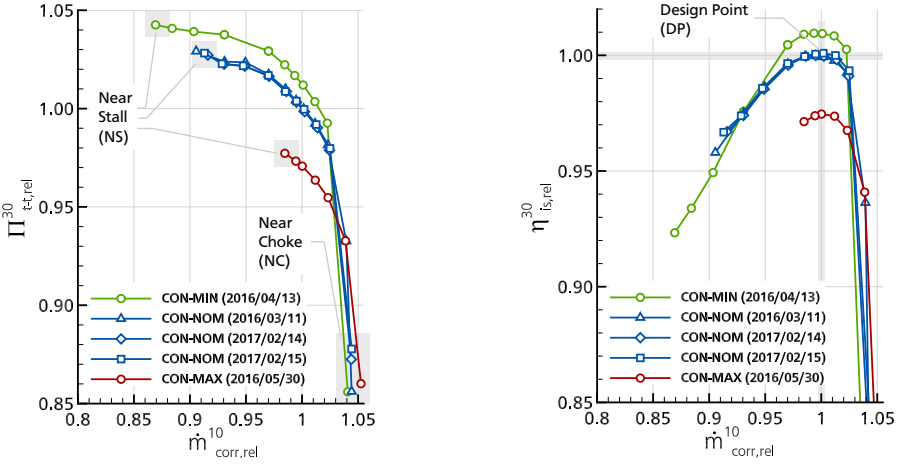

(a) Stage total pressure ratio against corrected inlet mass flow

(b) Stage isentropic efficiency against corrected inlet mass flow

Figure 4.1: Three redundant measurements of the nominal configuration relative to small and large tip clearance setup. DP is used as reference for mass flow, pressure rise and efficiency.

CON-NOM (1.25% chord) and CON-MAX (2.5% chord). As a result, the pressure ratio is in between these corresponding concentric settings.

ECC-MAX is throttled further than CON-MAX, although both have the same maximum gap. Hence, the stability margin of ECC-MAX is not determined by its largest clearance. However, it must be considered that the limiting phenomena of this state-of-the-art rotor design are not purely aerodynamic and depend on tip clearance.

In general, the evolution of pre-stall disturbances results in blade vibrations near stall. In case of configuration CON-MAX, this limits further throttling. Consequently, for configurations CON-MAX and ECC-MAX, the operation is terminated differently. This is worth noting, but the comparison remains valid for a front stage. The individual mechanisms that limit the operating range are further addressed in subsequent sections[1].

In Figure 4.2b, the sensitivities regarding efficiency, peak pressure and stability margin are plotted against relative tip clearance. In case of stage efficiency, values

[1] CON-NOM and ECC-MIN are compared in Section 4.2.1. ECC-MAX is analysed in Sections 4.1.6 and 4.2. CON-MIN and CON-MAX are illustrated in the Appendix in Figure A.8 and Figure A.9, respectively. See Figure A.10 and Figure A.11d for the stall inception process of configuration ECC-MIN.

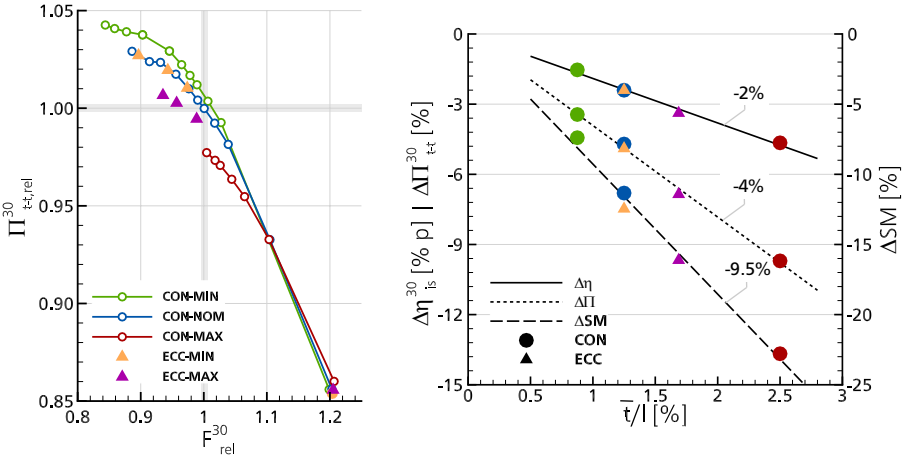

(a) Averaged stage pressure ratio against exit flow function

(b) Sensitivity of efficiency, pressure rise and stability margin (color code in accordance with Table 3.1)

Figure 4.2: Effect of varying average clearance on the compressor's performance

are shown in percent points. All configurations are related to the smallest clearance (configuration CON-MIN) and the linear fitted trend lines are shifted with their y-axis intercept in order to cross zero reduction at zero clearance. Consequently, comparisons to other investigations are possible. According to Section 2.4, a statement regarding the tip clearance range is needed, as the sensitivity to tip clearance varies from tight to large clearance.

In between the measured range, efficiency is reduced by -2% points and peak pressure by -4% for an increase of tip clearance by 1% tip chord. The eccentric settings are in line with the concentric cases. This indicates the dependency of non-uniform designs on the circumferentially averaged clearance in case of efficiency and peak pressure rise. The stability is reduced by -9.5%. A specific influence of eccentricity cannot be fully quantified with the current dataset. A study of several configurations with constant average gap and varying eccentricity was not carried out. Previous investigations showed a dependency of stability on the level of eccentricity (Young et al., 2016). In accordance with their findings, the current dataset illustrates that the largest clearance is not expedient to address the stability margin of eccentric compressors. Stability is rather determined by the average clearance.

These findings for design speed are supplemented by results at part speed, shown in the Appendix in Section A.3.

4.1.2 Effect on Radial Flow Redistribution

As a result of varying tip clearance and the associated secondary flow in the tip region, mass flow is redistributed radially in the compressor. To illustrate this, the rotor exit flow of the concentric settings is examined in the following.

Figure 4.3 presents the radial distribution of the axial Mach number, tangential flow angle and entropy at the rotor exit (denoted as Station 21). For more detail on the derivation of the quantities refer to Section A.2. The measurements are carried out at NS for each of the three concentric configurations. Two redundant measurements with nominal clearance are shown (labelled as (1) and (2)). These measurements were repeated in between days without removing and reinstalling the probe traversing unit and five hole probe itself.

Figure 4.3a and 4.3b reveal that above 80% span, the axial Mach number is decreased and the flow angle is progressively increased compared to midspan and at the hub. For this rotor design, the aerodynamic loading is thus highest at the tip for a tip clearance range between 0.9% and 2.5% chord. The axial Mach number as well as the flow angle reach consistent extremes at the tip, just before stall is initiated. So these values mark the stability limit in terms of minimum axial through flow and maximum flow deviation at the tip.

Figure 4.3c shows that the generated loss is disproportionally high in the tip region compared to hub and midspan. It increases with clearance. Loss due to increased tip clearance flow is generated when it mixes out with the main flow (Wisler, 1985). For the rotor under investigation, this zone is located between 70 and 95% span.

With small clearance, entropy is increased at approximately 40% span. As more mass flow passes the rotor tip section, the loading at the hub is increased. This shows that the profile does not operate perfectly at midspan, but there is no indication that the profile is overloaded or that the flow breaks down at the hub. Consequently, even at the smallest clearance the rotor remains tip critical. So, stall is initiated at the tip for the clearance range of 0.9% to 2.5% chord.

To quantify the radial mass flow distribution - besides the axial Mach number - a straight forward approach is the use of mass flow density. This quantity is used in Figure 4.4 to illustrate the effect of tip clearance and eccentricity at the aerodynamic design point. Mass flow density is corrected by local pressure and temperature. Reference is the stage exit mass flow density at the DP. The measurements are all carried out at the same integral inlet mass flow.

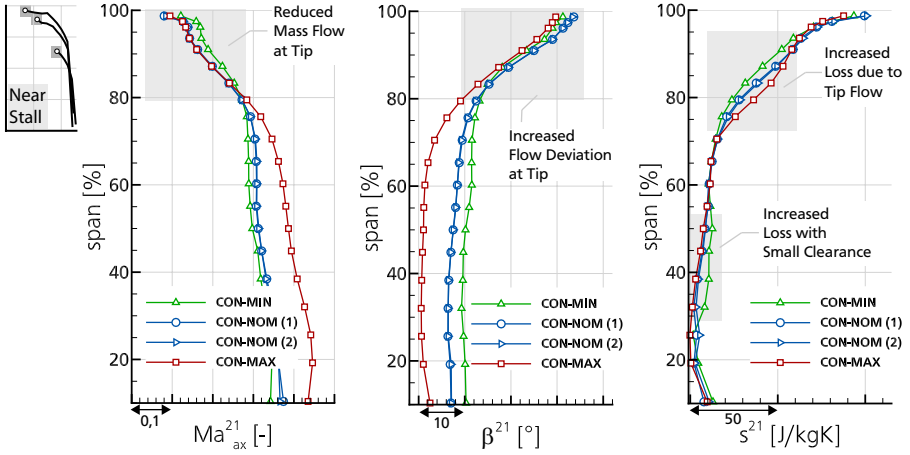

(a) Axial Mach number **(b)** Tangential flow angle **(c)** Entropy

Figure 4.3: Effect of increased uniform tip clearance on rotor exit flow. The NS operating points of concentric configurations are compared.

First, the measurements with concentric clearance are analysed. Figure 4.4a illustrates the effect of an increased concentric clearance. The two redundant measurements of CON-NOM visualize the precision of the measurement. By increasing the clearance, less mass flow passes the tip section above 80% span. As the total inlet mass flow is constant, an reduction of mass flow at the tip leads to an increase of mass flow rate at the hub.

In the case of configurations with eccentric clearance, the results are calculated by averaging eight radial profiles that are measured evenly distributed over the circumference.

In Figure 4.4b the influence of average clearance on the rotor exit flow is shown. The averaged mass flow at the tip in an eccentric casing (see configuration ECC-MIN with clearance $\overline{t}/l = 1.25\%$) is equal to that in a concentric casing (CON-NOM tip clearance is $t/l = 1.25\%$). Thus, the circumferentially averaged blockage, generated in an non-uniform casing is equivalent to that in an uniform casing with the same average clearance.

Figure 4.4c shows two out of eight measured profiles for configuration ECC-MAX. These represent the extreme levels of local mass flow. A comparison with the

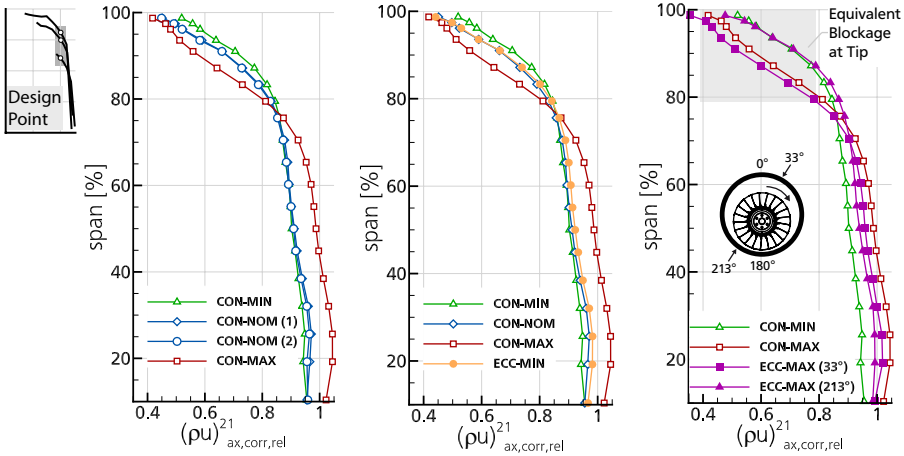

(a) Effect of increased concentric clearance

(b) Effect of average clearance

(c) Local mass flow in an eccentric casing

Figure 4.4: Effect of tip clearance and eccentricity on the radial flow distribution. Comparisons of the mass flow density at the rotor exit are made at the DP.

corresponding concentric clearances is illustrated, while the integral inlet mass flow is constant.

At 33° and 213° the local mass flow rates above 80% span are equivalent to the ones of the corresponding concentric configurations that geometrically represent the local extreme clearance. However, the circumferential offset of 33° must be considered. Below 80% span, the local mass flow rate does not vary with the same intensity. This result cannot be explained if the respective sector would locally work with the same inlet mass flow as the concentric configurations. Hence, there must be an upstream mass flow redistribution. This is analysed in the following.

Supplementary data of the radial distribution of mass flow in an eccentric casing is given in Figure A.5 in the Appendix.

4.1.3 Effect on Circumferential Flow Redistribution

The flow in an eccentric casing is redistributed radially according to its mean clearance. In addition to this, the pressure constraints at the inlet and exit of the stage result in a circumferential flow redistribution. This is addressed by the parallel compressor theory (refer to Section 2.4.3). It assumes constant static exit pressure,

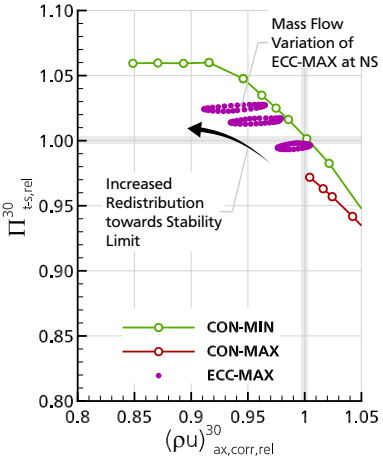

(a) Stage total-to-static pressure ratio against corrected mass flow density

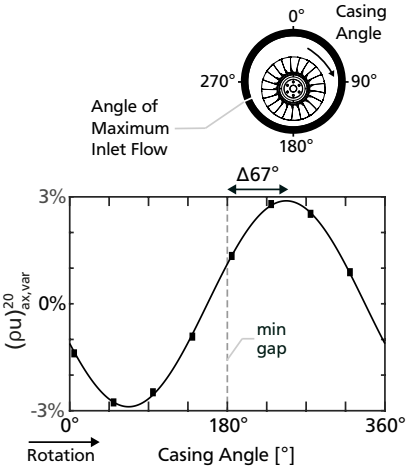

(b) Mass flow redistribution at the inlet. Operating point NS of configuration ECC-MAX is shown.

Figure 4.5: Mass flow redistribution in an eccentric casing

uniform total inlet pressure and - which is not valid in a transonic compressor - incompressibility.

This is reviewed, analysing the results shown in Figure 4.5a. The tip clearance in case of CON-MIN and CON-MAX correspond to the local extremes of ECC-MAX. Thus, these concentric configurations define the boundaries in terms of pressure rise and mass flow capacity of the stage. The total-to-static pressure ratio is plotted against the mass flow density for each stator exit passage. The calculation of Π^{30}_{t-s} is outlined in Section A.2. For the concentric settings, the flow is assumed to be periodic by one pitch and thus representative for the entire exit surface. So, the averaged values of one stator exit passage are illustrated. In case of configuration ECC-MAX, the averaged values of each individual stator exit passage are shown. Accordingly, the individual marker represent the variation of the local static pressure and mass flow rate at the exit of the stage. Reference pressure ratio and mass flow density are those at the DP.

The compressor stage delivers an approximately constant total-to-static pressure rise for all three throttling conditions illustrated. With increased throttling, the variation of the mass flow rises. This is a result of the larger blockage at NS compared to the DP, which leads to a larger extent of flow redistribution compared to the operation at a higher integral inlet mass flow.

At NS, the total-to-static pressure rise varies by ±0.25%, so the assumption of uniform static pressure at the exit of the stage is valid.

In Figure 4.5b, the mass flow redistribution is assessed via measurements at the stage inlet. Static pressure ports are positioned upstream of the IGV. The measured pressure is corrected to the rotor inlet, applying the method proposed by Morris et al. (2008), assuming an exponentially decaying potential field (compare Section A.2). Consequently, this analysis is an estimation and takes only the variation at the rotor tip into account.

The operating point with maximum redistribution is shown. Upstream of the rotor, the mass flow varies by ±3%. The flow redistributes at the inlet with a phase lag of approximately $\Delta 67°$ relative to the smallest and largest gap. This effect is most likely a result of a stationary potential field that results from the circumferentially varying blockage in the rotor. As the rotor passes the largest clearance, the actual blockage in the rotor passage is smaller because it was generated at a smaller clearance. Shortly after passing the maximum clearance, the blockage in the rotor passage reaches its maximum. Consequently, the circumferential delay is likely to depend on the time scale by which the flow in the passage adapts to the local gap. As a result, the circumferentially varying blockage is smallest and largest at about 67° after the minimum and maximum gap, respectively.

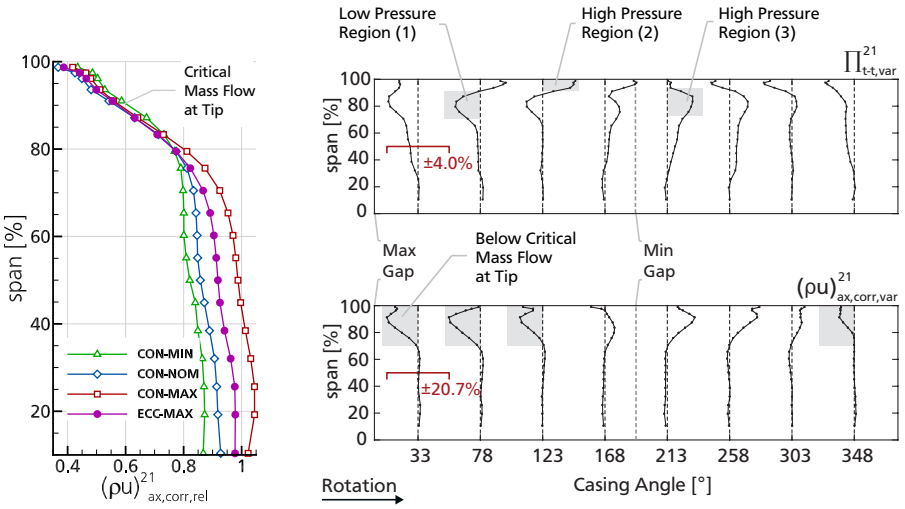

(a) Circumferential average of mass flow density

(b) Circumferential variation of total pressure ratio and mass flow density in an eccentric casing. Configuration ECC-MAX is illustrated.

Figure 4.6: Critical mass flow at the blade tip for NS conditions

In the following, the circumferential blockage distribution at the rotor exit is further investigated. Probe measurements are taken at eight - evenly distributed - casing angles at the rotor exit. Hence, there is an considerable angular uncertainty in this determination. Figure 4.6a illustrates a comparison of the eccentric configuration ECC-MAX to the concentric configurations for NS conditions. For ECC-MAX, the circumferential average of the eight measured radial profiles is shown. Above 80% span, the mass flow density of all configuration reaches a limit value (compare also Figure 4.3). The incidence at the rotor inlet is not measured in the framework of this thesis, but the mass flow at rotor in- and outlet implicitly contain the critical incidence at the tip of the blade.

Thus, on average, the aerodynamic loading in an eccentric casing is equivalent to configurations with an uniform clearance. However, there is a sector that operates with lower mass flow rate at the tip of the blade than the one needed for steady-state operation. Consequently, the compressor is locally unstable in this sector, but overall the compressor operation remains stable without evolving rotating stall (discussed in detail in Section 4.1.6).

Figure 4.6b shows the deviation of both, the mass flow density (bottom) as well as the total pressure rise (top) from the circumferentially averaged radial profile (average of configuration ECC-MAX). The location of the maximum gap is at 0°. Between 348° and 123°, the compressor operates with less mass flow compared to the critical one indicated in Figure 4.6a. The critical sector covers at least half of the circumference. Considering the circumferential resolution of the probe measurements, this is an estimation. At the rotor tip, the mass flow variation in circumferential direction is in the order of 20%.

The total pressure deviation is in the order of 4%. Major deviations occur at about 80% span that result from a low pressure region (1) in the large clearance sector and a high pressure region (3) in the sector with a small clearance. According to Figure 4.3c, this is accompanied with the generation of low and high loss. The high pressure region (2), close to the casing, is most likely a result of fluid with low axial momentum, which is transported with the rotor.

The effects, previously considered relative to the casing, are a result of the rotor relative flow that varies during one turn in an eccentric casing. This is analysed in the subsequent section.

4.1.4 Effect on Rotor Relative Flow

The effect of eccentricity on the rotor relative flow is presented for configuration ECC-MAX at NS, because mass flow redistribution is largest in this case and governing effects clearest. To display the rotor relative flow, measurements with the unsteady pressure probe are conducted. Data are measured at eight angles relative to the casing and superimposed during post-processing. This permits a 360° illustration of the rotor exit flow in a casing with non-uniform clearance.

In Figure 4.7, the contour of the total pressure ratio is shown. Reference is the design pressure ratio. The overlaid solid lines indicate constant relative standard deviation of the total pressure. These lines range between 3 and 10% and demonstrate the unsteadiness of the flow. They are calculated in accordance to Equation 3.2. In case of rotor exit flow, an increase of pressure fluctuations results mostly from higher turbulence in the blade wakes or vortex structures, which are a result of secondary flow. As before, the maximum clearance in this view is at top position.

In the sector with a large clearance, the rotor wakes are strengthened at midspan (from about 3% to 5%). The unsteadiness of the rotor wakes is largest after the rotor passed the maximum clearance. This is in agreement with the circumferential delay of the highest aerodynamic loading. In Figure 4.5b and Figure 4.6b, the maximum loading was indicated to occur at about 67° relative to the largest clearance. Just after the rotor passed the smallest gap at 180°, the unsteadiness of the rotor wakes is smallest.

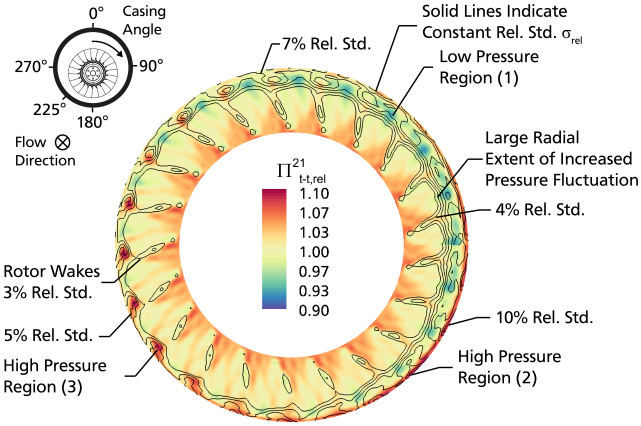

Figure 4.7: Full circumference visualization of the rotor relative exit flow. Operating point NS of configuration ECC-MAX is shown.

In the tip region, the relative standard deviation is increasing from 5% (between 225° and 270°) to 10% at about 90°. Also, the radial extent of the unsteady region at the tip is growing as the rotor moves from the small to the large clearance of the casing. In this sector, the increasing blockage leads to a decreased mass flow at the tip (reconsider Figure 4.6b).

Between 180° and 270° the pressure rise in the blade tip region is high. With increasing clearance, this high pressure region (3) in the blade passage is weakened and the higher pressure fluctuation is accompanied by low pressure region (1). The enlarged radial extent, accompanied with a total pressure loss and high unsteadiness indicates vortex breakdown in the tip region in the large clearance sector (Yamada et al., 2004). This is consistent with the eccentric configuration operating locally at mass flow rates that lead to rotating stall in a compressor with an equivalent concentric clearance. High pressure region (3) and low pressure region (1) correspond to the pressure deviation labelled evenly in Figure 4.6b.

As the operation is limited by a breakdown of the flow at the tip of the rotor blades, the rotor is tip critical. This is the area of interest with respect to compressor stability. Therefore, the effect of mass flow redistribution on the blade tip flow is examined below.

The static wall pressure at the tip of the rotor is measured simultaneously via four axial arrays (compare Figure 4.8a). The visualization is pseudo-spatial because the rotor moves across the probes at distinct casing angles. Figure 4.8b illustrates

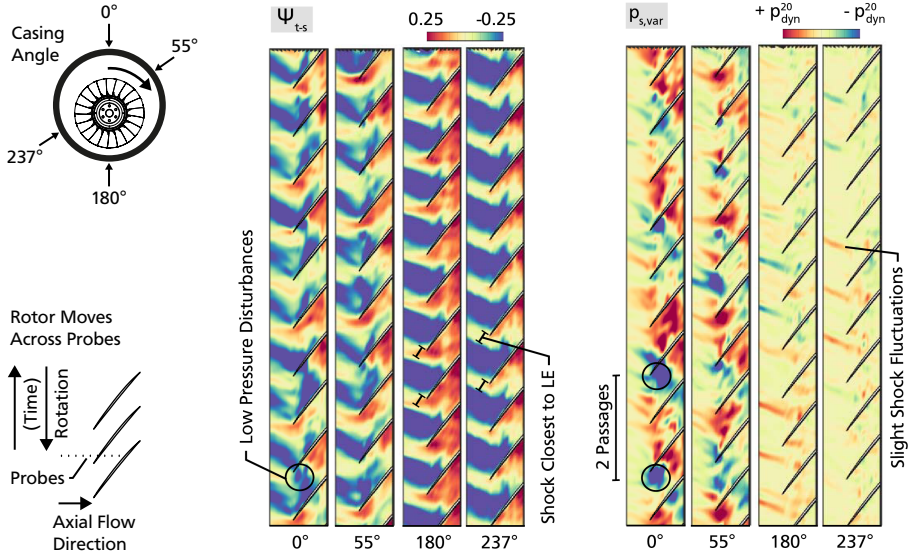

(a) Probe positions and measurement procedure

(b) Instantaneous distribution of total-to-static pressure rise coefficient

(c) Pressure deviation from ensemble average

Figure 4.8: Rotor tip flow measured via static wall pressure transducers. Operating point NS of configuration ECC-MAX is shown.

the wall pressure of a single revolution at steady-state operation NS. No averaging method is applied, the static wall pressure is only normalized in accordance to Equation 3.3.

The operating conditions vary considerably between the region with large (0° and 55°) and small (180° and 237°) tip clearance. As the mass flow rate in the sector of the large clearance is below critical values for steady-state, the passage flow is highly unsteady at the tip of the blades. The through flow varies from passage to passage. Strong disturbances in form of pressure drops occur between the leading edges of the blades. This results in large variations of the shock position that is indefinable in several passages. The shock is more evident in the sector with a small clearance. Compared to other casing angles, the shock front is closest to the LE of the blades at angle 237°. This is in agreement with the analysis based on Figure 4.5b and

4.6b because the local shock position is defined by the rotor inlet Mach number and blockage, which is highest and lowest in this sector, respectively.

The unsteadiness of the flow is more clearly demonstrated by subtracting the ensemble-averaged flow field from the given revolutions, based on Equation 3.4.

This pressure deviation is illustrated in Figure 4.8c. Reference pressure is the dynamic pressure at the rotor inlet. It is calculated, using the unsteady static pressure of the first upstream wall pressure transducer and the total pressure of the settling chamber. At 0° and 55°, low pressure disturbances occur in about every second passage, analysed in the stationary frame of reference. A calculation of the cell count in the reference system of the rotor would only be possible by knowledge of the propagation speed. The determination is not possible via the wall pressure sensors, as their circumferential distribution is not tight enough. However, assuming a propagation speed of about half the rotor speed (Young et al., 2011, Jüngst et al., 2015, Holzinger, 2017, Brandstetter et al., 2018), relative to the rotor each passage is actually disturbed.

At casing angles 180° and 237°, only slight variations of the shock position occur. These fluctuations at both angles result most likely from random disturbances in some of the passages. Due to this, the local inlet Mach number is altered by the blockage in respective blade passages, which influences the shock position. An equally valid approach to explain these random fluctuations are blade vibrations, which directly cause a variation of the shock position.

In short, the local operation of the rotor varies circumferentially. Even though large disturbances exist in some part of the annulus with an amplitude and size larger than in previous studies (e.g. Brandstetter et al. (2018)), the whole compressor operation remains steady-state and rotating stall does not evolve. More detail on the evolution of rotating stall and fluid-structure interaction, as a result of this flow unsteadiness, is given in subsequent sections.

4.1.5 Effect on Downstream Blade Rows

Previous to the analysis of stall inception, the analysis of the influence of eccentricity at steady-state is completed. This section's intend is to examine the effect of an eccentric front stage on subsequent stages. For this purpose, the stator exit flow of the 1.5-stage design is analysed. A circumferential variation of the mass flow rate results in an inlet distortion for downstream blade rows.

In Figure 4.9a, the total pressure ratio at the exit of the stator is shown. Values are referenced to the averaged total pressure at the DP. The investigated stator design is hub critical, which is quite common (Cumpsty, 2004). Thus, stator designs usually tend to flow separation at the hub that leads to a circumferentially uniform pressure loss in the present case.

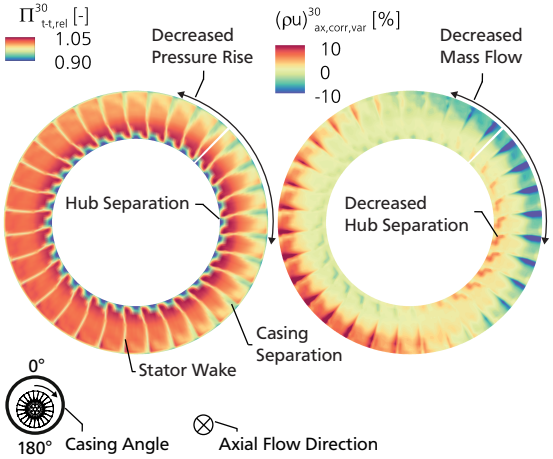

(a) Variation of stage total pressure ratio (left) and mass flow density (right) at the stator exit

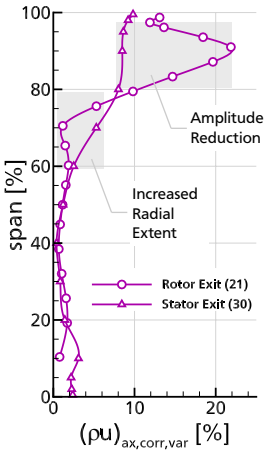

(b) Comparison of circumferential mass flow density variation at rotor and stator exit

Figure 4.9: Operation of the stator row, downstream of an eccentric casing. Operating point NS of configuration ECC-MAX is shown.

The variation of the stator inlet flow rate is largest close to the casing (refer to measurements of the rotor exit flow in Figure 4.6b). As a result, the decreased flow rate between 348° and 123° results in a locally reduced stage pressure rise that indicates increased flow separation at the casing, i.e. in the stator tip section.

Mass flow density varies with up to ±10% (see Figure 4.9a, right). All values are corrected by local pressure and temperature. Its variation is largest at the casing (above 70% span). As a consequence of the reduced mass flow in the tip section of the stator blades, the mass flow is redistributed radially and increased at the hub. This results in a lower stator incidence and consequently to a reduction of the hub separation. The maximum mass flow at the hub has a circumferential delay of about three passages compared to the minimum mass flow at the tip.

In Figure 4.9b, the effects across the stator blade row are summed up. Compared to the rotor exit, the amplitude of the circumferential mass flow density variation is reduced from ±20% to ±10%. In addition, due to the flow phenomena in the stator, the radial extent of the circumferential mass flow variation increases.

In a multi-stage assembly, upstream blade rows affect downstream ones and vice versa. As the upstream effect of a downstream row is neglected here, these multi-stage effects need further assessment. However, it can be deduced from the 1.5-stage build that eccentricity (in the presented case $\xi = 96\%$) can result in inlet distortions of up to ±10% mass flow density for downstream blade rows.

4.1.6 Effect on Stall Inception

The rotor incidence varies circumferentially, which has an impact on the stall inception process. Consistently to the analysis before, stall inception is examined for configuration ECC-MAX. For data acquisition, the transient measurement procedure illustrated in Figure 3.3b is used.

Eight sensors at the rotor LE are used to analyse the throttling process. The signal is processed according to Equation 3.4. As illustrated in Figure 4.10a, the maximum and minimum pressure deviation per revolution are detected.

1000 revolutions prior to rotating stall are shown in Figure 4.10b. The initial condition of the measurement, i.e. revolution -1000, represents steady-state at NS. Revolution 0 refers to the first revolution with fully developed, rotating stall cell.

As discussed above for steady-state operation, the rotor tips operate below the critical mass flow between 348° and 123° (compare Figure 4.6b). During stall inception, this results in large pressure disturbances at the leading edge of the

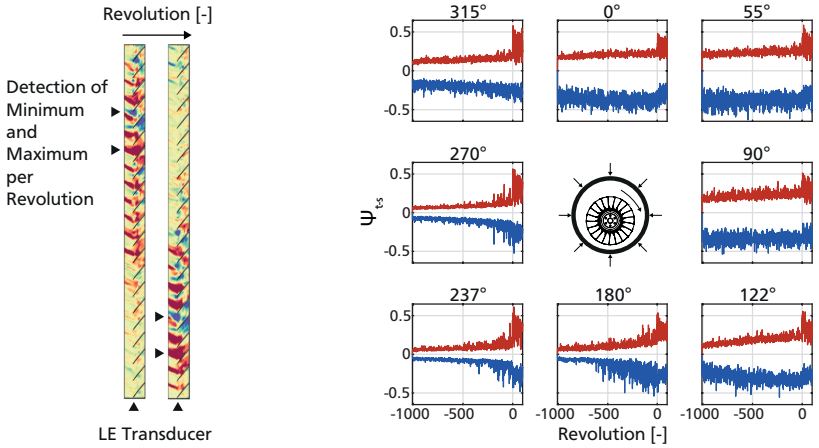

(a) Analysis Procedure

(b) Minimum and Maximum Disturbance per Revolution

Figure 4.10: Non-uniform disturbance growth during stall inception in an eccentric casing. Configuration ECC-MAX is shown.

blades. Until rotating stall occurs, they do not grow further. Instead, in the sector between 0° and 90°, the pressure drops remain constant in amplitude and size.

At 122°, the amplitude of the disturbances increases from the beginning of the throttling process. Between revolution -500 and 0, the intensity of the associated pressure drops starts to remain constant as well. At the same time, the growth of disturbances occurs at casing angle 180°. So, via continuous throttling, the unstable part of the annulus is extended and the time, blades spend in the unstable sector increases. Also, the probability rises that pressure drops evolve in the magnitude of the rotating stall cell. However, at 237° and 270°, the rotor recovers and it is likely that it runs undisturbed for several revolutions after large pressure drops occurred in this sector.

In short, the local flow field strongly depends on the history of the rotor during one turn and is linked to growth and decay of disturbances. Even though the local gap at 122° and 237° is the same (equivalent at 90° and 270°), the local operation varies fundamentally. The flow within the passages recovers on the way through the small clearance sector and disturbances decrease in count, amplitude and length-scale.

In Figure 4.11a, the last 100 revolutions prior to stall are illustrated. In the sector with decreasing clearance (0° to 180°), the pressure fluctuations remain constant. In contrast, between 180° and 315° spike-type disturbances occur. In the example shown, spikes occur between revolutions -100 and -80 as well as between -40 and -20. They are damped and periods of recovery exist, before rotating stall is initiated. Some of these spikes lead to a complete breakdown of the flow in several passages.

To demonstrate this, complete revolutions of the throttling process are shown in Figure 4.11b. The signal is processed equivalently to Figure 4.8c. It is shown, how amplitude, length-scale and axial extent of the disturbances evolve at casing angle 237°. As a result of disturbed passages during revolution -89, the flow is redistributed locally. The generated blockage leads to retarded flow in neighbouring passages and detached shocks. During the periods of recovery, only slight shock fluctuations occur at casing angle 237°. The evolving rotating stall cell in revolution 0 has an increased circumferential and axial extent compared to previous pre-stall disturbances. The stall cell is initiated by a spike, which is not damped, but constantly growing in size over several revolutions (compare Figure 4.11a). The initial spike occurs during revolution -1. The rotating stall cell propagates with a speed of about 53% of the rotor speed. As the stall cell rotates at a fraction of the rotor speed, its size is not true-scale in Figure 4.11b. The fully developed cell is enlarged by a factor of $1/0.53 \approx 1.9$.

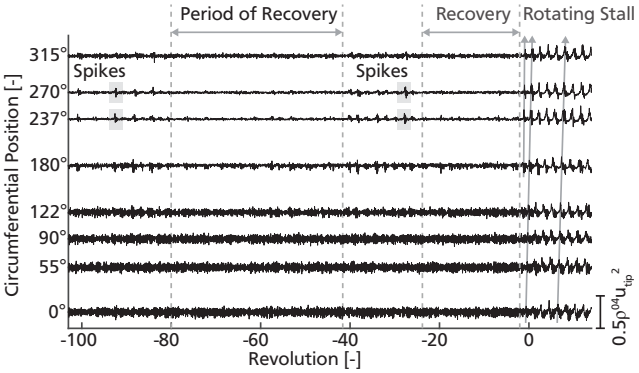

(a) Unsteady wall pressure signals at the leading edge, low pass filtered at EO = 12.5, i.e. about 60% blade passing

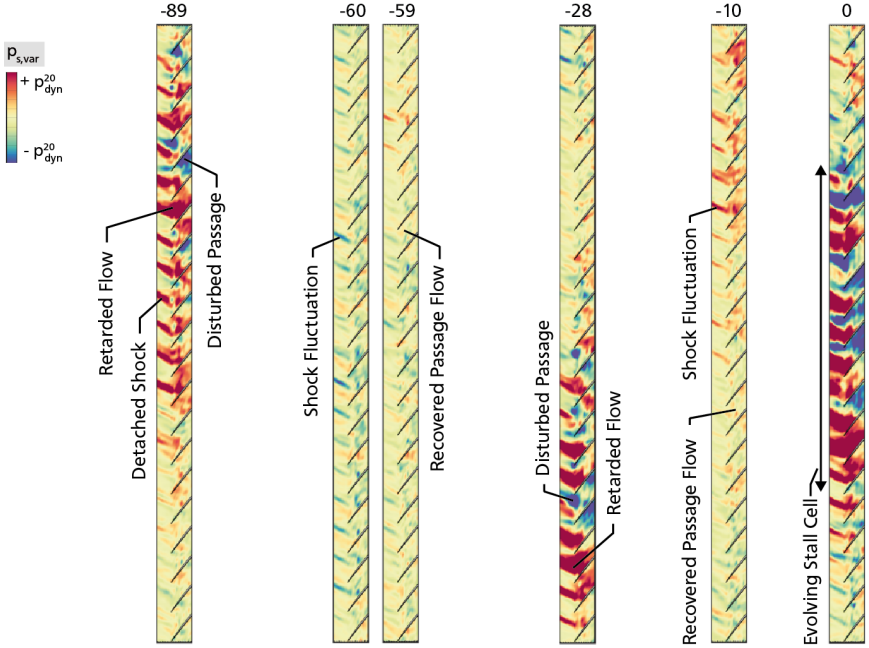

(b) Axial wall pressure deviation at casing angle 237°

Figure 4.11: Evolution of rotating stall in an eccentric casing. Configuration ECC-MAX is shown.

4.1.7 Intermediate Conclusion

Previous sections illustrated the effect of tip clearance and eccentricity on aerodynamics in a modern transonic compressor. In short, the main findings are:

- The efficiency of the stage is reduced by about -2% points and peak pressure rise by -4% per 1% $\overline{t}/l$ increase. This is in agreement to earlier findings (Smith, 1958, Schäffler, 1979a, Moore, 1982, Freeman, 1985, Berdanier and Key, 2015). The tip clearance sensitivity is thus not reduced by modern features, e.g. such as forward sweep. However, it must be noted that the stage loading $\Delta h_t/u_m^2$ of the stage is higher compared to previous studies throughout the last century.

- The reduction of efficiency and pressure rise due to an eccentric tip clearance is equivalent to a concentric compressor with the same average clearance. This is in line with studies by Graf et al. (1998) and Young et al. (2016).

- The stability margin of the stage is reduced by -9.5% per 1% $\overline{t}/l$ increase. Similar sensitivity was found before by Baghdadi (1995) and Young et al. (2016) in tests of core compressors on low and high speed rigs. In contrast to earlier findings by Freeman (1985) and Graf et al. (1998), the largest clearance does not limit the compressor operation of the measured eccentric designs (60% and 96% eccentricity). Others also reported that the largest gap of an eccentric configuration is not an appropriate way to predict the stability margin of an eccentric machine (Young et al., 2016). They found a dependency of stability margin on eccentricity. This cannot be quantified with the current dataset, because several eccentric configurations with identical mean gap have not been analysed.

- An uniform increase of the clearance, generates larger blockage primarily in the tip region above 70% span. Mixing losses increase between 70 and 95% span. Even at the smallest clearance (0.9% chord), the rotor design remains tip critical. So, rotating stall is initiated at the tip throughout the investigated tip clearance range.

- There is a critical rotor tip mass flow below which rotating stall is triggered in a concentric casing. With an eccentric clearance, the rotor operation remains stable, though operating with less tip mass flow in a sector of at least 180°. Hence, the extent of the unstable sector is larger compared to earlier studies in low speed facilities by Young et al. (2016).

- Two aspects have to be considered by analytical models of eccentric compressor stages. First, mass flow is shifted circumferentially at rotor inlet due to the

upstream influence of varying blockage in the rotor. This leads to decreased mass flow in sectors with increased clearance and vice versa. Second, the sectional blockage in the tip region of the eccentric casing is regulated by the local tip gap, identical to the blockage of an equivalent concentric configuration.

- The inlet mass flow to a stage with a tip clearance eccentricity of 96% varies with an amplitude of up to ±3% and a phase of about 67°, relative to the minimum and maximum clearance. Although not shown, a 60% eccentric clearance results in an inlet mass flow variation of up to 1.8% with a phase lag of 66°.

- In the current dataset (high speed), the phase lag is larger compared to the low speed investigation by Young et al. (2016). Morris et al. (2008) found a 60° to 80° phase lag for a transonic compressor at 70% speed, which is in good agreement with the current dataset. The results indicate that the phase lag depends on the time scale of the blockage formation in the rotor passage, which is associated to the adjustment of the flow relative to the local tip gap.

- The investigated stator tends to flow separation at the hub. This is common for stator designs in aero engines (Cumpsty, 2004). Current findings indicate that flow redistribution in a compressor with non-uniform clearance affects the hub loading non-uniformly and reduces the stator hub separation in some part of the annulus. This may have severe effects in a multi-stage assembly. Berdanier and Key (2016) even observed that increasing the rotor clearance prevented stator hub corner separation.

- Due to eccentricity in a front stage, inlet distortions for downstream stages occur with up to ±10% mass flow and ±3% total pressure deviation (for the case with 96% eccentricity and 1.7% average clearance). Although not shown, for a setup with 60% eccentricity and an average clearance of 1.25%, mass flow varies with ±6% and total pressure with ±1.5% at the stator/stage exit.

- As a result of non-uniform clearance, the local operation of the rotor varies in circumferential direction. The maximum clearance of an eccentric casing is not limiting the stable operation of the entire compressor stage. The flow within the rotor passages recovers on the way through the small clearance sector because disturbances decrease in count, amplitude and length-scale. In some part of the annulus, large disturbances exist with an amplitude and size larger than in previous studies with concentric clearance (Brandstetter et al., 2018). However, the whole compressor operation still remains stable, although the intensity of the existing disturbances led to rotating stall in case of settings with an equivalent uniform clearance.

Non-uniform tip clearance has no negative impact on the pressure rise and efficiency of a stage. In terms of stability, the influence of eccentricity is not as severe as simple rules of thumb suggested since the mid-1980s.

The mass redistribution in an eccentric stage results in inlet distortions for subsequent stages with a magnitude of 3% total pressure. Wartzek (2017) investigated the effect of total pressure distortions in the order of 20% to 30% that affected the stability of a transonic compressor, similar to the compressor used in the current study. The stability margin was reduced by 1 to 2% in terms of exit flow function. The distortions due to eccentricity are one order of magnitude smaller, which is why the loss of stability in downstream stages is likely to be negligible. Based on these findings, aerodynamic design conservatism regarding eccentricity might be reduced.

The strong blockage and mass flow deficit in segments of the compressor leads to a locally increased positive incidence relative to the circumferential average. This affects the stall inception process and results in strong pressure fluctuations between the leading edges of the blades that rise and decay. The influence on associated blade vibrations is assessed below.

4.2 Effect of Eccentricity on Aeroelasticity at Design Speed

Recent investigations have highlighted that the rotor design used here is prone to blade vibration. The vibrations are caused by pressure fluctuations on the blade leading edge, as a result of propagating radial vortex structures (Jüngst et al., 2015, Holzinger, 2017, Brandstetter et al., 2018).

In the following, the fluid-structure interaction in case of configuration ECC-MAX is investigated. For this setup, the stall inception process was analysed in the previous section from a pure aerodynamic viewpoint. Compared to a build with an uniform tip clearance, the intensity of the disturbances is stronger in parts of the casing. However, the amplitude and count rise and decay during one turn of the rotor.

In Figure 4.12, spectra of the throttling process from steady near stall to rotating stall are shown for the same transducers as in Figures 4.10 and 4.11a. The spectrogram and the maximum amplitudes during the manoeuvre are plotted. For sufficient resolution in both, the time and the frequency domain, engine orders are resolved by $\Delta EO = 0.025$ and revolutions by $\Delta revolution = 21$.

At casing angle 0°, the pre-stall unsteadiness is increased between $EO_{stat} = 6$ and $EO_{stat} = 15$. This unsteadiness is present in the sector with decreasing clearance only (from casing angle 0° to 122°). It is the result of disturbances, which occur approximately within every second passage in this part of the annulus (stationary frame of reference, compare Figure 4.8c).

Two peaks occur that result from an interaction between an aerodynamic disturbance that propagates with 19 cells and the CWB mode. Although not shown, inter-blade variations of the CWB mode range from $EO_{rot} = 10.01$ to $EO_{rot} = 10.07$,

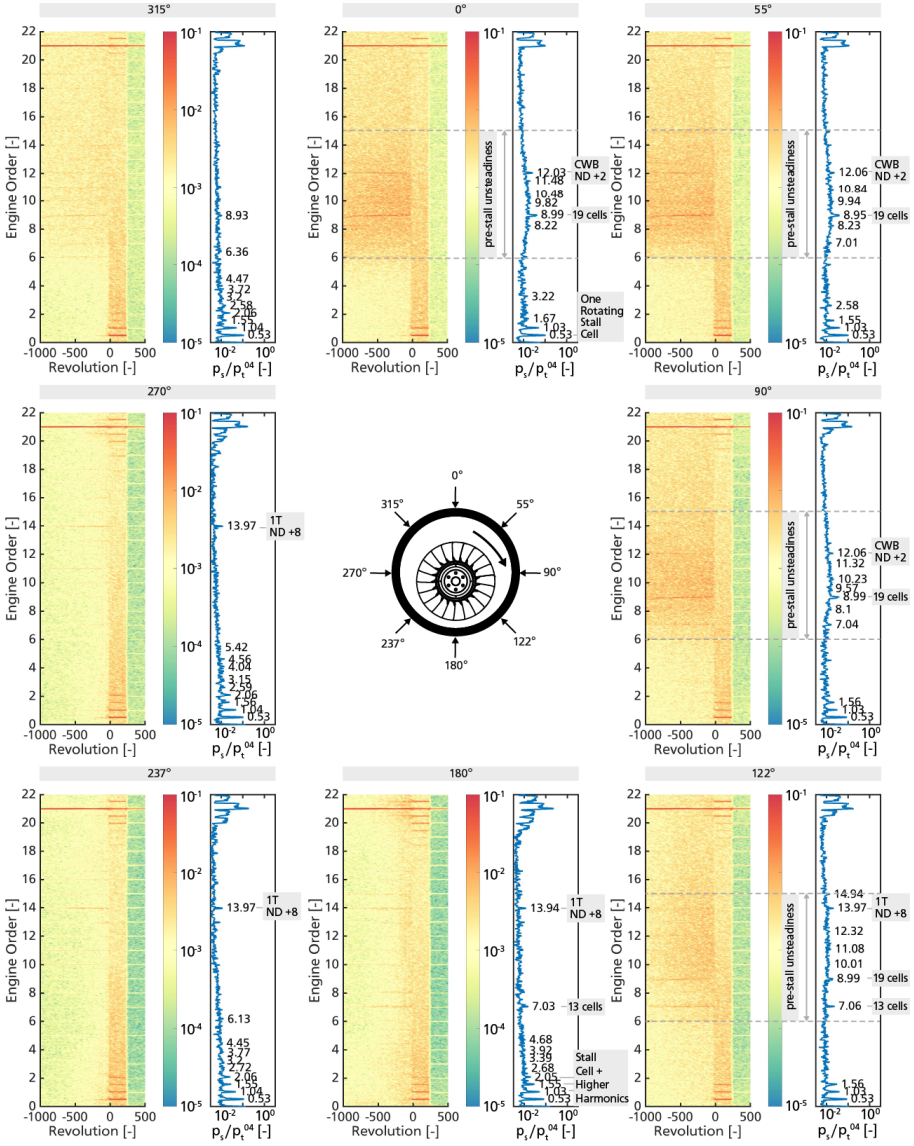

Figure 4.12: Fluid-structure interaction during stall inception in a casing with eccentric clearance. Configuration ECC-MAX is shown. Unsteady pressure transducers at 8% chord, downstream of the rotor LE are illustrated.

measured with blade mounted strain gauges in the rotating frame of reference (strain gauge response on Blade No. 1 is shown in Figure A.11b). Using Equation 2.11, a cell count of 19 is derived. To match the phase between the aerodynamic propagation and the structural vibration, the rotor blades vibrate primarily with nodal diameter +2.

The spectrum to spectrum variation of EO_{stat} (12.03 to 12.06) results most likely from both, blade-to-blade variations and the discrete EO resolution.

Peaks, associated with the CWB mode are present until casing angle 122°. In addition to these, two peaks with small amplitude occur at 122°. These are a result of an interaction of the 1T mode (structural vibration with ND +8) with 13 aerodynamic cells.

The pre-stall disturbances vanish in the sector between 180° and 237°, but the structural vibration remains until 270° (EO_{stat} = 13.97). This is most likely due to the low mechanical damping of the blade vibrations and a result of the 1T mode accumulating only about six cycles per revolution. At annulus angle 315°, no pre-stall disturbances and no fluid-structure interaction are visible in the wall pressure spectrum. Only the full rotating stall cell is present for revolutions larger than zero. The measured frequencies indicate a single rotating stall cell that propagates with a speed of 0.53 times rotor speed in the stationary frame of reference.

Summed up, in the sector with a large clearance, the cell count of the disturbances is high (19 cells) and preferentially the CWB mode interacts with the fluid. As the tip gap decreases, the 1T mode interacts with fewer aerodynamic cells (13 cells). In some part of the annulus, the blade motion is not synchronized with the occurrence of pre-stall disturbances. A stated cell count of 19 does not mean that 19 cells exist at the same time. It simply represents that the spatial distance of the cells is smaller (compared to 13 cells), specifically 1/19 of the circumference.

This result is significant as it shows that the fluid-structure interaction in an eccentric casing varies circumferentially. It is a consequence of the circumferential distribution of aerodynamic disturbances, which is never uniform prior to stall and which varies the aerodynamic force on the blades during one turn.

4.2.1 Analysis of Blade Vibration Amplitudes

Eccentricity has an effect on fluid-structure interaction. With regard to the influence of eccentricity on the vibration level, a valid comparison are the configurations CON-NOM and ECC-MIN, because both setups have an identical average clearance and both stall at about the same mass flow and loading (compare Figure 4.2a).

Figure 4.13 shows the stall inception process of CON-NOM at a glance. This

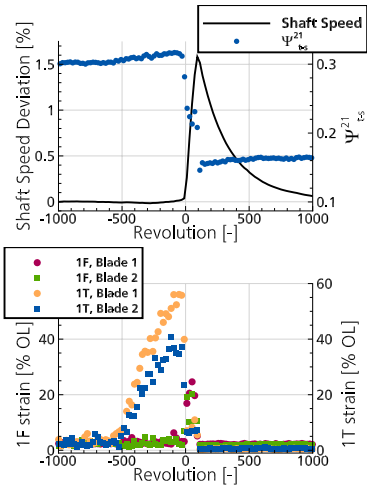

(a) Shaft speed, total-to-static pressure rise at rotor TE and the rise of blade vibration amplitudes

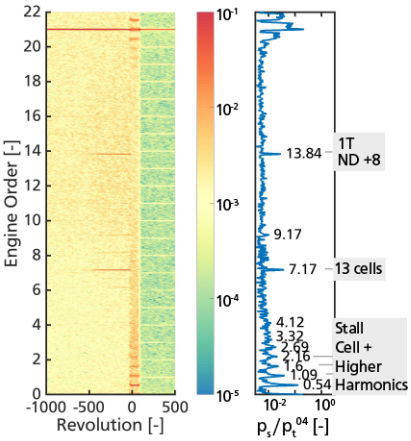

(b) Spectrogram of wall pressure at rotor LE and the maximum pressure amplitudes during stall inception

Figure 4.13: Stall inception of CON-NOM at design speed - analysis of stall induced vibrations

overview separates individual aeroelastic phenomena and introduces the nominal behaviour of the compressor during stall inception[2].

Revolution 0 refers to the first revolution with a fully developed, rotating stall cell. Since the work input is immediately reduced from the stage when the flow breaks down, the rotor accelerates with a steep gradient. As a result, the shaft speed rises by about 1.5% (see Figure 4.13a). Also, as the work input is reduced, the total-to-static pressure rise drops at the rotor TE.

Before stall, pre-stall disturbances result in high blade vibration responses of the first torsion mode. The blade vibration amplitudes can vary significantly between the blades. To illustrate this, the amplitudes of two blades (measured via two strain gauges on different blades) are plotted relative to the rig operating limit (OL). In the given case, the maximum amplitudes of the 1T mode vary by about 20% of the OL.

As the rotating stall cell evolves, the disturbance size expands (reconsider Figure 4.11b). Due to the fact that the cell count drops to a single cell, the 1T

[2] In Figure A.8 and Figure A.9, the stall inception process of the configurations with small and large tip clearance are presented. The data are analysed equivalent to the one carried out in detail within the current section.

amplitudes are lowered. Instead, the large axial extent of the flow breakdown results in increased amplitudes of the 1F mode. By opening the outlet throttle (at approximately revolution 100), the rotor inlet mass flow increases, which lowers the rotor incidence. As a result, the blades recover from stall and the blade amplitudes are lowered. Afterwards the rotor speed is regulated back to design speed by the DC drive control.

In Figure 4.13b, a spectrogram of this throttling process is shown. In the rotating frame of reference, the 1T mode occurs at $EO_{rot} = 5.83$ (strain gauge spectrogram is shown in Figure A.11a). Via Equation 2.11, the aerodynamic cell count calculates to 13. These interact with the 1T mode and result in increased blade amplitudes. Using Equation 2.8, the propagation speed of the 13 aerodynamic cells concludes to 0.55 times rotor speed. The rotating stall propagates with a similar speed of about 0.54 times rotor speed in the stationary frame of reference.

The analysis highlights the difference of stall induced vibration prior and during rotating stall. As a result of pre-stall disturbances that occur with a high count at the rotor tip and leading edge, the blades are interacting with the fluid via the 1T mode. This does not result in a drop of the work input into the fluid. When the flow breaks down and expands axially and circumferentially, the cell count drops to a low number of aerodynamic cells. This excites primarily the 1F mode and results in a reduction of the work input to the fluid. These two types of stall induced vibrations must be separated.

Similarly, Dodds and Vahdati (2014) distinguish low and high frequency stall. They suggest EO 5 to divide the individual aerodynamics of the two categories. The focus of the current analysis is on non-synchronous vibrations, which occur as a result of pre-stall disturbances with a high cell count. The term NSV is used for this phenomenon (reconsider Section 2.3.2).

The stall inception process of configuration ECC-MIN is similar to the concentric case. However, the NSV amplitudes are lower. Figure 4.14 illustrates the 1T blade vibration amplitudes that occurred for the concentric and the eccentric configuration with average clearances of 1.25% tip chord.

The vibration amplitudes, presented in Figure 4.14a appear at steady-state operation during performance measurements[3]. The time scales of these measurements are long. In terms of the rotor blade stress, these vibrations can result in a matter of high cycle fatigue.

The measurements are taken at the same corrected rotational speed. Due to varying inlet temperature, the mechanical speed varies. At near stall operation,

[3] Corresponding performance data are given in Figure A.7a.

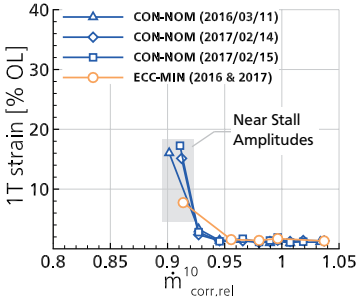

(a) Vibration amplitudes of Blade No. 1 at steady-state operating points.

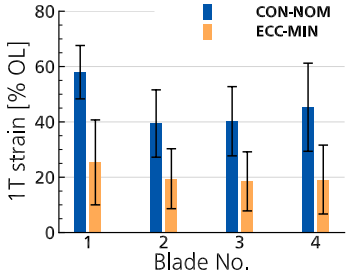

(b) Average blade amplitudes and their deviation that results from mechanical rotor speed and throttle speed variations during transient throttling from NS to rotating stall.

Figure 4.14: Effect of eccentricity on 1T blade vibration amplitudes at design speed

blade vibration amplitudes rise due to increased flow unsteadiness and pre-stall disturbances in the rotor passage. For CON-NOM, three repeated measurements are illustrated. The intent is to demonstrate that the last stable operating point is reproducible from an aerodynamic as well as an aeroelastic point of view. Taken this into account, the reliability of the results is increased, because the steady-state blade vibrations occur with high repeatability. For the eccentric configuration, the steady-state vibration amplitudes are lower compared to the concentric case.

Figure 4.14b illustrates the 1T strain of about 20 transient throttling manoeuvres per configuration from steady NS to rotating stall (measurement procedure illustrated in Figure 3.3b). The full database of these measurements is summed up in Table A.3. Due to the short time scales of the phenomenon, slight differences of the exit throttle opening, throttle speed and rotational speed, variations in amplitude can occur during distinct manoeuvres. To account for these variations, the measurements are repeated several times at different inlet conditions and for different throttle speeds. These variations are indicated via deviation ranges that represent the minimum and maximum amplitude for each blade. Four different strain gauges have been analysed to account for blade-to-blade variations. Differences of the average blade amplitude for each configuration are most likely a result of slight mistuning of the rotor blades and inaccuracies that result from the strain gauge application. For all blades, the vibration amplitudes of the eccentric case are lower.

So the reduction of the vibration amplitude appears blade independent, but varies in intensity from blade to blade. Considering that the rotor stalls at approximately the same mass flow and loading for both configurations, the effect is absolutely significant.

4.2.2 Intermediate Conclusion

This section illustrated the effect of tip clearance and eccentricity on aeroelasticity in a modern transonic compressor. The main findings are:

- In an eccentric casing, pre-stall disturbances evolve circumferentially non-uniform.
- In the sector with a large tip clearance, the aerodynamic cell count is higher than in sectors with tight clearance.
- A high count of disturbances between the rotor leading edges excites primarily the 1T and CWB blade modes. The CWB mode is interacting with higher cell counts than the 1T mode. The phenomenon does not result in a drop of the work input to the fluid. According to the suggestion by Kielb et al. (2003) the phenomenon is named NSV.
- In the sector with a high inlet mass flow, rotor tip flow unsteadiness is reduced, which causes pre-stall blade vibrations to decay.
- Rotating stall cells with a low count but large axial and circumferential extent, excite primarily the 1F mode. These rotating stall cells prevail in the duct for more than one revolution. The larger extent of the flow breakdown results in a drop of the work input to the fluid. These vibrations are not of the same category as the ones with a high aerodynamic cell count.
- For two configurations with an average clearance of 1.25% tip chord and one with an eccentric clearance of 60%, the maximum 1T vibration amplitudes are lower during stall inception. In average of all blades, the amplitudes are reduced by about -25% of the rig operating limit.

The major results of the previous sections are illustrated in Figure 4.15. In an eccentric casing, the non-uniform rotor tip blockage has an upstream effect on the inlet mass flow. The rotor incidence varies circumferentially, which leads to a non-uniform distribution of pre-stall disturbances. This results in a circumferential variation of the aerodynamic force on the blades - in both, amplitude and frequency - and prevents the growth of coherent structural and aerodynamic waves.

From a purely aerodynamic viewpoint, an eccentric casing is not a drawback compared to a concentric configuration with the same average clearance. Instead,

the significant reduction of pre-stall blade vibrations suggests an aeroelastic benefit, which might be used as a measure to reduce stall induced vibration levels.

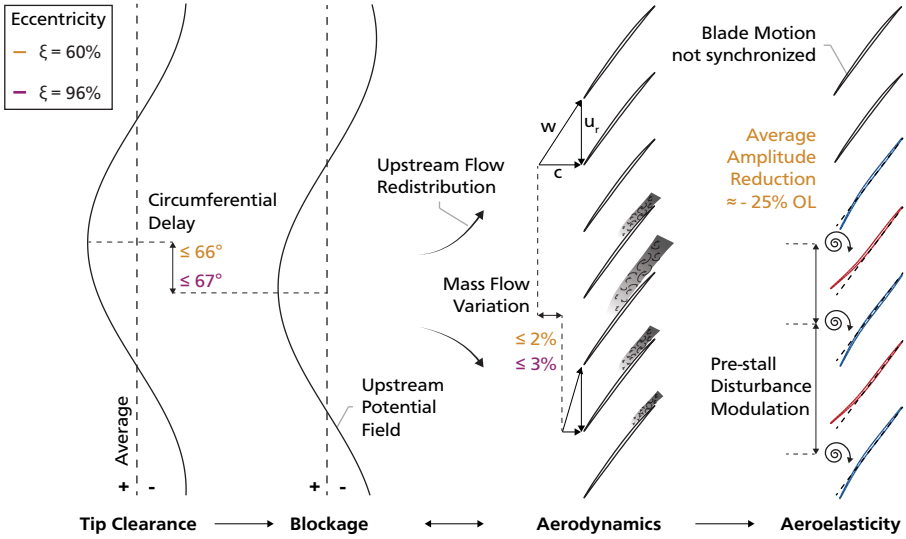

Figure 4.15: Effect of non-uniform clearance on aerodynamics and aeroelasticity

4.3 Effects on the Compressor's Stability at Part Speed

The previous section illustrated the effect of tip clearance and eccentricity on aerodynamics and aeroelasticity at design speed. In a multi-stage compressor, the front stages are highly loaded at part speed. As the current investigation uses a front stage design, issues in terms of stability are best addressed at part speed conditions with varying rotor speed and inlet guide vane angle (IGVA).

An unstable front stage turns into a problem if it leads to blade failure. The following analysis is therefore directed towards the occurrence of NSV and its avoidance.

So far, the results were largely based on individual measurements. Within the scope of this part speed study, five different rotor speeds and up to five different IGVA are investigated per configuration. The full database is summed up in Table A.4 in the Appendix.

4.3.1 Characteristics of Non-Synchronous Vibrations (*NSV*)

In this section, characteristics of NSV are analysed regarding tip clearance size (configurations CON-NOM, CON-MIN, CON-MAX) and eccentricity (configurations ECC-MIN, ECC-MAX). All tests are carried out, using the measurement procedure introduced in Figure 3.3b. The data are analysed in accordance to the analysis presented in Section 4.2.1. This analysis reveals the *total-to-static pressure rise*, *mechanical rotor speed*, *maximum vibration amplitudes* and the *count* and *speed of pre-stall disturbances*.

The subsequent evaluation includes all measurements during which NSV amplitudes of at least 15% operating limit (OL) occurred on any blade equipped with strain gauges[4]. The 1F mode is not included in the analysis, because according to the previous section - in case of this rotor - it should not be assigned to the identical vibration category.

Propagation Speed. In Figure 4.16a, the propagation speed of the aerodynamic disturbances during NSV (for lock-in conditions) are plotted. The propagation velocity is stated relative to the stationary frame of reference and in the direction of rotation. In the rotating frame of reference, the propagation direction is against the direction of rotation. Relative to the rotor speed, the propagation speed remains between 0.4 and 0.6 times rotor speed for all measurements carried out. In this range, the propagation speed is independent of tip clearance size, eccentricity and

[4] The vibrations occurred during the stall inception process, prior to rotating stall (1T and CWB mode). The maximum amplitude is taken, so the following data preparation is a worst case estimation.

also the number of aerodynamic cells. Tip clearance size is illustrated via marker size and eccentric measurements are highlighted via triangular markers.

The independence from cell count is worth noting because the variation of the cell count between 10 and 30 is large. However, this statement must be evaluated independently of the disturbance size. In the current thesis, no measurement equipment is used to resolve their radial extent.

The statement of constant propagation speed can most likely be generalized for compressors with a similar design, as numerous investigations of front stages revealed the same speed range for NSV (compare Table 2.1).

Disturbance Cell Count. An aerodynamic disturbance that consists of several cells and propagates relative to the rotor with a distinct speed results in a harmonic force on the rotor blades. This force can be expressed by reformulating Equation 2.9 and Equation 2.10:

$$f_{\mathrm{blade}} = \left(1 - \frac{v_{\mathrm{abs}}}{u_{\mathrm{tip}}}\right) f_{\mathrm{r}}\, n_{\mathrm{aero}} \tag{4.1}$$

Assuming constant propagation speed, this equation can be rearranged to evaluate the cell count n_{aero} that is required to excite the 1T and CWB mode at a certain speed. As a function of rotor speed, both modes are illustrated in Figure 4.16b, using an upper and lower theoretical boundary. For each natural frequency, the upper limit is calculated assuming a propagation speed of 0.6 times rotor speed. The lower one is defined by a speed of 0.4 times rotor speed. For instance, in case of the 1T mode, the cell count range decreases from about 30 at 6,000 rpm to about 12 cells at 20,000 rpm.

According to the presented dataset, NSV occurs across the whole mechanical speed range. Both, the 1T and CWB mode are subject to NSV, because the number of aerodynamic cells adjusts in a broad range between 10 and 30. If the aerodynamic cell counts during stall inception were known and remained constant for a given speed, NSV might be avoided. However, predicting the number of aerodynamic cells during stall inception - which includes pre-stall disturbances and rotating stall cells - is extremely difficult. Also, the findings by Holzinger (2017) and Brandstetter et al. (2018) or Figure A.9 show that the disturbance cell count varies over time during stall inception. Therefore, avoiding NSV remains a major issue.

Effect of Tip Clearance on Cell Count. A large clearance increases the probability of higher cell counts during stall inception. This results in an excitation of the CWB mode for configuration CON-MAX at high speed and configuration CON-NOM at part speed[5]. These findings are in agreement with numerical investigations by

[5] Due to reduced centrifugal forces, the tip clearance is also increased at low speed in this case.

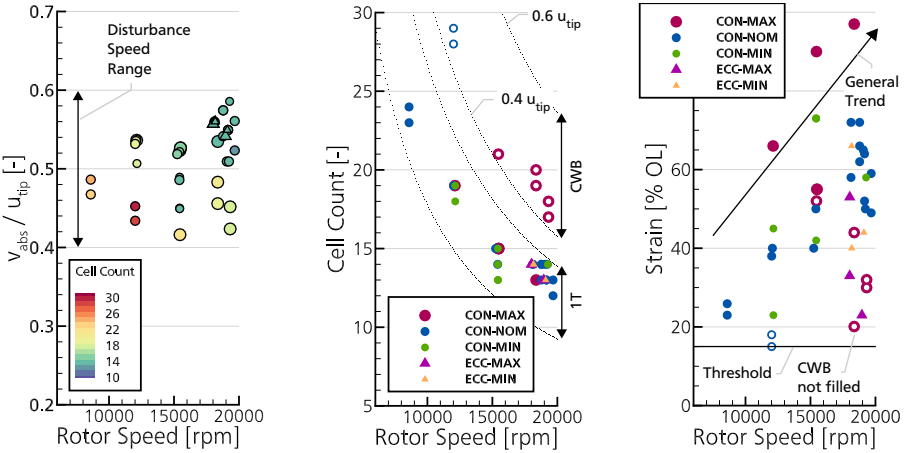

(a) Propagation speed of the aerodynamic disturbances

(b) Cell count of the aerodynamic disturbances

(c) Effect of clearance and eccentricity on NSV amplitude

Figure 4.16: Effect of tip clearance and eccentricity on NSV[a].

[a] Further illustration regarding the vibration amplitudes and the effect of IGVA is provided in the Appendix in Figure A.13

Möller et al. (2017) and fit to the observation that higher cell counts exist in the large clearance sector of an eccentric casing compared to the sector with a decreasing clearance (see Figure 4.12). Consequently, as wear mechanisms in an aero engine lead to an increase of the average clearance, excitations of higher modes become more likely in service.

However, a tight clearance does not necessarily lead to the prevention of NSV either. Even with a small clearance such as CON-MIN, NSV occurs at part speed conditions. So, a tight clearance cannot be used ultimately to avoid NSV. The statement is assumed valid until the rotor becomes hub-critical due to a clearance reduction.

Effect of Clearance and Eccentricity on Blade Vibration Amplitude. Figure 4.16c illustrates the amplitudes during NSV. There is a general trend of the maximum amplitudes that increase with rotor speed. This is most likely a result of the higher absolute pressure level with increased speed. For a multi-stage design, this means that R1 should preferably be exposed to flow separation at the

lowest speed possible via IGV scheduling. At high speeds, the risk of increased NSV amplitudes rises.

Of all configurations, the most critical rig commissioning was the one with a large concentric clearance (CON-MAX). 1T vibrations in the range 80 to 100% OL limit occur in this case. This is a result of an amplification of the tip flow unsteadiness (Möller et al., 2017, Holzinger, 2017). The increased blade tip fluctuations in turn cause higher blade vibration levels.

The effect of eccentricity on the amplitudes of 1T vibrations was described in the previous section at design speed. The stated trend is apparent at all speeds. The amplitudes of 1T and CWB vibrations are reduced by eccentricity in the entire operating range. No NSV data is viewed at low speeds in this case because the maximum amplitudes dropped mostly below the threshold of 15% OL.

Furthermore, Figure 4.16c shows that 1T vibrations are more severe than non-synchronous vibrations of the CWB mode. It is likely that a larger tip deflection of the 1T mode is the source for an increased amplification of the vibration amplitude. An increased leading edge deflection leads to an increased incidence, which in turn results in an amplified blockage generation and vortex development (reconsider Figure 2.6a). Assuming constant mechanical stress in the blade, the tip deflection of the 1T vibration is larger compared to the CWB mode.

Effect of Blade Design. Whether a blade design is susceptible to NSV or not, depends on both the natural frequency and the mode shape.

According to Equation 4.1, compressor blades with similar *natural frequency* are excited by an equivalent count of disturbances at a given speed (assumed constant propagation speed). Influence on blade aerodynamics aside, a varying blade count leads only to a change of the ND, meaning that the structural inter blade phase angle adjusts to the altered propagation time per passage. This also explains the stepwise changes of NDs during NSV if the blade natural frequency or mechanical rotor speed is varied. This was observed in numerical studies (Leichtfuss, 2015) and experimentally (Kielb et al., 2003). The influence of *mode shape* is implicitly included in Figure 4.16b. The 1T mode is of order two and the CWB mode is of order four. So the natural frequency of mode three is in the range of a possible excitation, but it is not an issue in terms of NSV. 1T and CWB vibrations have in common that both modes exhibit a strong deflection of the blades' leading edge (see Figure 2.6a). This is most likely the reason for their sensitivity to NSV because deflections of the leading edge vary the blade tip incidence.

The findings imply that during the design phase of a new compressor rotor, computation times might be reduced. As early as the natural frequencies of the blades are known, computations can focus on the stability of specific NDs because possibly exciting cell counts are pre-determined according to Figure 4.16b. In a sense, this

figure reveals NSV excitation in a certain speed range, comparable to a Campbell diagram regarding synchronous vibrations.

Effect of Mechanical Rotor Speed. As expressed by Equation 4.1, the mechanical rotor speed has an effect on the excitation frequency. A large amount of measurements with configuration CON-NOM in the speed range between 17,000 and 20,000 rpm revealed that the synchronisation of the 1T mode with pre-stall disturbances can also be avoided via mechanical speed changes. At this point, the data preparation used here has disadvantages because operating points without NSV are not displayed.

The dependency on rotor speed complicates the task of measuring aeroelastic phenomena in open cycle facilities. Ideally, mechanical rotor speed and corrected rotor speed are both considered. However, if the corrected speed remains constant, the vibration amplitudes are influenced by varying inlet temperature. For the comparison in Section 4.2.1, mechanical rotor speed variations ensure reliability of the findings. In this case, it is reasonable to assume that the interpretation in this form is consistent. However, caution is required if measurements involve several months of highly varying inlet conditions.

On the Mechanism of NSV. The concept of non-synchronous vibrations as blade instability (flutter) on the one hand and fluid dynamic instability (rotating stall) on the other was introduced in Section 2.3.2. In some cases, one instability dominates. For pure flutter for example, all self-sustaining pressure forces vanish if the blade motion is locked (Kielb, 2018).

This is not the case for NSV. However, the current results suggest that the mechanism is neither purely dominated by the blade nor the fluid. It seems that although the blade provides a very limited and well known unstable range (the blades' natural frequency), the instability of the fluid adapts in a broad range via various cell counts, which complicates predictions. The only constant of the fluid instability is its convective speed. For this reason, NSV is a concern throughout the entire operating range. A comparison of flutter design rules and NSV prediction methods are shown in the Appendix in Section A.7. Until today, simple analytical models fail regarding NSV.

The unsteady pressure forces and cell counts are not solely caused by the blade movement, they occur prior to the vibration onset. Holzinger (2017) and Brandstetter et al. (2018) showed that in the further course of the mechanism, large blade tip deflections lead to a self-enhancing mechanism whereby the blade vibration enforces a dominant wavelength. In other words, at certain blade vibration amplitudes, the periodic vortex separation is blade dominated (Brandstetter et al., 2018).

4.3.2 Application of Countermeasures

If future trends, such as higher overall pressure ratios, force front stage stall in a multi-stage compressor, IGV scheduling may reduce NSV amplitudes. However, this clearly seems to be no ultimate solution. Another approach are countermeasures that support the avoidance of NSV by an extension of the front stages' operating range.

A well-known method to extent the operating range of a compressor is the use of casing treatments (CTs, compare Section 2.3.3). Generally, the method is based on an aerodynamic optimization that aims to reduce blade tip blockage. The blockage reduction lowers stochastic flow fluctuations in the blade passage, which is in turn beneficial from an aeroelastic viewpoint (Möller et al., 2017, Holzinger, 2017).

The rotor under investigation is tip critical, which is a basic requirement to use the full potential of casing treatments (Greitzer et al., 1979). Previous studies have shown that a half-heart casing treatment leads to a discharge of the blade tip and a significant gain in stability. With regard to the aerodynamic design point, it was shown that the compressor does not suffer any loss of efficiency due to the treatment (Brandstetter, 2015). However, resonance phenomena that forced large blade vibrations were observed at design speed and raised concern regarding its use in an engine (Brandstetter et al., 2016, Holzinger, 2017).

In the following, this CT360 is examined with the aim of an engine application to improve the compressor's part speed stability.

Non-uniform tip clearance has shown potential in terms of reducing NSV amplitudes (Section 4.2.1). Consequently, in addition to the full-circumference CT360, a non-uniform configuration (named CT180) is investigated. In this setup, only a segment of 180° is treated with axial grooves. The remaining part is designed as smooth casing and corresponds to the clearance of the concentric reference CON-NOM[6].

The application of both casing treatments is reviewed in two steps. *First*, the comparability of configuration CT180 to the eccentric builds is examined aerodynamically. Therefore, performance measurements at design speed and static wall pressure measurements in the treated and untreated segment are analysed.

Second, the effect on vibration amplitudes and the extension of the stable operating range are investigated relative to configuration CON-NOM. In line with the previous section, the rotor speed and IGVA are varied.

[6] Without consideration of the grooves, the clearance is also equivalent to CON-NOM in the CT segment

Design Considerations. In order to describe the mass flow redistribution upstream of the inlet in a compressor with a non-uniform tip clearance, the parallel compressor theory is used. It was demonstrated for a compressor with an eccentric tip gap that the assumptions are also valid to model the throughflow of a transonic compressor. Concentric setups corresponding to the respective extreme clearance of the eccentric case were examined. The same analysis is now applied to the measurements with smooth casing, full-circumference and segmental CT.

In the present case, the smooth casing configuration and the full-circumference CT360 define the boundaries for CT180 in terms of local pressure rise and mass flow capacity of the stage. In Figure 4.17a, the total-to-total pressure ratio is plotted against mass flow density for each stator exit passage. The calculation of Π^{30}_{t-t} is outlined in Section A.2. Pressure ratio and mass flow density are referenced to the DP. For the uniform configurations, the flow is assumed to be periodic by one stator pitch and thus representative for the entire exit surface. So, the averaged values of one stator exit passage are illustrated. In case of configuration CT180, the averaged values of each stator exit passage are shown individually. Accordingly, the individual

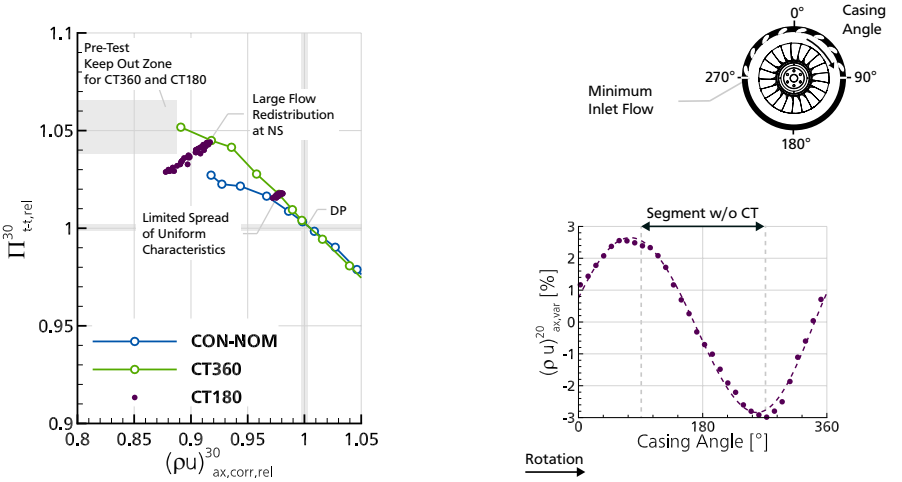

(a) Stage pressure rise against mass flow density at stator exit

(b) Maximum and minimum inlet mass flow relative to treated segment of CT180 at NS operation

Figure 4.17: Evaluation of casing treatment configurations at design speed

marker represent the variation of the local total pressure and mass flow rate at the exit of the stage.

Figure 4.17a reveals that the total pressure rise and mass flow rate of the segmental CT180 are limited by the two extreme cases. The circumferential redistribution of mass flow occurs comparable to an eccentric casing. In that case, more mass passed the sector with a small clearance. With the partial CT180, blockage is reduced in the sector of the casing treatments, which leads to an increased mass flow capacity.

It was found in Section 4.1.5 that non-uniform tip clearance results in an inlet distortion for subsequent stages. This distortion was discussed as total pressure distortion. To address this aspect, the total-to total pressure rise at stator exit is selected for visualisation in Figure 4.17a[7]. In other words, the total pressure distortion to a downstream stage is shown. The distortion is small close to the DP and grows when stall is approached. Note that in case of CT360 and CT180, the dataset does not represent the stability limit. The measurements were stopped prematurely, due to resonance effects at design speed (Brandstetter et al., 2016, Holzinger, 2017). Whether resonance effects occur for configuration CT180 is questionable, but remains undetermined, because measurements were prohibited in that area.

Close to the aerodynamic design point, the pressure rise and mass flow characteristic of CON-NOM and CT360 differ only slightly. Consequently, only a limited amount of flow redistributes in the compressor with the segmental CT. However, for NS operation[8], the blockage in the CT segment is significantly reduced, which results in a greater circumferential redistribution of the mass flow.

The amount of redistributed mass is based on the characteristics of the uniform configurations. Thus, if the spread of the uniform characteristics is large, the amount of redistributed mass is large and vice versa. As long as the operation of both configurations remains stable, the redistribution in a non-uniform casing is a direct result of CFD simulations of the local extremes. This is of great value during the aerodynamic design of a compressor.

The axial position of the grooves determines the impact of the casing treatments from choke to stall (reconsider Figure 2.9). Consequently, the present spread of the smooth casing and CT360 characteristic is a result of this axial position. It is still difficult to evaluate the optimal axial position, pitch and groove size of casing treatments. The stated aspect is a further example of the necessity to improve numerical tools in order to better understand and optimize CT designs.

[7] In Figure 4.5a, The total-to-static pressure rise was used to illustrate the inlet and outlet pressure constraints of the stage that enforce circumferential flow redistribution. Higher local mass flow generates an circumferential variation of the dynamic pressure, which influences the total-to-total pressure rise.

[8] The integral inlet mass flow is the mass flow near stall of the smooth casing reference.

In Figure 4.17b, the redistribution of the inlet mass flow is shown. The variation is calculated in the same way as in Figure 4.5b. The segment without CT spans from 90° to 270°. The lowest inlet mass flow occurs at angle 270°. Considering the direction of rotation, this angle corresponds to the end of the segment without CT. Through the region without CT, the mass flow continuously decreases, which is related to the increase of the blockage in the rotor. Vice versa, the reduction of the blockage causes an increase of the mass flow in the CT segment.

Thus, according to the local blockage in the rotor, the mass flow is redistributed circumferentially at the stage inlet. This is absolutely similar to the eccentric configurations. In contrast to a compressor with eccentric clearance, the highest and lowest inlet mass flow enter the stage right at the border between the casing treatment segment and the smooth casing. Hence, the circumferential delay of the blockage growth and its degradation relative to the local clearance is smaller. This is most likely a result of the abrupt change of the casing geometry and the immediate blockage reduction via the casing treatment.

The spread of the uniform compressor characteristics indicates the amount of mass flow that is redistributed. As a result, the increase of the redistribution from DP to the stability limit is different in case of the segmental CT180 compared to an eccentric casing. This is illustrated in Figure 4.18.

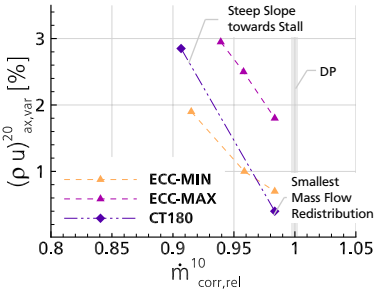

Figure 4.18: Mass flow redistribution at stage inlet - Cross-comparison of configurations with eccentric clearance to segmental CT

The circumferential variation of the inlet mass flow is plotted against the integral mass flow at the inlet. The mass flow is referred to the DP. Towards stall, the flow redistribution at the inlet rises less strongly in case of configuration ECC-MIN, compared to the case with large eccentric clearance (ECC-MAX). This results from the greater clearance variation across the circumference and the stronger blockage variation.

For the segmental CT180, the slope of the redistribution is largest. Whether the increase is linear or non-linear remains undetermined. Close to the DP, the CT180 exhibits the lowest inflow asymmetry. Towards the stability limit, the blockage variation is increasing the most. So regarding mass flow, blockage and incidence variation, CT180 is an extreme form of tip clearance non-uniformity.

Note that in case of the partial CT180, a ±3% mass flow variation is not the extreme case. The measurements at lower mass flow were prohibited.

These findings are an advantage regarding engine design, if the partial casing treatment is applied to aerodynamically mistune the part speed operation only. At design conditions, the engine operates without an additional circumferential total pressure distortion. Towards the stability limit, rotor tip incidence varies circumferentially (just as in a compressor with eccentric clearance), which was found being beneficial regarding NSV. This is demonstrated for configuration CT180 below.

Effect of Segmental Casing Treatment on Rotor Tip Flow. In the following, the rotor relative flow is analysed at part speed N80. The analysis further evaluates the comparability to the eccentric configurations.

Measurements of the casing static pressure at the rotor tip are shown in Figure 4.19. The probes are located 34° ahead of the exit of both segments.

The largest and smallest mass flow enters the stage at 90° and 270°, respectively (reconsider Figure 4.17b). Hence, the probes have an offset of about 34° to the location with the largest and smallest mass flow. However, the measurement positions are located well within the respective segment, so that the result of decreasing and increasing tip blockage is demonstrated.

In order to interpret the measurements, it must be considered that the measuring positions of the wall pressure were not moved relative to the CT slots (see Figure 4.19a). Only the rotor moves past the probes and slots.

Data are recorded simultaneously in the smooth and treated segment. The data analysis is similar to Figure 4.8.

At casing angle 56°, the higher inlet mass flow results in a stronger static pressure reduction upstream of the leading edge. Compared to the segment without CT, the rotor generates more static exit pressure, i.e. it is subjected to a higher aerodynamic loading in the CT region.

The measurements are conducted at steady-state conditions NS. At casing angle 236°, however, disturbances occur between the leading edges of the blades. This is very similar to the observations made for the eccentric configuration ECC-MAX at design speed (compare Figure 4.8).

In Figure 4.19c, the disturbances in the individual passages are highlighted. Reference pressure for the pressure deviation is the dynamic pressure at the rotor inlet. It is calculated, using the unsteady static pressure of the first upstream wall pressure transducer and the total pressure of the settling chamber. Downstream of the CT slots, small-scale disturbances occur. These are most likely a result of the interaction of the CT injections with the tip leakage flow. In the segment without CT, pre-stall disturbances evolve between the leading edges of the blades. On average,

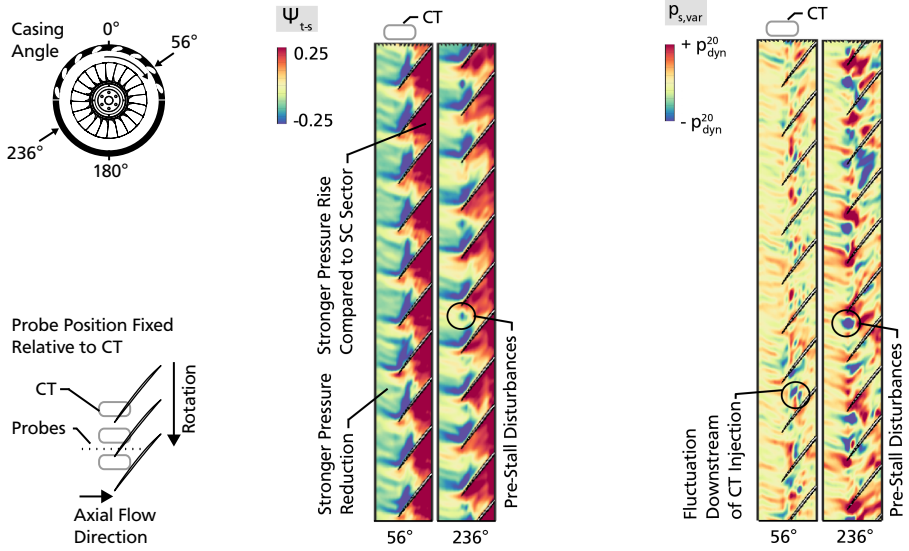

(a) Probe positions and measurement procedure

(b) Instantaneous distribution of total-to-static pressure rise coefficient

(c) Pressure deviation from ensemble average

Figure 4.19: Part speed operation N80 with segmental treatment CT180 at NS operation

these are measured in the stationary frame of reference at a distance of less than two blade passages.

Therefore, for configuration CT180, the leading edge position is best in order to analyse stall inception circumferentially.

The spectra of seven leading edge sensors are shown in Figure 4.20. They are recorded during stall inception at part speed N80. Their circumferential measurement position is indicated in the centre of Figure 4.20. The spectrogram and the maximum amplitudes during the manoeuvre are plotted. Engine orders are resolved by $\Delta EO = 0.025$ and revolutions by $\Delta revolution = 21$ for sufficient resolution in both, the time and the frequency domain.

The probe positions are not close enough to identify the evolution of disturbances in detail and to obtain the exact boundaries of increasing, constant and decreasing

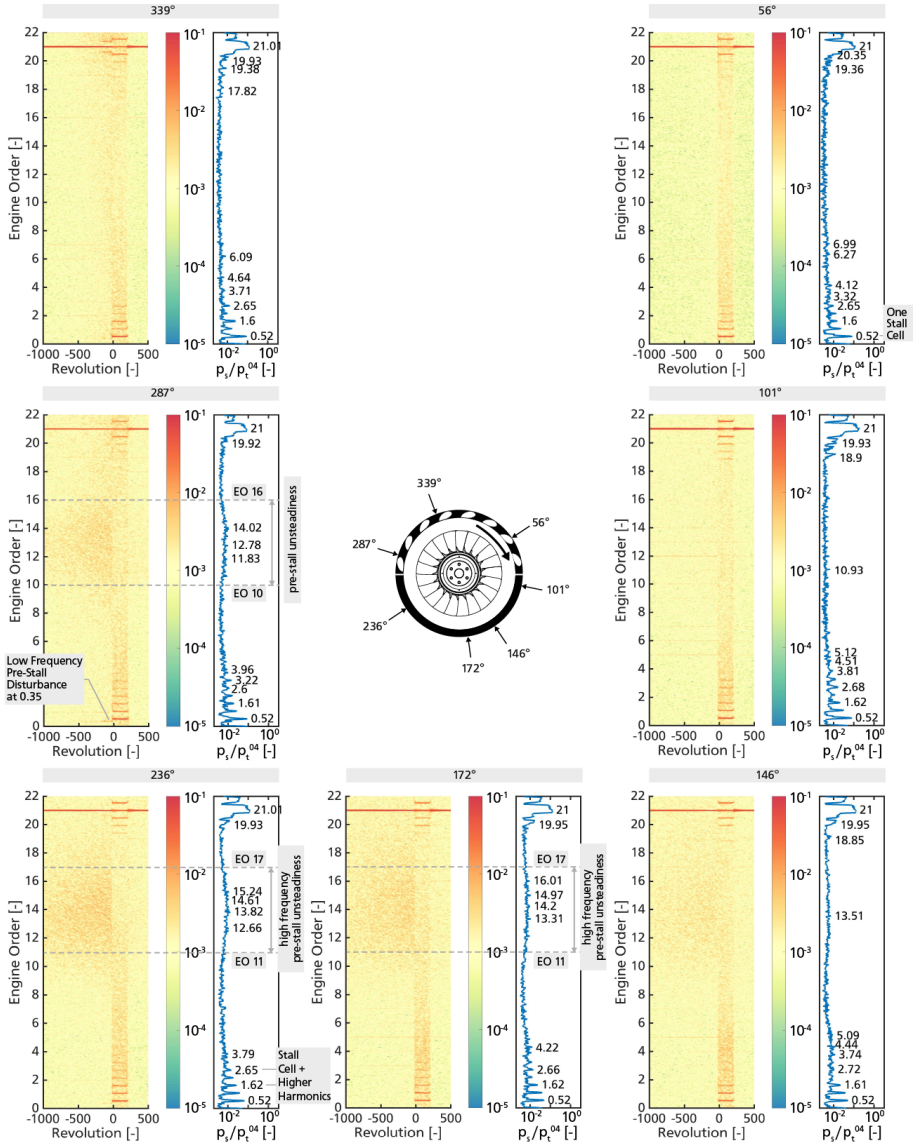

Figure 4.20: Stall inception in a configuration with segmental casing treatment (CT180) at part speed N80. Unsteady pressure transducers at 8% chord, downstream of the rotor LE are illustrated.

disturbance size. However, some statements can still be made regarding their rise and decay.

In the segment between 172° and 270°, pre-stall disturbances occur. The largest amplitudes are reached at the end of the smooth casing segment. From casing angle 236° to 287°, the upper and lower limit of the pre-stall unsteadiness decrease from EO 17 to 16 and EO 11 to 10, respectively. Assuming a constant propagation speed, this implies a reduction of the disturbance count.

As the rotor passes 70° (probe position at 339°) of the treated segment, the disturbances decay. Thus, a sector of 70° might be sufficient to suppress an uniform evolution of pre-stall disturbances and subsequently reduce NSV amplitudes.

Already Cumpsty (1989) assumed that the sector without CT controls the stall margin. For the current case, it takes about 146° (begin of smooth casing segment until probe at 236°) for the disturbances to evolve and increase in amplitude. Hence, an equally efficient setting (compared to configuration CT180) to reduce NSV amplitudes without the cost of stability, might consist of two treated segments, which are 180° apart and cover 70° each.

The operation is limited by a rotating stall cell that propagates with a cell speed of about 52% rotor speed. Before, a disturbance occurs at EO = 0.35 that is measured at the entry to the treated segment at casing angle 287° and reduced in amplitude at 339°. This is a common propagation speed for modal waves, i.e. long-lengthscale disturbances. A closer analysis indicates their occurrence in the region of minimum inlet mass flow only (see Figure A.12). It is likely that these low frequency disturbances evolve in the smooth casing segment, are measured at angle 287° (with smaller amplitude at 339°) and decay in the treated segment. The exact cause of this change to modal activity that occurs only at certain casing angles, remains unclear. However, similar changes of the stall inception mechanism (that becomes a combination of both spike and modal type) were observed before in compressors with large clearance and eccentricity (Young et al., 2016) as well as in compressors with distorted inflow (Longley, 1990).

Supplementary, the spectrum of the strain gauge signal is illustrated in Figure A.11c in the Appendix.

Effect of Casing Treatments on NSV and the Stability Margin. According to the previous analysis, the operation with a partial casing treatment is aerodynamically comparable to the operation with an eccentric casing. The circumferential redistribution of mass flow and tip incidence variation is accompanied by the rise and decay of pre-stall disturbances.

The aeroelastic results of measurements at three different part speeds and up to four IGVA are outlined in the following[9]. The full-circumference CT360 and the segmental casing treatment CT180 are compared to the reference with solid wall CON-NOM. The outcome is used to derive recommendations for the use in an engine.

All measurements are analysed equivalently to Section 4.2.1. The focus of the analysis is to determine the 1T vibration amplitude of the blades during the throttling process and the stability margin improvement. As described in Section 4.2.1, variations of the individual blade amplitudes occur. To take this blade to blade variation into account, the maximum and minimum amplitudes of four strain gauges are evaluated and displayed.

In order to analyse the stability improvement, exit flow function was suggested in Section 2.4.2. For the results presented in the current section, exit pressure and temperature can not be determined with sufficient accuracy, as no stage exit area traverses exist for these unsteady measurements. Instead, the minimum inlet mass flow is evaluated. At part speed, defining the stability improvement via mass flow instead of pressure rise is appropriate, because the slope of the characteristics is rather flat. The common definition

$$\Delta \mathrm{SM} = \frac{\dot{m}^{10}_{\mathrm{corr,ref}} - \dot{m}^{10}_{\mathrm{corr,min}}}{\dot{m}^{10}_{\mathrm{corr,ref}}} \tag{4.2}$$

is used. There are some uncertainties in the determination of the stability margin, which is difficult to quantify. However, for the full-circumference CT360, all measurements were performed twice, which is illustrated in Figure 4.21b via error bars. This is not intended as an indication of a statistical error, but to emphasize the limited resolution of the measurements. The results are normalized by the stability margin of the reference CON-NOM.

Figure 4.21a illustrates the vibration amplitudes of the 1T mode during stall inception at three part speeds (N45, N63 and N80). For the smooth casing configuration, the maximum vibration amplitudes reach up to 50% of the rig operating limit (OL). The amplitudes vary between 5% (not considered as NSV)[10] and 50% across all speeds and IGVA[11]. In case of the full-circumference CT360, the measurements show that the application of the casing treatments leads to even stronger 1T vibrations. The maximum vibration amplitudes reach up to 80% of the OL limit. On average,

[9] For configuration CT360, all corrected speeds are measured twice at different inlet conditions. For an overview of the full database refer to Table A.4.

[10] For the previous analysis in Section 4.3.1, 15% OL was used as reasonable threshold.

[11] IGVA is varied between 0% and 100% according Table A.3. The extensive influence of IGVA closure on total-to-static pressure rise is indicated in Figure A.13b.

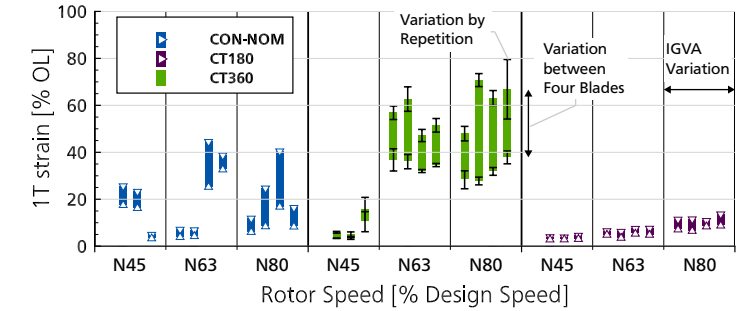

(a) 1T vibration amplitude at various speeds and IGVA closures (i.e. rotor pre-swirl)

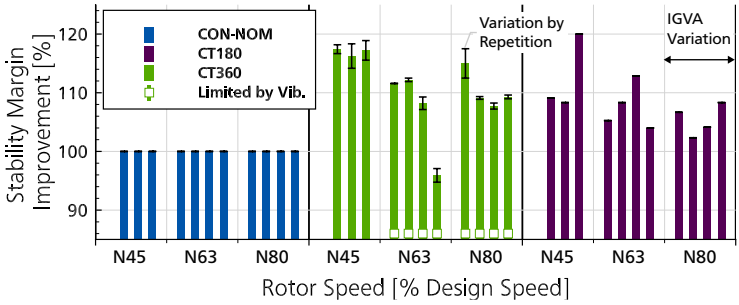

(b) Stability margin at various speeds and IGVA closures (i.e. rotor pre-swirl)

Figure 4.21: Overview on part speed improvements with full-circumference CT360 and segmental CT180 compared to smooth casing reference CON-NOM

the maximum amplitude is 49% for rotor speeds N63 and N80. Therefore, the average level of NSV amplitudes is higher than for the reference with a smooth wall. However, for configuration CT180, the maximum amplitudes remain below 15% at all part speeds. In that case, the average amplitude level increases continuously from 3.5% at N45 to 5.7% at N63 to 9.7% at N80.

For configuration CT360, high vibration amplitudes (at least one blade above 50% OL) limited further throttling in some cases. These measurements are aborted prior to the evolution of rotating stall and labelled as *Limited by Vibration* in Figure 4.21b. This means that the amplitudes shown for configuration CT360 in Figure 4.21a, are not even worst case.

Previously assumed that the stability limit of the segmental CT180 is in between the smooth casing reference CON-NOM and the full-circumference CT360, the results in Figure 4.21b are rather heterogeneous. This is most likely a result of the measurement uncertainty and also due to the fact that the operation is not purely constraint by aerodynamics. Hence, the comparison of these configurations in terms of stability margin does not reveal a clear pattern. Only at N80, the stability margin in case of the full-circumference casing treatment is extended compared to the partial casing treatment for all IGVA. For one inlet guide vane angle at part speed N63, due to large pre-stall amplitudes the stability limit of configuration CT360 does not even exceed the reference, which highlights more disadvantages of a full circumference casing treatment.

However, the stability improvement in case of the partial CT180 compared to the smooth casing is significant. At all speeds and IGVA, the operating range is extended. Taking into account the reduction of the 1T vibration amplitudes, configuration CT180 not only expands the operating range, but also reduces NSV amplitudes considerably. Thus, a segmental treatment is a more effective method of reducing NSV than a full-circumference casing treatment.

4.3.3 Intermediate Conclusion

In this section, characteristics of NSV were discussed. The analysis suggests potential to reduce computational effort regarding the aeroelastic design process of compressors in the future and shows that measures against NSV are needed. Novel approaches of these measures were examined. The findings support the investigations with an eccentric rotor clearance and highlight non-uniform tip clearance as a new idea in the context of aerodynamic mistuning. In short, the analysis revealed:

- For lock-in conditions, the propagation speed of aerodynamic disturbances varies in a range between 0.4 to 0.6 times rotor speed. This is in agreement with numerical results from Möller et al. (2016). In this range, the propagation speed is independent of tip clearance size, eccentricity and number of cells. The finding can most likely be generalized for aero engine front stages as it is in good agreement with the literature (compare Table 2.1).

- The broad range of cell counts between 10 and 30, leads to interactions with the 1T and CWB mode. As a result, NSV occurs in a wide range of rotational speeds. For a certain rotor speed and natural frequency of a blade, the interacting cell counts are pre-determined so that the number of aeroelastic simulations required might be limited in the future.

- Day (2016) emphasized that predicting the number of cells and their speed is still problematic in case of rotating stall. The prediction of NSV is at least as

complicated as a pure aerodynamic prediction of the failure mechanism. An improvement of the stall cell prediction and the stall evolution might also help in predicting NSV more accurately.

- A large clearance increases the probability that higher aerodynamic cell counts evolve. This is in agreement with the numerical analysis by Möller et al. (2017). Wear mechanisms in an aero engine lead to an increase of the average clearance that is likely to increase excitations of higher modes, such as CWB. Additionally, the blade vibration amplitudes of 1T are amplified by large clearances. However, a tight clearance can not be used to ultimately avoid NSV. The statement is assumed valid until the rotor becomes hub critical due to a clearance reduction.

- Eccentricity reduces NSV amplitudes at part speed. This adds to the analysis at design speed presented in Section 4.2.1. The operation with a partial casing treatment is comparable to the operation with an eccentric casing. The circumferentially varying blockage results in a redistribution of mass flow and an altered tip incidence that is accompanied by the rise and decay of pre-stall disturbances between the leading edges of the blades.

- In a non-uniform casing treatment, the highest and lowest inlet mass flows occur right at the transition from the casing treatment segment to the smooth casing and vice versa. This is in agreement with previous findings by Cumpsty (1989). This example highlights that the circumferential delay of the largest blockage formation depends on the adjustment of the flow relative to the local tip clearance. Whether the clearance is continually changing, such as in an eccentric casing (reconsider Section 4.1.3), or by sudden changes, such as with partial casing treatment, is decisive for the underlying time scale.

- At the design point, the partial casing treatment does not lead to an additional distortion at the exit of the stage. However, towards the stability limit, mass flow is redistributed circumferentially. The amount of redistributed mass increases stronger compared to an eccentric casing. From that perspective, dependent on CT design, a partial casing treatment is an extreme form of tip clearance non-uniformity. This is highly beneficial regarding an engine application.

- The amount of redistributed mass is based on the characteristics of the uniform configurations that represent the local extremes of a non-uniform configuration. So, if the spread of the uniform characteristics is large, the amount of redistributed mass flow is large and vice versa. This aspect can be used for future non-uniform casing treatment designs (e.g. for a redesign of the axial

groove position, groove size/depth or count). The finding corresponds to the investigation by Plourde and Stenning (1968), who found equivalent results regarding compressors with distorted inflow. In that case, the impact on flow redistribution also depends on the slope of the characteristic.

- A full-circumference casing treatment does not necessarily lead to a reduction of NSV amplitudes and an extended stability margin. There exists a possibility of a negative impact on blade vibrations. In contrast, a partial casing treatment can significantly reduce NSV amplitudes (below 15% rig operating limit) and expand the stability compared to a smooth casing.

- For the current case, it takes about 146° (begin of smooth casing segment until probe at 236°) for pre-stall disturbances to evolve and increase in amplitude. Hence, an equally efficient setting (compared to configuration CT180) to reduce NSV amplitudes without the cost of stability, might consist of two treated segments, which are 180° apart and cover 70° each.

The results of this section support and extend the already presented findings on eccentric casings. In general, the so far rather negative understanding of casing asymmetries seems inequitable. In the future, these asymmetries might represent a novel design strategy for aero engines.

4.4 The Research Results in an Expanded Field of Vision

Aero engine compressors are built increasingly lightweight. This can be achieved firstly through thinner structural designs and secondly by reducing the number of individual stages. At the same time, there is a trend towards increased overall pressure ratios across the compressor. Taken these future goals together, the front stages are at risk in terms of non-synchronous vibrations.

Non-synchronous vibrations are caused by the unsteadiness of the flow close to the stability limit. In the part speed regime of an engine, the front stages of the compressor are operated near or beyond the stability limit at any point. This operating point can be shifted, for example, via variable guide vanes or interstage bleed. However, as the vibrations do not only occur in a certain operating range and at a certain speed, countermeasures such as mistuning must be taken (Section 4.3.1).

For the rotating component - the rotor - two types of mistuning exist. First, random mistuning that is caused e.g. by wear or geometry deviations as a result of manufacturing. Second, intended mistuning that is a concious choice of engineers to reduce the risk of non-synchronous blade vibrations. Both can lower the amplitude of blade vibrations (Castanier and Pierre, 2002). The use of intended mistuning requires more than one aerodynamic rotor design of the same quality or the will

to sacrifice compressor performance. However, a loss of efficiency is usually not acceptable. So far, research addressed rotor mistuning in the context of flutter. Whether rotor mistuning also reduces blade vibration levels with regard to NSV remains to be demonstrated. First experimental results that connect both topics are promising (Holzinger, 2017).

For the first time, the results of this thesis demonstrate that random and intentional mistuning exist for the stationary part - the rotor casing - in the context of NSV. In general, the approach is novel regarding non-synchronous vibrations and might also work for blade flutter.

Thin and unevenly cooled compressor casings or in-service rub-ins result in permanent *random mistuning* of engine casings. This could have a stabilizing influence on vibration amplitudes during operation (Section 4.2.1). In addition, there is potential to reduce blade vibration amplitudes via *intended mistuning* of the casing e.g. via partial casing treatments (Section 4.3.2).

There is no loss of performance if the casing treatment has no negative effect on efficiency (Section 4.1.1 and 4.3.2). As a bonus, the stability margin of the rotor is extended compared to a smooth casing (Section 4.3.2).

As non-uniform casings cause excitations at low multiples of the rotor speed, such a geometry must be questioned regarding a negative effect on synchronous vibrations. In service of an engine, low engine order excitations such as inlet distortions, non-uniform intakes or side winds demand design strategies. An approach that appears rather simple, is to design the natural frequency of the lowest blade mode above a certain engine order at maximum engine speed. Although not shown, this is the case for the test rig. Consequently, a strain gauge analysis of accelerations and decelerations in the entire operating range of the rig clearly revealed no negative effect on synchronous vibrations.

Inlet distortions to downstream stages that originate from non-uniform front stages are also in an acceptable order of magnitude (Section 4.1.1). In case of partial casing treatments, the circumferential mistuning evolves only close to the stability limit (Section 4.3.2).

The advantages of intended casing mistuning are considerable. Aero engine casings are often split in two halves (Figure 1.3a). If the casing treatments are designed in the upper half of the compressor, there exists a lower risk of casing treatment malfunction due to icing. The other half of the casing can be run with an abradable liner to achieve tight clearances and high compressor efficiency. For this reason, the use of the results is large for the aero engine industry and in a wide range of applications. In principle, only the rotor design must be tip critical. Together with

Rolls Royce Deutschland Ltd & Co KG, a patent application has been filed that covers fans and front stages of intermediate and high pressure compressors (Giersch et al., 2018).

Partial casing treatments are not a completely new idea. To improve stability, they were also suggested by Page et al. (2017). Their viewpoint was purely aerodynamic. They stated the idea in the context of inlet distortions to fan stages, because inlet distortions vary the aerodynamic loading of the rotor during one turn. The investigation of partial casing treatments on fan stages may also be potential from an aeroelastic point of view.

Related studies are also available in the field of inter-stage compressor bleed. Non-uniform bleed extraction was analysed by Grimshaw et al. (2015, 2016). They found a significant variation of the rotor incidence that had an impact on stall inception. In their analysis, an investigation of non-synchronous vibrations was not included. Common bleed rates are in the order of 5 to 20% (Di Mare et al., 2006, Young et al., 2011). In the scope of the current work, significant improvements regarding blade vibrations were already found for an inlet mass flow variation of about 3%. Hence, there is also potential in the field of non-uniform bleed take-off. Its use to prevent stall induced vibrations was covered by a patent from General Electric (Schirle et al., 2008).

5 Conclusion

The findings of this work weaken aerodynamic and mechanical concerns regarding axial compressors for small core applications. The work highlights potential to reduce design conservatism and introduces non-uniform rotor tip clearance as a novel approach to aerodynamic mistuning.

5.1 The Big Picture

In order to design future aircraft engines more efficient, less polluting and more silent, it is essential to further improve the compression system. Via improvements of the compressor's overall pressure ratio, the core engines are reduced in size while their power output is maintained. In particular, this increases the bypass ratio, which essentially contributes to an improvement of the engine in terms of efficiency, pollution and noise.

Downsizing of the core engine increases the relevance of rotor tip clearance effects and any non-uniform shape of the casing. Additionally, contacts of the rotor with the casing occur in service of an engine. As a result, abradable liner are evenly and unevenly removed by these rub-ins, which in turn leads to a deterioration of the compressor. The reduction of the sensitivity to tip clearance effects is hence one of the major goals of current compressor research.

In a multi-stage axial compressor, front stages operate with supersonic flow at the blade tip. At part speed of an engine, the stable operation of these stages is endangered, which results in mechanical problems, blade cracks or a loss of rotor blades in the worst case.

The development towards higher overall pressure ratios increases these blade vibration problems, as it is increasingly difficult to match the individual stages at off-design conditions. Therefore, stabilizing measures such as casing treatments are part of today's design processes.

In the current work, a compressor front stage was operated at high speed. The investigation was carried out on TRL 4, i.e. all relevant characteristics of front stages were replicated at the test rig. Measurements revealed the effect of uniform tip clearance, eccentric tip clearance and partial casing treatments on aerodynamics and aeroelasticity with a detail unattained so far. The major findings are as follows.

Regarding Uniform Clearance. The measurements reveal that modern features, such as forward sweep, do not significantly reduce the tip clearance sensitivity compared to previous studies. Instead, the measured performance degradation is in

line with previous studies throughout the last century. However, it must be noted that the aerodynamic loading of the stage is substantially higher compared to early research.

Large tip clearance increases the risk of non-synchronous vibration with severe amplitudes and higher blade mode excitations. Thus, in future engines, wear mechanisms or larger initial clearance contribute to an amplification of the blade vibrations in front stages. A tight clearance does not solve the problem of NSV either. As long as the rotor design remains tip critical, a reduction of the tip clearance size does not ultimately prevent non-synchronous vibrations at part speed. Aerodynamic cells with counts in a broad range between 10 and 30 propagate with a speed of about 0.4 to 0.6 relative to the rotor and result in an excitation of the blade vibrations in the entire rotational speed range.

Regarding Eccentric Clearance. As long as the average clearance remains constant, an eccentric tip clearance does not have a negative impact on the pressure rise and efficiency of a stage. In terms of stability, the influence of eccentricity is not as severe as simple rules of thumb suggested since the mid-1980s. Instead, the current findings highlight that the largest clearance does not limit the compressor operation. The tests reveal that inlet distortions to downstream blade rows due to eccentricity in front stages are negligible. Moreover, no negative effect on synchronous vibrations exist if the lowest natural frequency of the blades is above fundamental engine orders at maximum rotational speed. Consequently, the current work suggests potential to reduce compressor design conservatism regarding non-uniform tip clearance.

The parallel compressor theory is generally used, in order to describe the mass flow redistribution upstream of the inlet in a compressor with a non-uniform clearance. It was demonstrated that the assumptions are valid to model the throughflow of a transonic compressor. The circumferential delay of the largest blockage relative to the largest clearance depends on the time scale of the blockage generation and its reduction. This time period is associated to the adjustment of the flow relative to the local tip clearance. Whether the clearance is continually changing, such as in an eccentric casing, or suddenly changing, such as with partial casing treatment, is decisive.

The mass flow redistribution generated upstream of the compressor results in a circumferential incidence variation which in turn varies the aerodynamic force on the blades. Consequently, the rotor relative flow recovers during one turn, which lowers blade vibration amplitudes.

Regarding Non-Uniform Clearance. As non-synchronous vibrations occur in fact throughout the entire operating range of a compressor, countermeasures such

as mistuning must be taken. To lower vibration amplitudes, the current findings highlight potential of random and intended mistuning of the compressor casing. The circumferentially varying aerodynamic force on the blades prohibits an evolution of coherent aerodynamic and structural waves that lowers blade vibration amplitudes.

Thus, slight clearance imperfections in engines have a stabilizing influence on blade vibration. E.g. an eccentric tip clearance reduces the amplitudes of non-synchronous vibrations by -25% of the rig operating limit, compared to an uniform casing with the same average clearance.

Partial casing treatments benefit from the equivalent effect and are hence a novel design tool to consciously avoid non-synchronous vibrations. In contrast to a circumferentially uniform casing treatment, non-uniform designs are a smart solution to the problem of non-synchronous vibrations at off-design conditions.

5.2 Recommendations for Future Research

Limitations of the current work demand future investigations. These fall into three categories: *Experimental Work, Numerical Studies and Engine Applications.*

Experimental Work in Low Speed Facilities. For the current thesis, the circumferential variation of fluid-structure interaction was derived from measurements in the stationary frame of reference. Blade mounted pressure transducers on a rotor that is run in a non-uniform casing would deepen the insight, because they would directly resolve the unsteady pressure force on the blade surface.

Unfortunately, the last approach at the Darmstadt Transonic Compressor in the framework of the FUTURE project highlighted that this is very challenging in a high speed facility. The transducers were lost early during the measurements and the rig infrastructure was at risk.

A study of the unsteady blade surface pressure is consequently worth carrying out in a low speed facility. These measurements would clarify the aerodynamic forcing on the rotor in a non-uniform casing - even if these blades are not susceptible to blade vibrations.

Experimental Work in High Speed Facilities. To extend the findings of the current work, a subsequent study is needed to investigate a variety of eccentric casings with constant average clearance. This variation would provide a correlation of the blade vibration amplitudes to the amount of redistributed mass flow at the stage inlet. During the current work, eccentricity was not varied for several designs with the same average clearance. Such an analysis would also reveal the influence of tip clearance non-uniformity on the stability margin at more detail.

Work in a high speed facility is also needed to further investigate other concepts of stationary aerodynamic mistuning as well as rotor mistuning in the context of

NSV. First, by varying the inlet guide vane angle non-uniformly. In that context, the current results indicate that a variation with a large circumferential wavelength in the order of the compressor circumference is promising. Second, mistuning could be applied by designing an axial groove casing treatment with altered spacing or groove sizes/depths. Such a design might solve the problem of casing treatment resonances at design speed and can benefit from the results of the current work. Third, a casing with segments that are treated with grooves of variable circumferential extent would reveal the necessity of a minimum covered angle (the current work suggests 70°) and its effect on stability margin. Fourth, experiments are needed that connect intended rotor mistuning to the topic and mechanism of NSV.

Detailed analyses of the evolution of pre-stall disturbances and the NSV mechanism are still needed. High speed PIV in a transonic compressor would resolve adjacent rotor pitches and both, the blade tip deflection and the associate passage flow in one image. Such measurements would provide valuable insight to the mechanism of stall inception and stall induced vibrations for a compressor with flexible blades.

Also, a rotor that does not suffer NSV - e.g. Darmstadt Rotor 1 - would provide worthwhile information on the evolution of rotating stall. Large clearance widths and operating conditions that result in an evolution of rotating instabilities are of particular interest.

If a high speed PIV cannot be made available, a novel use of the PIV system already available at the Institute of Gasturbines and Aerospace Propulsion would be to analyse stall inception via steady-state measurements. The stall inception process is normally a brief transient with an unknown start time, but can be studied quasi-steady in the unstable sector of a compressor with non-uniform clearance, as the entire operation of the stage remains stable. These measurements would be insightful regarding the onset of rotating stall.

The process of stall inception is still part of ongoing research. Mass flow fluctuations downstream of the rotor, measured via a highly sampled hot wire would uncover effects unconsidered at the Darmstadt Transonic Compressor so far. In combination with unsteady pressure transducers, e.g. such measurements can resolve the hysteresis during stall. Radially distributed hot wires might additionally expose the stall cell size evolution during stall inception.

Also, upstream of the rotor, hot wire probes measuring unsteady incidence variations at the rotor inlet are a feasible alternative to optical measurement technologies, which are mostly of high effort. However, the durability of these probes at high speed remains the major problem for their application.

Numerical Studies. CFD is needed to analyse non-uniform tip clearance effects. The most insightful case is an unsteady setup of a high speed stage that is simulated using a coupled aeroelastic approach. A time-varying analysis of the blade force would extend the findings of the current work.

This suggestion is of high numerical effort and complexity, as it would take unsteady calculations of the full annulus to resolve these effects. If partial casing treatments and fluid-structure interaction are simulated in a coupled approach, the task is considered extremely challenging as further code developments might be needed.

Applications for Fan Stages and the Core Compressor. In previous purely aerodynamic studies, to address the threat of inlet distortions, partial casing treatments were suggested for the use in fan stages. The current work highlights that such designs might also benefit regarding blade vibration. Partial casing treatments might also compensate these inlet distortions, which is an advantage for integrated engine concepts. One engineering challenge of these future designs is the unavoidable ingestion of the airframe boundary layer, which is circumferentially non-uniform.

In core compressors, non-uniform interstage compressor bleed might have the same potential to reduce vibration amplitudes, as non-uniform tip clearance. Until today, during compressor design, a single passage is often assumed representative for the entire circumference in order to simplify design computations. According to the current results, the first simple design computations should be followed by strategies that treat the compressor as a full circular system, because there is high potential and possibilities for future engines.

Bibliography

J. J. Adamczyk, M. L. Celestina, and E. M. Greitzer. The role of tip clearance in high-speed fan stall. *Journal of Turbomachinery*, 115(1):28, 1993. ISSN 0889-504X. doi: 10.1115/1.2929212.

Airbus. Flying on demand: Global market forecast, 2018.

J. S. Alford. Protecting turbomachinery from selfexcited whirl. *ASME Transactions, Series A, Journal of Engineering Power 87, No. 10*, 1965.

S. Baghdadi. Modeling tip clearance effects in multi–stage axial compressors. In *International Gas Turbine and Aeroengine Congress & Exposition*, 1995.

M. Baumgartner, F. Kameier, and J. Hourmouziadis. Non-engine order blade vibration in a high pressure compressor. In *Proceedings of 12th International Symposium on Airbreathing Engines (ISABE)*, 1995.

0. Bendiksen. Recent developments in flutter suppression techniques for turbomachinery rotors. *Journal of Propulsion and Power*, 4(2):164–171, 1988. ISSN 0748-4658. doi: 10.2514/3.51283.

M. A. Bennington, M. H. Ross, J. Du, S. C. Morris, F. Lin, J. D. Cameron, and C. Jingyi. An experimental and computational investigation of tip clearance flow and its impact on stall inception. In *Proceedings of ASME Turbo Expo 2010: Power for Land, Sea and Air*, 2010.

R. A. Berdanier and N. L. Key. Experimental investigation of factors influencing operating rotor tip clearance in multistage compressors. *International Journal of Rotating Machinery*, 2015:1–13, 2015. ISSN 1023-621X. doi: 10.1155/2015/146272.

R. A. Berdanier and N. L. Key. The effects of tip leakage flow on the performance of multistage compressors used in small core engine applications. *Journal of Engineering for Gas Turbines and Power*, 138(5):052605, 2016. ISSN 0742-4795. doi: 10.1115/1.4031625.

R. A. Berdanier, N. R. Smith, A. M. Young, and N. L. Key. Effects of tip clearance on stall inception in a multistage compressor. *Journal of Propulsion and Power*, 34(2):308–317, 2018. ISSN 0748-4658. doi: 10.2514/1.B36364.

Fanny M. Besem, Joshua D. Kamrass, Jeffrey P. Thomas, Deman Tang, and Robert E. Kielb. Vortex-induced vibration and frequency lock-in of an airfoil at high angles of attack. In *Proceedings of ASME Turbo Expo 2014: Turbine Technical Conference and Exposition GT2014*, page V07BT35A008, 2014. doi: 10.1115/GT2014-25648.

C. Biela. *Experimental Investigation of the Aerodynamic Influence of Inlet-Guide-Vanes on the Flow Features of a One-And-A-Half Stage Axial Transonic Compressor*. Dissertation, Technische Universität Darmstadt, Germany, 2012.

Boing. Current market outlook, 2018.

C. Bopp. *Weiterentwicklung stationärer Kennfeldmesstechnik an einem 1.5-stufigen transsonischen Verdichter im Rahmen einer Messkampagne mit Schaufelspitzenspaltvariation*. Bachelor thesis, Technische Universität Darmstadt, Darmstadt, 2015.

M. O. Borel, A. R. Nicoll, H. W. Schläpfer, and R. K. Schmid. The wear mechanisms occurring in abradable seals of gas turbines. *Surface and Coatings Technology*, 39-40:117–126, 1989. ISSN 02578972. doi: 10.1016/0257-8972(89)90046-7.

C. Brandstetter. *Aerodynamische Stabilisierung transsonischer Axialverdichter: Eine experimentelle Untersuchung der Blattspitzenströmung unter dem Einfluss von Gehäusestrukturierungen*. Dissertation, Technische Universität Darmstadt, Darmstadt, 2015.

C. Brandstetter and H. P. Schiffer. PIV measurements of the transient flow structure in the tip region of a transonic compressor near stability limit. *Journal of the Global Power and Propulsion Society*, 2(1), 2018. ISSN 2515-3080. doi: 10.22261/JGPPS.JYVUQD.

C. Brandstetter, F. Wartzek, J. Werner, H. P. Schiffer, and F. Heinichen. Unsteady measurements of periodic effects in a transonic compressor with casing treatments: GT2015-42394. In *Proceedings of ASME Turbo Expo 2015: Turbine Technical Conference and Exposition*, 2015.

C. Brandstetter, F. Holzinger, H. P. Schiffer, S. Stapelfeld, and M. Vahdati. Near stall behaviour of a transonic compressor rotor with casing treatment. In *ASME Turbo Expo 2016: Turbomachinery Technical Conference and Exposition*, 2016.

C. Brandstetter, M. Jüngst, and H. P. Schiffer. Measurements of radial vortices, spill forward and vortex breakdown in a transonic compressor. *Journal of Turbomachinery*, 2018. ISSN 0889-504X. doi: 10.1115/1.4039053.

W. J. G. Bräunling, editor. *Flugzeugtriebwerke*. Springer Berlin Heidelberg, Berlin, Heidelberg, 2009. doi: 10.1007/978-3-540-76370-3.

K. D. Broichhausen and K. U. Ziegler. Supersonic and transonic compressors: Past, status and technology trends. *Proceedings of GT2005*, pages 63–74, 2005. doi: 10.1115/GT2005-69067.

T. R. Camp and I. J. Day. A study of spike and modal stall phenomena in a low-speed axial compressor. *Journal of Turbomachinery*, (Vol. 120):V001T03A109, 1998. doi: 10.1115/97-GT-526.

T. Cao, P. Hield, and P. G. Tucker. Hierarchical immersed boundary method with smeared geometry. *Journal of Propulsion and Power*, 33(5):1151–1163, 2017. ISSN 0748-4658.

M. P. Castanier and C. Pierre. Using intentional mistuning in the design of turbomachinery rotors. *AIAA journal*, 40(10):2077–2086, 2002. doi: 10.2514/2.1542.

R. Clark, D. Cox, H. C. Curtiss, E. H. Dowell, J. W. Edwards, K. C. Hall, D. A. Peters, R. Scanlan, E. Simiu, F. Sisto, and T. W. Strganac, editors. *A Modern Course in Aeroelasticity*, volume 116 of *Solid Mechanics and Its Applications*. Springer Science + Business Media, Inc, Dordrecht, fourth revised and enlarged edition edition, 2005. ISBN 1-4020-2106-2.

N. A. Cumpsty. Part-circumference casing treatment and the effect on compressor stall. In *Gas Turbine and Aeroengine Congress and Exposition*, 1989.

N. A. Cumpsty. *Compressor aerodynamics*. Krieger Publishing Company, Malabar, 2004. ISBN 9781575242477.

N. A. Cumpsty and J. H. Horlock. Averaging nonuniform flow for a purpose. *Journal of Turbomachinery*, 128(1):120, 2006. ISSN 0889-504X. doi: 10.1115/1.2098807.

I. J. Day. Stall inception in axial flow compressors. *Journal of Turbomachinery*, 115 (1):1, 1993. ISSN 0889-504X. doi: 10.1115/1.2929209.

I. J. Day. Stall, surge, and 75 years of research. *Journal of Turbomachinery*, 138(1): 011001, 2016. ISSN 0889-504X. doi: 10.1115/1.4031473.

I. J. Day, E. M. Greitzer, and N. A. Cumpsty. Prediction of compressor performance in rotating stall. *Journal of Engineering for Power*, 100(1):1, 1978. ISSN 00220825. doi: 10.1115/1.3446318.

J. D. Denton. The 1993 IGTI scholar lecture: Loss mechanisms in turbomachines. *Journal of Turbomachinery*, 115(4):621, 1993. ISSN 0889-504X. doi: 10.1115/1.2929299.

L. Di Mare, G. Simpson, B. Mueck, and A. I. Sayma. Effect of bleed flows on flutter and forced response of core compressors. In *Proceedings of GT2006*, pages 1115–1122, 2006. doi: 10.1115/GT2006-90683.

L. Di Mare, M. Imregun, and J. S. Green. Effect of real geometry on compressor performance predictions. In *Proceedings of ASME Turbo Expo 2009*, pages 263–271, 2009. doi: 10.1115/GT2009-59824.

DIN Deutsches Institut für Normung e. V. Raumfahrtsysteme - Definition des Technologie-Reifegrades (TRL) und der Beurteilungskriterien, 2016.

DIN Deutsches Institut für Normung e.V. Durchflussmessung von Fluiden mit Drosselgeräten, 2004.

J. Dodds and M. Vahdati. Rotating stall observations in a high speed compressor: Part 1 – experimental study. In *Proceedings of ASME Turbo Expo 2014: Turbine Technical Conference and Exposition GT2014*, 2014.

O. Domercq and J.-F. Escuret. Tip clearance effect on high-pressure compressor stage matching. *Proceedings of the Institution of Mechanical Engineers, Part A: Journal of Power and Energy*, 221(6):759–767, 2007. ISSN 0957-6509. doi: 10.1243/09576509JPE468.

M. Drolet, H. D. Vo, and N. W. Mureithi. Effect of tip clearance on the prediction of nonsynchronous vibrations in axial compressors. *ASME Journal of Turbomachinery*, 135(1):011023, 2013. doi: 10.1115/1.4006401.

M. Eck, S. Geist, and D. Peitsch. Physics of prestall propagating disturbances in axial compressors and their potential as a stall warning indicator. *Applied Sciences*, 7 (3):285, 2017. ISSN 2076-3417. doi: 10.3390/app7030285.

European Commission. *European Aeronautics: A vision for 2020, meeting society's needs and winning global leadership: Report of the Group of Personalities*. Off. for Off. Publ. of the Europ. Communities, Luxembourg, 2001. ISBN 92-894-0559-7.

European Commission. *Flightpath 2050: Europe's vision for aviation*. Policy / European Commission. Office for official publications of the European communities, Luxembourg, 2011. ISBN 978-92-79-19724-6.

F. Figaschewsky, A. Kühhorn, B. Beirow, J. Nipkau, T. Giersch, and B. Power. Design and analysis of an intentional mistuning experiment reducing flutter susceptibility and minimizing forced response of a jet engine fan. In *Proceedings of ASME Turbo Expo 2017: Turbomachinery Technical Conference and Exposition*, page V07BT36A020, 2017. doi: 10.1115/GT2017-64621.

C. Freeman. Effect of tip clearance flow on compressor stability and engine performance. *van Karman Institute for Fluid Dynamics, Lecture Series*, 1985.

J. Friedrich. *Implementierung eines kapazitiven Messsystems zur Messung von Schaufelspitzenspalt und Schaufelschwingungen an einer transsonischen Verdichterstufe*. Master thesis, Technische Universität Darmstadt, Darmstadt, 2015.

Y. C. Fung, editor. *An introduction to the theory of aeroelasticity*. Dover Phoenix Edition. Engineering. Dover, New York, 2002. ISBN 0486495051.

M. Furukawa, M. Inoue, K. Saiki, and K. Yamada. The role of tip leakage vortex breakdown in compressor rotor aerodynamics. *Journal of Turbomachinery*, 121 (3):469, 1999. ISSN 0889-504X. doi: 10.1115/1.2841339.

T. Giersch, F. Heinichen, B. Becker, P. Grothe, and M. Jüngst. Strukturbaugruppe für einen Verdichter einer Strömungsmaschine, 2018.

K. A. Gordan. *Three-dimensional Rotating Stall Inception and Effects of Rotating Tip Clearance Asymmetry in Axial Compressors*. Ph.d., Massachusetts Institute of Technology, Boston, 1999.

M. B. Graf, T. S. Wong, E. M. Greitzer, D. C. Wisler, F. E. Marble, C. S. Tan, and H.-W. Shin. Effects of nonaxisymmetric tip clearance on axial compressor performance and stability. *Journal of Turbomachinery*, 120(Vol. 120 // 4):648, 1998. doi: 10.1115/1.2841774.

E. M. Greitzer, J. P. Nikkanen, D. E. Haddad, R. S. Mazzawy, and H. D. Joslyn. A fundamental criterion for the application of rotor casing treatment. *Journal of Fluids Engineering*, 101(2):237, 1979. ISSN 00982202. doi: 10.1115/1.3448945.

H. Grieb. *Turboverdichter für Flugtriebwerke*. Springer, Dordrecht, 2007. ISBN 978-3-540-34374-5.

H. Grieb. *Verdichter für Turbo-Flugtriebwerke*. Springer Berlin Heidelberg, Berlin, Heidelberg, 2009. ISBN 978-3-540-34373-8. doi: 10.1007/978-3-540-34374-5.

S. D. Grimshaw, G. Pullan, and T. Walker. Bleed-induced distortion in axial compressors. *Journal of Turbomachinery*, 137(10):101009, 2015. ISSN 0889-504X. doi: 10.1115/1.4030809.

S. D. Grimshaw, G. Pullan, and T. P. Hynes. Modeling nonuniform bleed in axial compressors. *Journal of Turbomachinery*, 138(9):091010, 2016. ISSN 0889-504X. doi: 10.1115/1.4032845.

C. Hah. Effects of double-leakage tip clearance flow on the performance of a compressor stage with a large rotor tip gap. In *ASME Turbo Expo 2016: Turbomachinery Technical Conference and Exposition*, page V02AT37A005, 2016. doi: 10.1115/GT2016-56050.

C. Hah, J. Bergner, and H. P. Schiffer. Tip clearance vortex oscillation, vortex shedding and rotating instabilities in an axial transonic compressor rotor. In *Proceedings of ASME Turbo Expo 2008: Power for Land, Sea and Air GT2008*, pages 57–65, 2008. doi: 10.1115/GT2008-50105.

F. Haselbach, A. Newby, and R. Parker. Next generation of large civil aircraft engines - concepts & technologies. In *11th European Turbomachinery Conference (ETC)*, pages 1–22, 2015. doi: 10.1002/9781119197249.ch1.

M. Hathaway. Passive endwall treatments for enhancing stability. *StabilityNASA Technical Report No. NASA/TM-2007-214409*, 2007.

D. K. Hennecke. Tip clearance effects in axial turbomachines: Active and passive tip clearance. *van Karman Institute for Fluid Dynamics, Lecture Series*, 1985.

M. Hewkin-Smith, G. Pullan, S. D. Grimshaw, E. M. Greitzer, and Z. S. Spakovszky. The role of tip leakage flow in spike-type rotating stall inception. In *Proceedings of ASME Turbo Expo 2017: Turbomachinery Technical Conference and Exposition*, page V02DT46A009, 2017. doi: 10.1115/GT2017-63655.

P. Hoeveler. Europäischer Kraftakt: Fortschritte beim Forschungsprogramm LEMCOTEC. *Flug Revue*, (09.01.2014), 2014.

P. Hoeveler. Bausteine fuer die Zukunft: Das europäische Forschungsprogramm E-BREAK soll Schlüsseltechnologien für weitere Verbesserungen künftiger Triebwerke bereitstellen. *Flug Revue*, (14.09.2015), 2015.

W. Hofmann. *Topologie und Entstehung von Blattspitzenwirbeln in transsonischen Verdichterrotoren und ihr Einfluss auf die Stabilitätsgrenze*. Dissertation, Technische Hochschule Aachen, Aachen, 2006.

F. Holzinger. *Coupling of tip leakage flow and blade vibration in transonic compressors - Mechanism and countermeasures*. Dissertation, Technische Universität Darmstadt, Darmstadt, 2017.

F. Holzinger, F. Wartzek, M. Jüngst, S. Leichtfuss, and H. P. Schiffer. Self-excited blade vibration experimentally investigated in transonic compressors - rotating instabilities and flutter. In *Proceedings of ASME Turbo Expo 2015: Turbine Technical Conference and Exposition*, 2015.

S. Hormel. *Projektplanung, Konzeptionierung und Vorbereitung von experimentellen Untersuchungen einer transsonischen Verdichterstufe*. Master thesis, Technische Universität Darmstadt, Darmstadt, 2015.

D. Hoyniak and S. Fleeter. The effect of circumferential aerodynamic detuning on coupled bending-torsion unstalled supersonic flutter. *Journal of Turbomachinery*, 108(2):253, 1986. ISSN 0889-504X. doi: 10.1115/1.3262045.

M. C. Huppert, H. F. Calvert, and A. J. Meyer. Experimental investigation of rotating stall and blade vibration in the axial-flow compressor of a turbojet engine: Lewis flight propulsion laboratory. *Research Memorandum*, (NACA RM E54A08), 1954.

M. Inoue and M. Kuroumaru. Structure of tip clearance flow in an isolated axial compressor rotor. *Journal of Turbomachinery*, (Vol. 111), 1989.

M. Inoue, M. Kuroumaru, T. Tanino, and M. Furukawa. Propagation of multiple short-length-scale stall cells in an axial compressor rotor. *Journal of Turbomachinery*, 122(1):45, 2000. ISSN 0889-504X. doi: 10.1115/1.555426.

E. Johann and M. Hembera. Turbomachine with annulus duct wall recess, 2015.

A. John, N. Qin, and S. Shahpar. The impact of realistic casing geometries and clearances on fan blade tip aerodynamics (GT2017-64403). *Journal of Turbomachinery*, 2017. ISSN 0889-504X. doi: 10.1115/1.4038834.

M. Jüngst. *Blade vibration characterization of a transonic compressor rotor by experimental data and numerical studies*. Master Thesis, Technische Universität Darmstadt, Darmstadt, 2014.

M. Jüngst, F. Holzinger, S. Leichtfuss, and H. P. Schiffer. Analysing non-synchronous vibration in a transonic compressor rotor. In *11th European Turbomachinery Conference (ETC)*, 2015.

M. Jüngst, D. Franke, T. Giersch, and H. P. Schiffer. Aeroelastic effects in a transonic compressor with nonaxisymmetric tip clearance. In *Proceedings of GPPS Forum 18*, 2018a.

M. Jüngst, S. Liedtke, B. Becker, and H. P. Schiffer. Aerodynamic effects in a transonic compressor with nonaxisymmetric tip clearance. In *Proceedings of the ASME Turbo Expo 2018*, 2018b.

S. Kablitz. *Beeinflussung der Spaltströmung von Transsonischen Axialverdichtern durch Forward Sweep*. Dissertation, Technische Universität Darmstadt, Darmstadt, 2003.

F. Kameier and W. Neise. Rotating blade flow instability as a source of noise in axial turbomachines. *Journal of Sound and Vibration*, 203(5):833–853, 1997.

C. Keller, A. Kellersmann, J. Friedrichs, and J. R. Seume. Influence of geometric imperfections on aerodynamic and aeroelastic behavior of a compressor blisk. In *Proceedings of ASME Turbo Expo 2017: Turbomachinery Technical Conference and Exposition*, page V07BT36A007, 2017. doi: 10.1115/GT2017-63556.

S. A. Khalid. *The Effects of tip Clearance on Axial Compressor Pressure Rise*. Dissertation, Massachusetts Institute of Technology, Boston, 1995.

R. E. Kielb. Definition of classical flutter and NSV: Panel session on vibrations in axial compressors at the GPPS, 2018.

R. E. Kielb, J. W. Barter, J. P. Thomas, and K. C. Hall. Blade excitation by aerodynamic instabilities: A compressor blade study. In *Proceedings of the ASME Turbo Expo 2003: Power for Land, Sea, and Air*, 2003.

C. Kunkel. *Konstruktion und Inbetriebnahme einer neuen Austrittsinstrumentierung für den transsonischen Verdichterprüfstand*. Master Thesis, Technische Universität Darmstadt, Darmstadt, 2013.

S. Leichtfuss. *Zum Einfluss des Spaltwirbels auf das aeroelastische Verhalten transsonischer Verdichter*. Dissertation, Technische Universität Darmstadt, Darmstadt, 2015.

S. Liedtke. *Kalibration kapazitiver Abstandssensoren zur berührungslosen Schaufelspaltmessung*. Interner Bericht, Institut für Gasturbinen, Luft- und Raumfahrtantriebe, Darmstadt, 2016.

S. Liedtke. *Analysis of Aerodynamics in a 1.5-Stage Transonic Compressor Based on Measurements With Variable Size and Eccentricity of Blade Tip Clearance*. Master thesis, Technische Universität Darmstadt, Darmstadt, 2017.

J. P. Longley. Measured and predicted effects of inlet distortion on axial compressors: Paper no. 90-GT-214. In *ASME 1990 International Gas Turbine and Aeroengine Congress and Exposition*, page V001T01A067. 1990. doi: 10.1115/90-GT-214.

R. Mailach, I. Lehmann, and K. Vogeler. Rotating instabilities in an axial compressor originating from the fluctuating blade tip vortex. *Journal of Turbomachinery*, 123 (3):453–460, 2001. ISSN 0889-504X. doi: 10.1115/1.1370160.

J. März, C. Hah, and W. Neise. An experimental and numerical investigation into the mechanisms of rotating instability. *Journal of Turbomachinery*, 124(3):367–374, 2002. ISSN 0889-504X. doi: 10.1115/1.1460915.

K. Mathioudakis and F. A. E. Breugelmans. Development of small rotating stall in a single stage axial compressor: ASME Paper No. 85-GT-227. In ASME, editor, *Gas Turbine Conference and Exhibit*, 1985.

R. S. Mazzawy. Multiple segment parallel compressor model for circumferential flow distortion. *ASME Journal of Engineering for Power*, 1977:288–297, 1977.

N. M. McDougall, N. A. Cumpsty, and T. P. Hynes. Stall inception in axial compressors. *Journal of Turbomachinery*, 112(1):116, 1990. ISSN 0889-504X. doi: 10.1115/1.2927406.

R. E. McNair. Tip clearance effects on stalling pressure rise in axial flow compressors. In *ASME 1960 Gas Turbine Power and Hydraulic Divisions Conference and Exhibit*, page V001T03A011, 1960. doi: 10.1115/60-GTHYD-12.

D. Möller, M. Jüngst, F. Holzinger, C. Brandstetter, H. P. Schiffer, and S. Leichtfuss. Numerical investigation of tip clearance flow induced flutter in an axial research compressor. In *ASME Turbo Expo 2016: Turbomachinery Technical Conference and Exposition*, page V07BT34A010, 2016. doi: 10.1115/GT2016-56956.

D. Möller, M. Jüngst, H. P. Schiffer, T. Giersch, and F. Heinichen. Influence of rotor tip blockage on near stall blade vibrations in an axial compressor rig. In *Proceedings of ASME Turbo Expo 2017: Turbomachinery Technical Conference and Exposition*, 2017.

D. R. Moore. Rotor tip clearance effects on overall and blade-element performance of axial-flow transonic fan stage. *NASA Technical Paper*, 1982.

S. C. Morris, J. D. Cameron, M. A. Bennington, G. S. McNulty, and A. Wadia. Performance and short length-scale disturbance generation in an axial compressor with non-uniform tip clearance. In *Proceedings of ASME Turbo Expo 2008: Power for Land, Sea and Air GT2008*, pages 667–679, 2008. doi: 10.1115/GT2008-51372.

J. H. Page, P. Hield, and P. G. Tucker. Effect of inlet distortion features on transonic fan rotor stall. In *Proceedings of ASME Turbo Expo 2017: Turbomachinery Technical Conference and Exposition*, page V001T01A028, 2017. doi: 10.1115/GT2017-64612.

R. C. Pampreen. *Compressor Surge and Stall*. Concepts ETI, Vermont, USA, 1993. ISBN 0933283059.

B. Pardowitz, A. Moreau, U. Tapken, and L. Enghardt. Experimental identification of rotating instability on an axial fan with shrouded rotor. In *11th European Turbomachinery Conference (ETC)*, 2015.

H. Pearson and A. B. McKenzie. Wakes in axial compressors. *Journal of the Royal Aeronautical Society*, 1959.

J. E. Penner, D. H. Lister, D. J. Griggs, D. J. Dokken, and M. McFarland. *Aviation and the Global Atmosphere: Summary for Policymakers*. 1999. ISBN 92-9169-.

G. A. Plourde and A. H. Stenning. Attenuation of circumferential inlet distortion in multistage axial compressors. *Journal of Aircraft*, 5(3):236–242, 1968. ISSN 0021-8669. doi: 10.2514/3.43933.

G. Pullan, A. M. Young, I. J. Day, E. M. Greitzer, and Z. S. Spakovszky. Origins and structure of spike-type rotating stall. *Journal of Turbomachinery*, 137(5):051007, 2015. ISSN 0889-504X. doi: 10.1115/1.4028494.

J. A. Reeder. Tip clearance problems in axial compressors. *AEC Research and Development Report*, 1966.

J. H. Richardson, G. P. Sallee, and F. K. Smakula. Causes of high pressure compressor deterioration in service. In *15th Joint Propulsion Conference*, 1979. doi: 10.2514/6.1979-1234.

H. Rick. *Gasturbinen und Flugantriebe*. Springer Berlin Heidelberg, Berlin, Heidelberg, 2013. doi: 10.1007/978-3-540-79446-2.

Rolls-Royce plc. *The Jet Engine*. Rolls-Royce plc, London, [5th ed.] edition, 2007. ISBN 0-902121-2-35.

S. Sakulkaew, C. S. Tan, E. Donahoo, C. Cornelius, and M. Montgomery. Compressor efficiency variation with rotor tip gap from vanishing to large clearance. *Journal of Turbomachinery*, 135(3):031030, 2013. ISSN 0889-504X. doi: 10.1115/1.4007547.

H. I. H. Saravanamuttoo. *Recommended Practices for Measurement of Gas Path Pressures and Temperatures for Performance Assessment of Aircraft Turbine Engines and Components: AGARD Advisory Report No.245*. 1990.

A. Schäffler. Aerodynamische Instabilitaet in mehrstufigen Axialverdichtern. *MTU Berichte*, (25):1–37, 1979a.

A. Schäffler. Experimental and analytical investigation of the effects of reynolds number and blade surface rughness on multistage axial flow compressors. *ASME: Journal for Engineering for Power*, (79-GT-2), 1979b.

S. M. Schirle, D. Kasperski, N. Martin, R. M. Zacharias, and T. E. Dejoris. Asymmetric compressor air extraction method, 2008.

S. Schlechtriem and M. Lötzerich. Breakdown of tip leakage vortices in compressors at flow conditions close to stall. In *Proceedings of the 1997 International Gas Turbine & Aeroengine Congress & Exposition*, page V001T03A004, 1997. doi: 10.1115/97-GT-041.

G. Schulze. *Betriebsverhalten eines transsonischen Axialverdichters*. Dissertation, Technische Universität Darmstadt, Darmstadt, 1996.

F. Sisto, W. Wu, S. Thangham, and S. Jonnavithula. Computational aerodynamics of oscillating cascades with the evolution of stall. *AIAA journal*, 27(4):462–471, 1989. doi: 10.2514/3.10134.

I. Sladojević, A. I. Sayma, and M. Imregun. Influence of stagger angle variation on aerodynamic damping and frequency shifts. In *Proceedings of GT2007 ASME Turbo Expo 2007: Power for Land, Sea, and Air*, pages 683–700, 2007. doi: 10.1115/GT2007-28166.

L. H. Smith. The effect of tip clearance on the peak pressure rise of axial-flow fans and compressors. *ASME Symposium on Stall*, pages 149–152, 1958.

G. Spelsberg-Korspeter. *Robust Structural Design against Self-Excited Vibrations*. Springer Berlin Heidelberg, Berlin, Heidelberg, 2013. doi: 10.1007/978-3-642-36552-2.

Joseph H. Spurk and Nuri Aksel. *Strömungslehre: Einführung in die Theorie der Strömungen*. Springer-Lehrbuch. Springer-Verlag Berlin Heidelberg, Berlin, Heidelberg, 8. aufl. edition, 2010. ISBN 978-3-642-13143-1. doi: 10.1007/978-3-642-13143-1.

A. V. Srinivasan. Flutter and resonant vibration characteristics of engine blades. In *Proceedings of the 1997 International Gas Turbine & Aeroengine Congress & Exposition*, pages 97–GT–533, 1997.

H. Stargardter. Subsonic/transonic stall flutter study. *Final Report, NASA CR-165256*, 1979, 1979.

K. Steffens. Advanced compressor technology key success factor for competitiveness in modern aero engines. *ISABE Conference on Airbreathing Engines, Bangalore*, (Paper 20011009), 2001.

A. F. Storace, D. C. Wisler, H.-W. Shin, B. F. Beacher, F. F. Ehrich, Z. S. Spakovszky, M. Martinez-Sanchez, and S. J. Song. Unsteady flow and whirl-inducing forces in axial-flow compressors: Part i—experiment. *Journal of Turbomachinery*, 123(3): 433, 2001. ISSN 0889-504X. doi: 10.1115/1.1378299.

J. A. Storer and N. A. Cumpsty. An approximate analysis and prediction method for tip clearance loss in axial compressors. *ASME 1993 International Gas Turbine and Aeroengine Congress and Exposition*, page V001T03A062, 1993. doi: 10.1115/93-GT-140.

A. J. Streit. *Zum Fortschritt transsonischer Axialverdichter: Gehäusestrukturierungen sinnvoll eingesetzt*. Dissertation, Technische Universität München, 2014.

K. L. Suder. Blockage development in a transonic, axial compressor rotor. *Journal of Turbomachinery*, 120(3):465, 1998. ISSN 0889-504X. doi: 10.1115/1.2841741.

H.-J. Thomas. Instabile Eigenschwingungen von Turbinenläufern, angefacht durch die Spaltströmungen in Stopfbuchsen und Beschaufelungen. *AEG-Sonderdruck Z10/5729*, 1958.

J. Thomassin, H. D. Vo, and N. W. Mureithi. Blade tip clearance flow and compressor nonsynchronous vibrations: The jet core feedback theory as the coupling mechanism. *Journal of Turbomachinery*, 131(1):011013, 2009. ISSN 0889-504X. doi: 10.1115/1.2812979.

J. Thomassin, H. D. Vo, and N. W. Mureithi. The tip clearance flow resonance behind axial compressor nonsynchronous vibration. *ASME Journal of Turbomachinery*, 133(4):041030–041030–10, 2011. doi: 10.1115/1.4001368.

O. Thomer, W. Schröder, and E. Krause. Normal and oblique shock-vortex interaction. *Proceedings of International Conference RDAMM–2001*, (6), 2001.

D. W. Thompson, P. I. King, C. Hah, and D. C. Rabe. Experimental and computational investigation of stepped tip gap effects on the flowfield of a transonic axial-flow compressor rotor. *Proceedings of the International Gas Turbine & Aeroengine Congress & Exhibition*, 1998.

Verein Deutscher Ingenieure. *Selbsterregte Schwingungen: Ursache, Analyse, Beherrschung : Tagung Fulda, 1. und 2. April 1992*, volume 957 of *VDI Berichte*. VDI-Verlag, Düsseldorf, 1992. ISBN 3-18-090957-9.

H. D. Vo. Role of tip clearance flow in the generation of non-synchronous vibrations. In *44th AIAA Aerospace Sciences Meeting and Exhibit*, 2006.

H. D. Vo, C. S. Tan, and E. M. Greitzer. Criteria for spike initiated rotating stall. *Journal of Turbomachinery*, 130(1):011023, 2008. ISSN 0889-504X. doi: 10.1115/1.2750674.

M. Vollmuth. EU technology programme ENOVAL launched: New technologies for next generation aero engines focus on lower CO2 and noise emissions, 2013.

R. von der Bank, S. Donnerhack, A. Rae, F. Poutriquet, A. Lundbladh, and A. Schweinberger. Advanced core engine technologies assessment & validation. In *11th European Turbomachinery Conference (ETC)*, 2015.

R. von der Bank, S. Donnerhack, A. Rae, F. Poutriquet, A. Lundbladh, A. Antoranz, L. Tarnowski, and M. Ruzicka. Compressors for ultra-high-pressure-ratio aeroengines. *CEAS Aeronautical Journal*, 7(3):455–470, 2016. ISSN 1869-5582. doi: 10.1007/s13272-016-0200-9.

F. Wartzek. *Aerodynamic Behaviour of the Transonic Compressor with Distorted Inflow*. Dissertation, Technische Universität Darmstadt, Darmstadt, 2017.

S. Weichert and I. J. Day. Detailed measurements of spike formation in an axial compressor. *Journal of Turbomachinery*, 136(5):051006, 2014. ISSN 0889-504X. doi: 10.1115/1.4025166.

A. J. Wennerstrom. Experimental study of a high-throughflow transonic axial compressor stage. *Journal of Engineering for Gas Turbines and Power*, page 106(3):552, 1984.

D. S. Whitehead. Bending flutter of unstalled cascade blades at finite deflection: Aeronautical research council reports and memoranda, 1965.

G. Wilde. Improvements in or relating to compressors, 1953.

D. C. Wisler. Tip clearance effects in axial turbomachines. *van Karman Institute for Fluid Dynamics, Lecture Series*, (1985-05), 1985.

K. Yamada, M. Furukawa, T. Nakano, M. Inoue, and K. Funazaki. Unsteady three-dimensional flow phenomena due to breakdown of tip leakage vortex in a transonic axial compressor rotor. In *Proceedings of ASME Turbo Expo 2004: Power for Land, Sea and Air*, 2004.

K. Yamada, K. Funazaki, and M. Furukawa. The behavior of tip clearance flow at near-stall condition in a transonic axial compressor rotor. In *Proceedings of GT2007 ASME Turbo Expo 2007: Power for Land, Sea, and Air*, pages 295–306, 2007. doi: 10.1115/GT2007-27725.

K. Yamada, H. Kikuta, M. Furukawa, S. Gunjishima, and Y. Hara. Effects of tip clearance on the stall inception process in an axial compressor rotor. In *Proceedings of the ASME Turbo Expo 2013: Power for Land, Sea and Air*, 2013.

A. M. Young, I. J. Day, and G. Pullan. Stall warning by blade pressure signature analysis. In *Proceedings of ASME Turbo Expo 2011*, pages 1589–1599, 2011. doi: 10.1115/GT2011-45850.

A. M. Young, T. Cao, I. J. Day, and J. P. Longley. Accounting for eccentricity in compressor performance predictions. In *ASME Turbo Expo 2016: Turbomachinery Technical Conference and Exposition*, page V02AT37A017, 2016. doi: 10.1115/GT2016-56681.

M. Zielinski and G. Ziller. Noncontact vibration measurements on compressor rotor blades. *Measurement Science and Technology*, 11(7):847–856, 2000. doi: 10.1088/0957-0233/11/7/301.

M. Zielinski and G. Ziller. Noncontact blade vibration measurement system for aero engine application. In *17th International Symposium on Airbreathing Engines (ISABE)*, 2005.

G. Ziller. Ovalität moderner Verdichtergehäuse: Schulung zur Berührungslosen-Schaufelschwingungsmessung, 2014.

A Appendix

A.1 Real Depiction of the Rig Design and Instrumentation

The central research focus of this work are the effects of a non-uniform rotor tip clearance with a wavelength that corresponds to the length of the circumference. In order to facilitate this research, the modular casing inserts are designed to be traversable by 360°. Two examples are shown in Figure A.1. In both cases, the traversable ring above the rotor is supported by a thin ring bearing towards the fixed downstream casing. The ring is moved from outside the casing via spur gearing.

In Figure A.1a an eccentric casing insert is shown. The tip clearance transitions upstream and downstream of the rotor are designed to be representative for eroded rub-ins. The ring diameter is altered and the casing is tilted in between. Figure A.1b depicts the segmental casing treatment design. To fill the grooves, counterparts were cast with two component epoxy resin and then glued in situ. This appeared to be a dentist's job. The instrumentation is covered to prevent collateral damage.

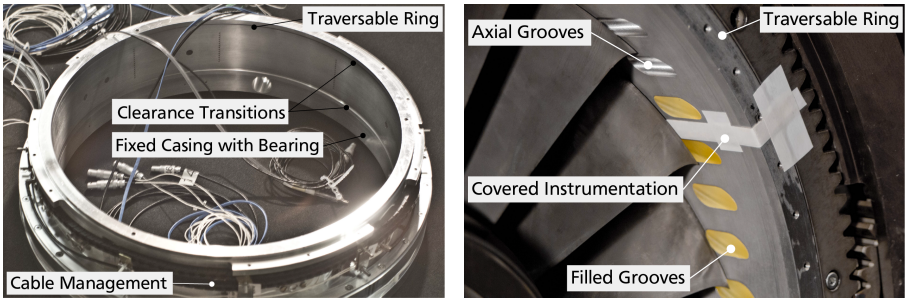

(a) Casing insert with eccentric tip clearance **(b)** Casing insert with segmental casing treatment CT180

Figure A.1: Modular non-uniform casing inserts and illustration of 360° traversing system

In Figure A.2, the steady-state and unsteady instrumentation is depicted. All pictures show the measurement technology in the installed state in the test rig. The only exception is the image of the tip timing and tip clearance sensors. In this case, the calibration setup is shown, for which the casing is modelled via a small ring segment only.

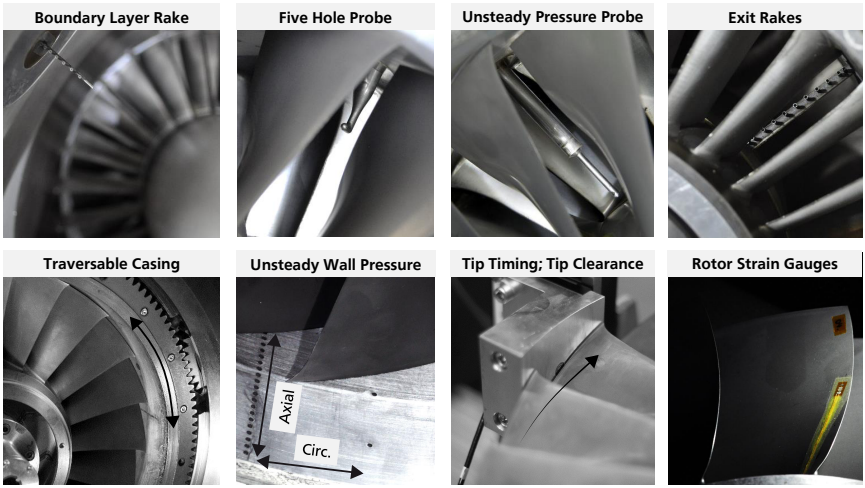

Figure A.2: Steady and unsteady measurement techniques

A.2 Determination of Steady-State Flow Quantities

This chapter contains further descriptions of the measured and derived steady-state quantities. The circumferential distribution of the sensors at the axial stations, an overview of all properties as well as the equations and assumptions used are explained.

Mass Flow. The measurement of the mass flow is based on the static pressure difference generated by the acceleration of the fluid through the inlet nozzle. According to DIN Deutsches Institut für Normung e.V. (2004), the mass flow can be calculated via

$$\dot{m}^{10} = \gamma \epsilon \pi r_{\mathrm{tip}}^2 \sqrt{2\rho^{04}(p_{\mathrm{s}}^{04} - p_{\mathrm{s}}^{10})}, \qquad \text{with} \qquad \epsilon = f(p_{\mathrm{s}}^{10}, p_{\mathrm{s}}^{04}), \tag{A.1}$$

where the area of the nozzle, the density of the fluid and the static pressure difference across the nozzle must be known or measured. In preliminary tests, the flow rate coefficient γ and expansion coefficient ϵ are calibrated. γ is a factor that takes into account the difference between the actual and the ideal, friction-free flow rate derived from the Bernoulli equation. It depends on Reynolds number only if certain design conditions are considered.

ϵ takes the compressibility of the fluid into account and becomes one if an incompressible fluid is used.

Stage Isentropic Efficiency. The isentropic work input to the fluid is calculated via the total pressure rise and related to the mechanical work input via the shaft by

$$\eta_{\mathrm{is}} = \frac{\dot{m}^{10} c_{\mathrm{p}} T_{\mathrm{t}}^{04} \left(\Pi_{\mathrm{t-t}}^{\frac{\kappa-1}{\kappa}} - 1 \right)}{P_{\mathrm{mech}}} \tag{A.2}$$

Exponential Decay. The static pressure variation p_{var}, resulting from tip leakage blockage, are maximum at the rotor inlet plane and decay exponentially upstream (Morris et al., 2008) according to

$$p_{\mathrm{var}}^{\mathrm{xx}}(x) = p_{\mathrm{var}}^{20} e^{-\frac{\Delta x}{2 r_{\mathrm{tip}}}} \tag{A.3}$$

Isentropic Relations.

$$\frac{T_{\mathrm{s}}}{T_{\mathrm{t}}} = \frac{p_{\mathrm{s}}}{p_{\mathrm{t}}}^{\frac{\kappa-1}{\kappa}} \qquad \text{and} \qquad \mathrm{Ma}^2 = \frac{2}{\kappa - 1} \left(\frac{p_{\mathrm{t}}}{p_{\mathrm{s}}}^{\frac{\kappa-1}{\kappa}} - 1 \right) \tag{A.4}$$

Density.

$$\rho = \frac{p_s}{RT_s} \tag{A.5}$$

Mach Number.

$$\mathrm{Ma} = \frac{c}{\sqrt{\kappa RT_s}} \tag{A.6}$$

Entropy.

$$s = c_p \ln \frac{T_s}{T_{s,\mathrm{ref}}} - R \ln \frac{p_s}{p_{s,\mathrm{ref}}} \tag{A.7}$$

Axial Flow Component.

$$\square_{ax} = \square \cdot \cos\beta \tag{A.8}$$

In Figure A.3, the circumferential positioning of all probes and rakes is illustrated. It contains the directly measured quantities only. Some physical values, such as mass flow density, are not directly measurable. To explain their determination, all quantities that are used in the scope of this work are listed in Tables A.1 and A.2. The tables indicate if the quantity is measured or determined using thermodynamic principles. In the case of measured parameters, the measurement method is displayed. If the parameter is derived, a link to the calculation procedure is included.

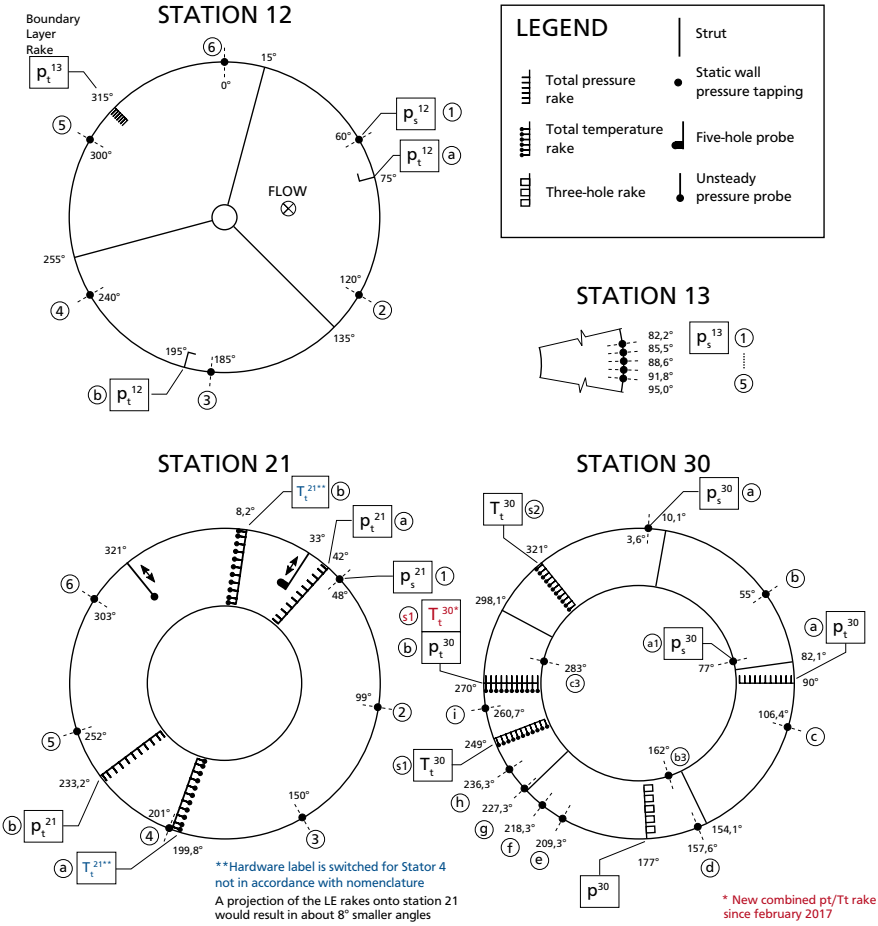

Figure A.3: Rake and probe positioning at measurement stations

Table A.1: Determination of steady-state quantities at stage inlet

Station	Quantity	Measured via	Derived via
00	p_{baro}^{00}	-	
01	κ^{01}	-	Wet air as ideal gas
	R^{01}	-	Wet air as ideal gas
	c_p^{01}	-	Wet air as ideal gas
10	$\dot{m}^{10}$	Calibrated inlet nozzle	Equation A.1, Equation A.5, T_{t}^{04}, p_{t}^{04}, p_{s}^{10}, T_{s}^{04}, p_{s}^{04}
	$\dot{m}_{\text{corr}}^{10}$	-	Equation 2.3, T_{t}^{04}, p_{t}^{04}, κ^{01}, R^{01}
	T_{t}^{04}	KHP[a]	-
	p_{t}^{04}	KHP	-
	p_{s}^{10}	WPT[b]	-
	T_{s}^{04}, p_{s}^{04}	-	Assuming negligible flow velocity in settling chamber
	ρ^{04}	-	Equation A.5
12	p_{t}^{12}	Boundary Layer Rake, KHP	p_{t}^{04} ,p_{t}^{13}, turbulent inlet profile
13	p_{s}^{13}	WPT	-
20	$(\rho u)_{\text{var}}^{20}$	-	$p_{\text{s,var}}^{20}$ via Equation A.3 and $p_{\text{s,var}}^{13}$, Equations A.4, Equation A.5, Equation A.6, T_{t}^{04}, p_{t}^{13}
	$(\rho u)_{\text{ax,var}}^{20}$	-	Assumed axial inlet velocity (only approximately valid for IGVA = 0°)

[a] Kiel head probes.

[b] Wall pressure tappings.

Table A.2: Determination of steady-state quantities at rotor and stator exit

Station	Quantity	Measured via	Derived via
21	p_{t}^{21}	FHP[a], UPP[b]	Free stream calibration
	p_{s}^{21}	FHP	Free stream calibration
	Ma^{21}	FHP	Free stream calibration
	β^{21}	FHP	Free stream calibration
	T_t^{21}	KHP at Stator LE	-
	T_s^{21}	-	Equation A.4, p_{s}^{21}, p_{t}^{21}, T_t^{21}
	Π_{t-t}^{21}	-	p_{t}^{21} relative to inlet reference pressure p_{t}^{12}
	$(\rho u)^{21}$	-	Equation A.4, Equation A.5, Equation A.6, p_{s}^{21}, p_{t}^{21}, T_t^{21}
	$(\rho u)_{\mathrm{ax,corr}}^{21}$	-	Equation 2.3, Equation A.8, $(\rho u)^{21}$, β^{21}, p_{t}^{21}, T_t^{21}
	s^{21}	-	Equation A.7, p_{s}^{21}, T_s^{21}, T_{s}^{04}, p_{s}^{04}, R^{01} and c_p^{01} assumed constant from inlet to exit
30	p_{t}^{30}	KHP	-
	T_{t}^{30}	KHP	-
	p_{s}^{30}	WPT at hub and tip	Linear interpolation, assuming no exit whirl, radial equilibrium $p_{\mathrm{s,hub}} < p_{\mathrm{s,tip}}$
	β^{30}	THP[c]	Free stream calibration
	$(\rho u)^{30}$	-	Equation A.4, Equation A.5, Equation A.6, p_{s}^{30}, p_{t}^{30}, T_{t}^{30}
	$(\rho u)_{\mathrm{ax,corr}}^{30}$	-	Equation 2.3, Equation A.8, $(\rho u)^{30}$, β^{30}, p_{t}^{30}, T_{t}^{30}
	$\Pi_{\mathrm{t-t}}^{30}$	-	p_{t}^{30} relative to inlet reference pressure p_{t}^{12}
	$\Pi_{\mathrm{t-s}}^{30}$	-	p_{s}^{30} relative to inlet reference pressure p_{t}^{12}
	η_{is}^{30}	-	Equation A.2, P_{mech} via torquemeter, assuming constant bearing loss for constant mechanical speeds

[a] Five hole probe.
[b] Unsteady pressure probe.
[c] Three hole rake.

A.3 Tip Clearance Sensitivity at Part Speed

In the main part of this document, tip clearance sensitivity at design speed is discussed. Figure A.4 presents the sensitivities of efficiency, pressure rise and stability margin at part speed. The investigated compressor stage is most sensitive at design speed.

At N63, efficiency is roughly a third as sensitive regarding tip clearance, compared to the design speed of the compressor (see Figure A.4a). The same accounts for the stage pressure ratio (compare Figure A.4b). This depends most likely on the decreasing efficiency level from high to low speeds as well as the characteristic of the compressor, which is rather flat for low speed compared to high speed.

In case of stability margin (Figure A.4c and Figure A.4d), tip clearance sensitivity is not decreasing continuously. Instead, there is a fundamental difference between subsonic (N63, N80) and transonic speeds (N95, N100). For transonic speeds, the stability of the stage is reduced by about -10% per 1% increase of tip clearance. For subsonic speeds, the sensitivity drops to roughly -7%.

It is likely that altered stall inception mechanisms are the driving force for the observed difference between high and low speed. E.g. the growth of tip blockage at near stall operation is fundamentally different if shock-vortex interaction leads to a sudden growth of the tip clearance vortex. However, the exact cause remains undefined in the scope of the current work.

With regard to eccentricity, the hypothesis already formulated in the main section applies to a large extent at part speed as well. With the exception of efficiency at part speed N80, the circumferential average clearance is decisive both for the performance and for the stability of an eccentric compressor stage.

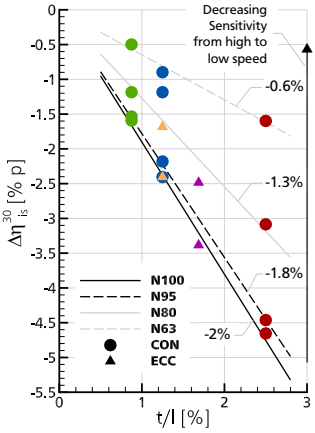

(a) Sensitivity of stage efficiency as a function of rotor speed, tip clearance and eccentricity

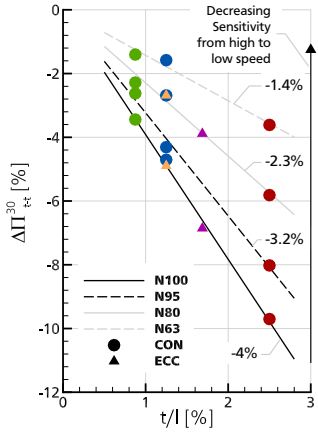

(b) Sensitivity of stage pressure rise as a function of rotor speed, tip clearance and eccentricity

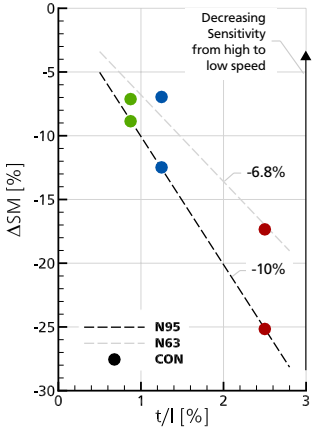

(c) Sensitivity of stability margin as a function of rotor speed and tip clearance

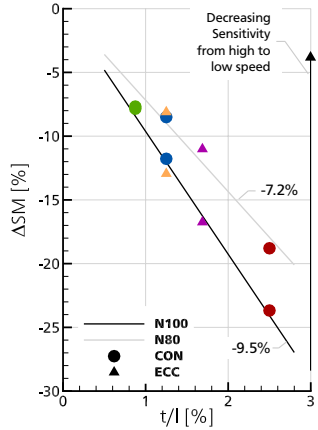

(d) Sensitivity of stability margin as a function of rotor speed, tip clearance and eccentricity

Figure A.4: Sensitivity of stage efficiency, pressure rise and stability margin regarding tip clearance and eccentricity. Inlet guide vane closure (i.e. pre-swirl) is nominal for each speed (N63, N80, N95, N100 with 0%, 25%, 78%, 73% IGVA, respectively).

A.4 Supplementary Results at Steady-State

In the main document, the analysis revealed that the circumferentially averaged blockage, generated in an non-uniform casing, is equivalent to that in a uniform casing with the same average clearance. For configuration ECC-MAX, eight radial profiles are measured evenly distributed over the circumference and presented as circumferential average in Figure A.5. In case of the concentric setups, one radial profile is measured representative for the whole circumference. The radial mass flow distribution in configuration ECC-MAX is in line with the findings in the main document.

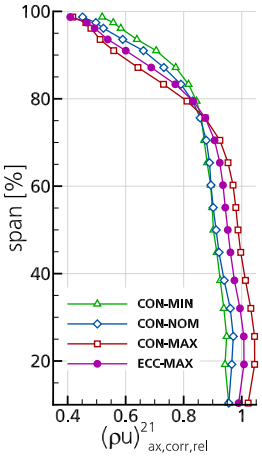

Figure A.5: Circumferentially averaged mass flow distribution of configuration ECC-MAX

With non-uniform tip clearance, the through flow of a compressor stage varies circumferentially at in- and outlet. As no numerical pre-analysis was carried out, it was difficult to analyse the variation and validate its measurability before the test. Therefore, redundant measurements are performed at the operating point of minimum circumferential variation for configuration ECC-MIN (see Figure A.6). These measurements show high repeatability, significance and accuracy of the performed measurements with non-uniform clearance.

Figure A.7 illustrates steady-state measurements and associated blade vibration amplitudes. For configuration ECC-MIN, additional measurements of the vibration amplitudes were carried out at constant mass flow. In some cases, no performance data is available. As a result, more data is displayed for configuration ECC-MIN in Figure A.7b compared to Figure A.7a.

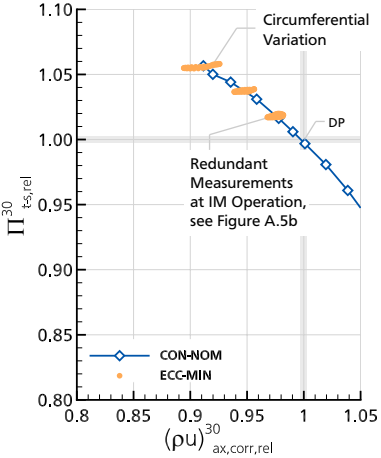

(a) Performance of configuration ECC-MIN, compared to configuration CON-NOM with similar average clearance. The reference for mass flow and pressure rise is the design point.

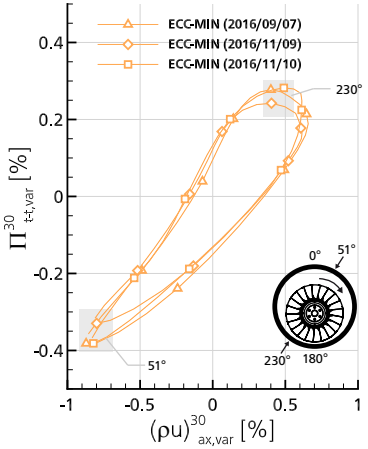

(b) Redundant measurements of circumferential variation at IM operation

Figure A.6: Measurements with small eccentricity ECC-MIN and reproducibility of circumferential variation.

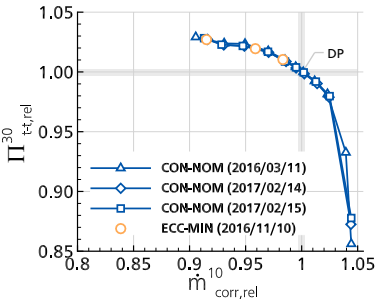

(a) Steady-state performance measurements

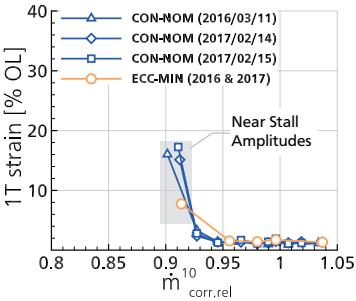

(b) Vibration amplitudes at steady-state operation

Figure A.7: Influence of eccentricity on 1T blade vibration amplitudes at design speed. For each figure, the mass flow is referred to the design point.

A.5 Supplementary Results regarding Unsteady Measurements

It is pointed out in the main document (in Section 4.1.1) that the operating limit of the individual configurations is not limited by identical phenomena. Hence, the wording *stability limit* is used instead of *stall limit*.

Figure A.8 and A.9 demonstrate the stall inception process and associated blade vibrations for configurations CON-MIN and CON-MAX.

In case of CON-MIN, the process is analogous to CON-NOM (compare Section 4.2.1). However, lower non-synchronous 1T vibrations occur. Quite similar findings are summed up in Figure A.10 and Figure A.11d for configuration ECC-MIN.

In case of CON-MAX, non-synchronous vibrations of the CWB mode limit further throttling. The rotor blades interact with a stepwise increasing number of cells with progressively increasing vibration amplitudes. The measurements were therefore aborted. Still, the static pressure at rotor exit constantly increases. The pressure drop is caused by the throttle opening. The main difference to measurements with smaller clearance is the formation of characteristic frequency patterns known as *rotating instabilities*. Fluid mechanically, the pattern is formed by a multi-cell pattern that propagates relative to the rotor Mathioudakis and Breugelmans (1985). Today, its formation is associated with the propagation of radial vortices Eck et al. (2017). For a detailed analysis of the failure mechanism of CON-MAX refer to Jüngst et al. (2015).

Rotating instabilities are associated with a broadband amplitude rise, which might be used to define a root mean square pressure criterion that justifies the abortion of the measurements from an aerodynamic perspective. This might also provide a consistent statement on the stability range and justify the use of the term stall margin. However, it is assumed in this work that a rotor blade vibration limit is more relevant and straight forward defined. Therefore, a combined aerodynamic and mechanical limit is used for the investigated front stage rotor.

Figure A.11 presents supplementary strain gauge measurements referenced in the main part of this document. These measurements reveal the interaction of the blades with the fluid flow. The number of rotating cells is determined via Equation 2.11. The propagation speed of the stall cell depends on the frame of reference (see Equation 2.10).

So relative to the rotor, it propagates in the opposite direction compared to the stationary frame of reference. This must be taken into consideration, when comparing the wall pressure spectra in the main document with the here presented strain gauge measurements.

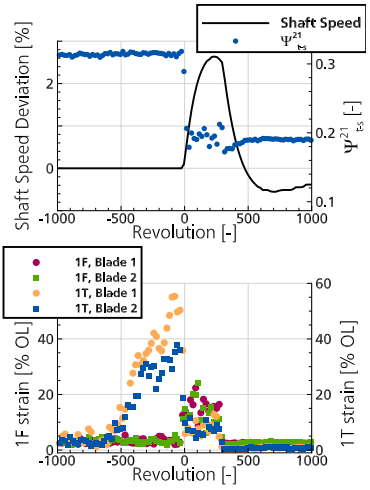

(a) Shaft speed, total-to-static pressure rise at rotor TE and the rise of blade vibration amplitudes

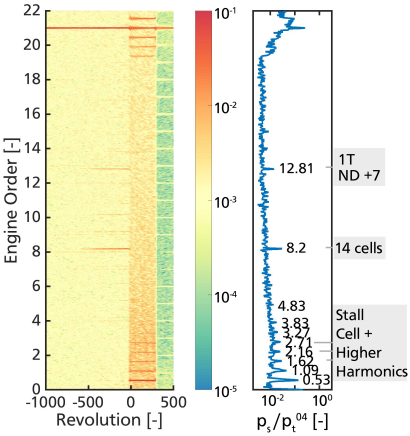

(b) Spectrogram of wall pressure at rotor LE and the maximum pressure amplitudes during stall inception

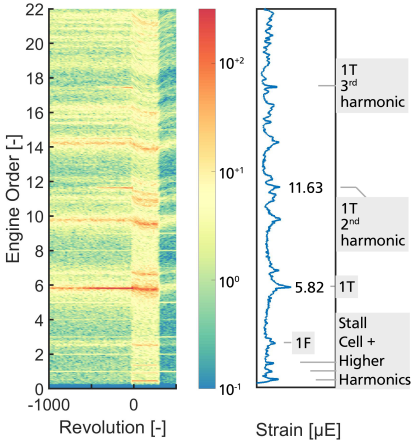

(c) Spectrogram of strain gauge response on Blade No. 1 and the maximum strain amplitudes during stall inception

Figure A.8: Stall inception of CON-MIN at design speed - analysis of stall induced vibrations

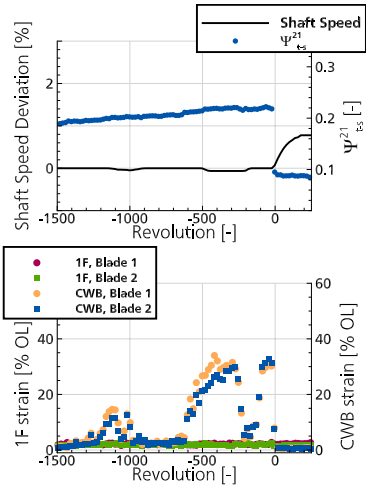

(a) Shaft speed, total-to-static pressure rise at rotor TE and the rise of blade vibration amplitudes

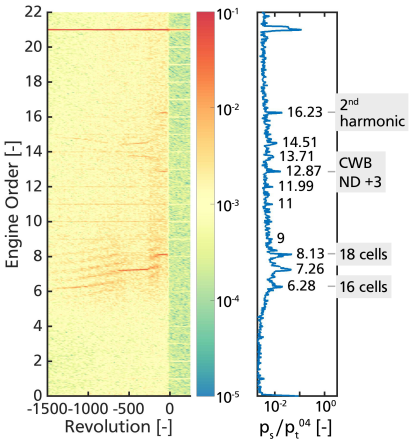

(b) Spectrogram of wall pressure at rotor LE and the maximum pressure amplitudes during stall inception

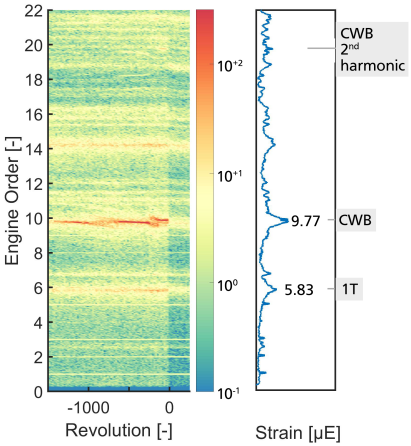

(c) Spectrogram of strain gauge response on Blade No. 1 and the maximum strain amplitudes during stall inception

Figure A.9: Stall inception of CON-MAX at design speed - analysis of stall induced vibrations

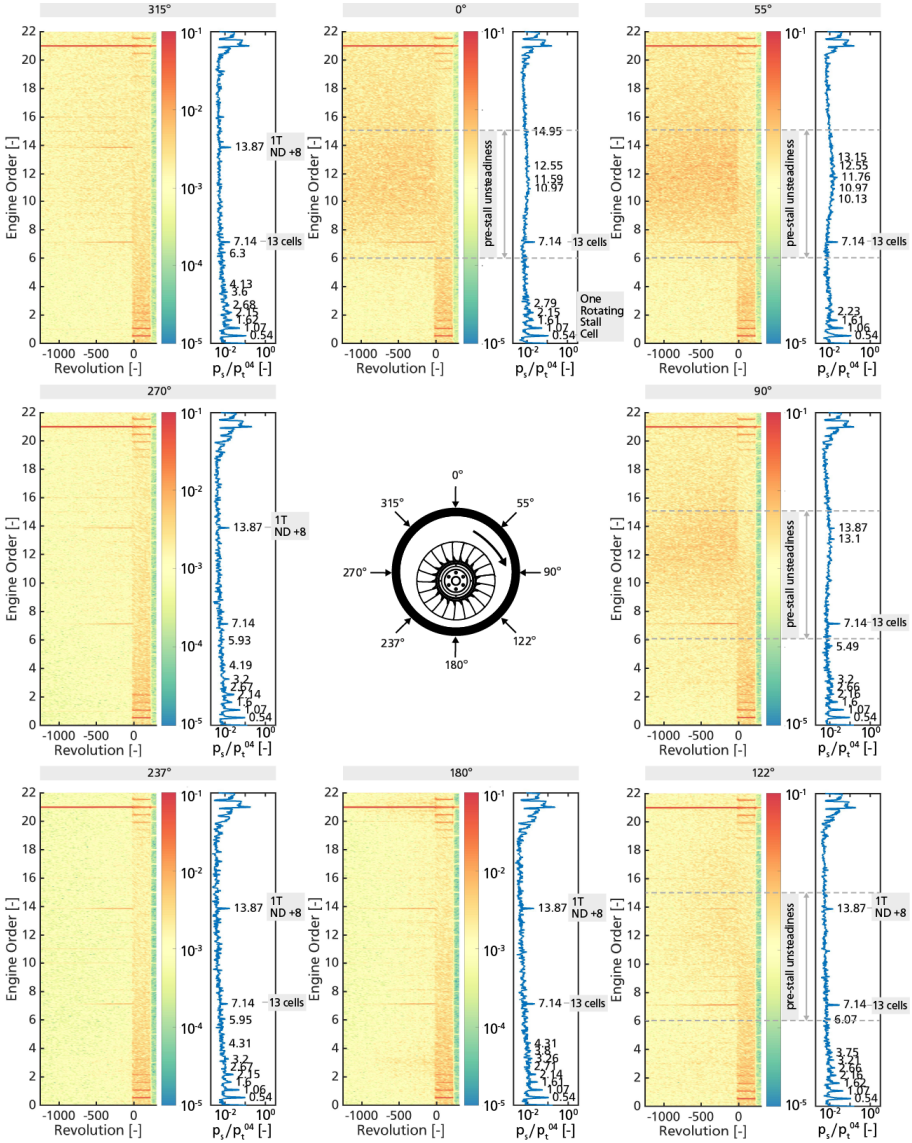

Figure A.10: Stall inception in a configuration with 60% eccentric clearance (ECC-MIN) at design speed

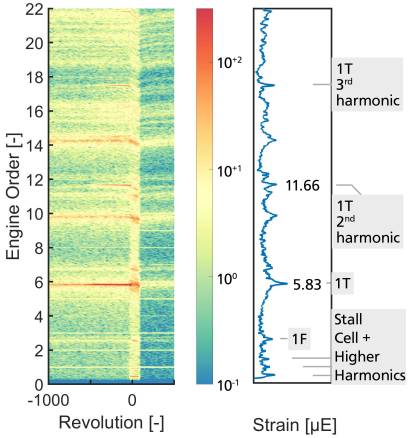

(a) Nominal clearance (CON-NOM) at design speed

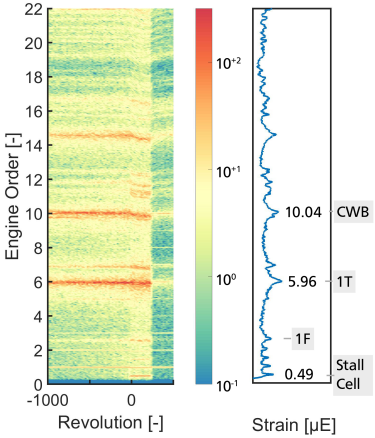

(b) Large eccentric clearance (ECC-MAX) at design speed

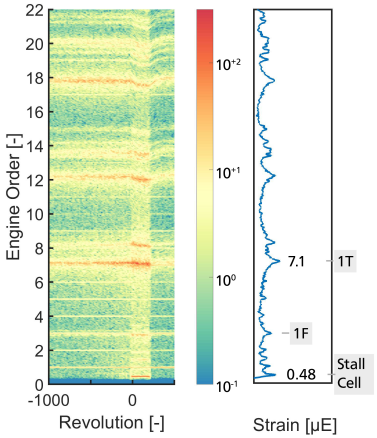

(c) Segmental casing treatment (CT180) at part speed N80

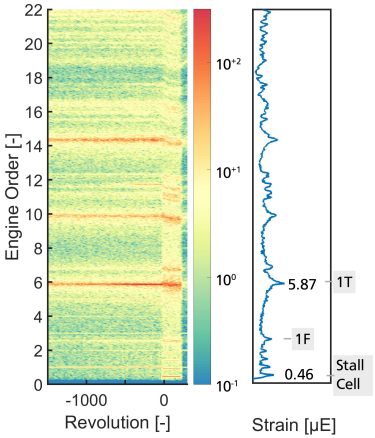

(d) Small eccentric clearance (ECC-MIN) at design speed

Figure A.11: Strain gauge measurements during stall inception. Spectra of strain gauge on Blade No. 1 are shown.

Nominally, the stall inception mechanism of the investigated rotor is clearly spike-type (Biela, 2012, Brandstetter et al., 2018). In a configuration with segmental casing treatment CT180, the stall inception mechanism is less clear-cut.

As the rotor passes the transition from the smooth to the treated segment, i.e. the region of lowest inlet mass flow approximately at 270°, disturbances occur at low frequency (see Figure A.12). These are commonly referred to as modal waves. In the current case, their propagation speed is about 0.35 times rotor speed that is measured at casing angle 287° and reduced in amplitude at 339° (see Figure 4.20). Hundreds of revolutions prior to the onset of rotating stall, these modal (i.e. long-lengthscale) disturbances are damped in the treated segment and do not develop into a mature stall cell (just as the disturbances at high frequency that are of short lengthscale). Five to six revolutions before revolution 0, a disturbance passes the treated segment and starts to grow continuously in size.

In the main part of the document, Figure 4.19c highlighted that pre-stall disturbances (low pressure spots between the leading edges of the blades) occur hundreds of revolutions prior to rotating stall in the segment with a smooth wall. These appear just like spike-type disturbances (Pullan et al., 2015, Brandstetter et al., 2018).

Hence, the stall inception of configuration CT180 rather becomes a combination of both, spike and modal type. Similar findings were published before for compressors with large clearance and eccentricity (Young et al., 2016) as well as compressors with distorted inflow (Longley, 1990). All of these cases have in common that the aerodynamic stage loading varies circumferentially.

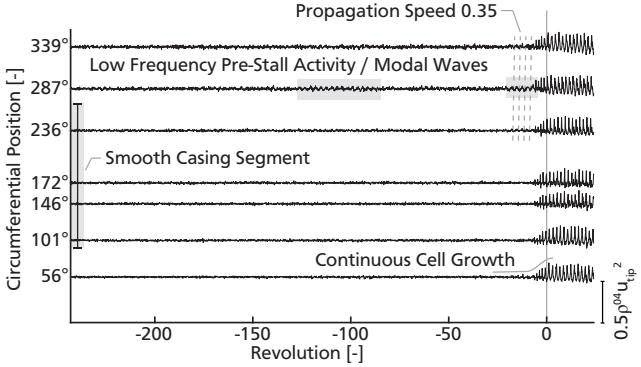

Figure A.12: Stall inception in a configuration with segmental casing treatment (CT180) at N80. Unsteady wall pressure signals at the leading edge, low pass filtered at EO = 4 to illustrate modal activity.

A.6 Full Database of Unsteady Measurements

Table A.3 sums up the database used for the amplitude comparison between configurations CON-NOM and ECC-MIN. It highlights varying rotational speed as well as throttle speed used for an averaged amplitude derivation.

In the main part of the document, characteristics of NSV are analysed using multiple transient measurements at part speed. The full database is presented in Table A.4. In the following, the severity of the blade vibration is shown. In addition, the influence of the inlet guide vane angle (IGVA) is illustrated.

Figure A.13a shows that for constant rotational speed, 1T vibrations are more severe than non-synchronous vibrations of the CWB mode. As pointed out in the main part, larger tip deflection might be the source for an increased amplification of the vibration amplitude. Assumed constant mechanical stress in the blade, the tip deflection of the 1T vibration is larger compared to the CWB mode.

The absolute IGVA setting is disclosed. In Figure A.13b, the total-to-static pressure rise across the rotor is shown, because it is a measure of the IGV closure. At constant speed, the maximum of the pressure rise across the rotor is reduced by both, an enlarged tip clearance and IGV closure. So to isolate the effect of IGV closure, the results are shown for configuration CON-NOM only.

At all speeds, closing the IGV (i.e. pre-swirl application) results in an increased propagation speed in the absolute frame of reference. At part speed, for a closure from 0 to 100%, we measured a speed increase from approximately 0.4 to 0.55. Consequently, the number of coupling aerodynamic cells increases. The modification of the propagation speed and coupling cell numbers is small. It can lead to an avoidance of NSV. However, simply closing the IGV to reduce the rotor loading does not reliably avoid NSV. Instead, it can amplify the problem if propagation speed and cell count match more accurate according to Equation 4.1.

Figure A.13c illustrates the effect of mechanical rotor speed for configuration CON-NOM only. In the main part of the document, the general trend towards increased amplitudes with speed was already pointed out. This is emphasized here.

Table A.3: Measurement database for configurations with the same average clearance. From this database, average amplitude and deviation are derived blade independently in Figure 4.14b. Throttle speed variations are indicated via internal rig nomenclature *Dr 1 & Dr 3*.

Configuration	Date	Speed Deviation from Design Speed [rpm]	Count of Repetitions	Throttle Speed Repetitions	
				Dr 1	Dr 3
CON-NOM	17.11.15	+194	2	1	1
	20.01.16	-250	5	3	2
	11.03.16	+6	5	2	3
	14.02.17	-86	3	2	1
	15.02.17	-64	2	1	1
	20.02.17[a]	-440	1		1
		-60	1		1
		+452	1		1
CON-NOM			**20**	9	11
ECC-MIN	21.07.16	+264	4	2	2
	10.11.16	-131	2	1	1
	30.01.17	-106	18	7	11
ECC-MIN			**24**	11	13

[a] These measurements were used to investigate the mechanical speed influence ($\approx \pm 450$ rpm). T_t^{04} did not vary during that day, so corrected speed was not kept constant.

Table A.4: All unsteady measurements at a glance

N_{corr}	N45			N63				N80						N95			N100		
IGVA [% max.]	0	50	100	0	50	87	100	0	14	28	50	73	100	0	12	25	0	12	25
CON-NOM[ab]	×	×	×	×	×	×	×	×		×	×	×	×	×	×	×	×	×	×
CON-MIN[c]						×		×				×				×	×		
CON-MAX						×		×	×	×		×				×	×		
ECC-MIN				×		×		×				×		×	×	×	×		
ECC-MAX				×		×		×				×		×		×	×		
CT360[de]	×	×	×	×	×	×	×	×			×	×	×						
CT180[f]	×	×	×	×	×	×	×	×			×	×	×						

[a] At N100, measurements were also taken with a *mechanical speed variation* by ± 450 rpm. Their goal was to point out the influence of mechanical speed on NSV. For some measurements, the corrected speed was not kept constant because the inlet temperature did not vary in the same extent.

[b] Two different *throttle closing speeds* were used for each configuration and condition because the speed has an influence on the amplitude rise during NSV. Rig nomenclature refers to these speeds by *Dr 1 & 3*.

[c] Concentric and eccentric clearance variations were run without measurements at N45 and with a reduced count of IGVA variations. This is a result of the initial main focus of the EBreak project, which was aerodynamic.

[d] To account for the mechanical speed influence on NSV, all corrected speeds were measured twice at *different inlet conditions* with $\Delta T^{04} = 12°\mathrm{K}$. The aerodynamic speed was held constant during the tests. As a result, the mechanical speeds were scaled by $\Delta N_r = N_{corr}\left(\sqrt{1+\Delta T^{04}/T_{ref}^{04}}-1\right)$ if humidity is assumed constant (just to make this simplified statement).

[e] A pre-test *keep out zone* prohibited measurements at N95 and N100.

[f] A pre-test *keep out zone* prohibited measurements at N95 and N100.

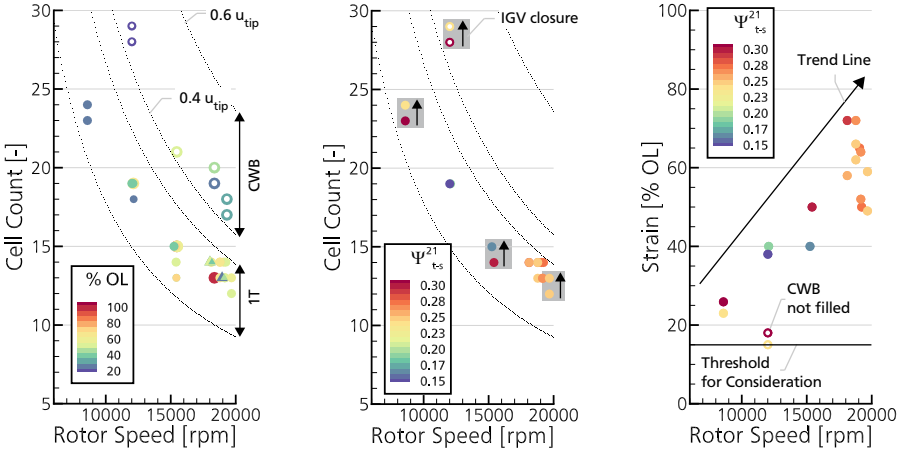

(a) Severity of blade vibrations in the entire operating range

(b) Influence of IGVA, shown for configuration CON-NOM only

(c) Effect of rotor speed and aerodynamic loading, shown for configuration CON-NOM only

Figure A.13: Characteristics of NSV - 1T and CWB vibration amplitudes for configurations CON-MIN, CON-NOM, CON-MAX, ECC-MIN, ECC-MAX

A.7 Reduced Frequency and Critical Rotor Speed Prediction

Historically, it was observed that flutter occurs if the flow velocity relative to an airfoil is above critical speeds (Fung, 2002). A well established parameter that considers the fluid motion relative to the motion of the airfoil is the reduced frequency. It can be written as

$$K = \frac{l/2}{w} \cdot \frac{2\pi f_{\text{blade}}}{1} \tag{A.9}$$

and represents the ratio of the time a fluid particle needs to pass half of the blade chord relative to one cycle of the blade vibration. Commonly, unstable values for 1T are between 0.4 to 0.8 (Srinivasan, 1997).

Srinivasan (1997) also highlighted that considering reduced frequency uniquely is not sufficient in order to distinguish stable and unstable flutter operating conditions. Early approaches of stall flutter rather used reduced frequency versus blade incidence (Stargardter, 1979).

Kielb et al. (2003) stated that NSV occur apart historically stable flutter regions. Holzinger (2017) questioned the usability of reduced frequency for modern front stage designs in general. For the investigated rotor, reduced frequencies vary between 3.4 and 1.4 for N45 and N100, respectively. For both speeds, the vibrations occur at near stall, which means at high tip incidence.

This review highlights that the use of reduced frequency is not reasonable in the present case. The blade design is stable regarding torsional flutter, but the design is not entirely stable from an aeroelastic point of view.

Thomassin et al. (2009, 2011) published a novel prediction method for critical rotor speeds regarding NSV. They assumed that vortices propagate from blade to blade and generate an acoustic feedback wave as they impinge on subsequent blades. In simple tests, apart from a rotating rig, they observed that the vortex formation is amplified if the shedding frequency coincides with the frequency of the vortex impingement. For the convective propagation of the vortices in the rotating rig or engine, they assumed 0.5 times rotor speed. This is valid in case of the currently investigated rotor and it is generally assumed that the observed phenomena are very similar.

According to Thomassin et al. (2011), critical rotational speeds are predictable via

$$N_r = k \cdot \frac{60}{2\pi r_{\text{tip}}} \cdot \left(\sqrt{\kappa R T_{\text{s,tip}}} - \frac{2\frac{2\pi r_{\text{tip}}}{N_{\text{blade}}} f_{\text{blade}}}{n} \right) \tag{A.10}$$

where k is a constant that depends on the convective vortex propagation ($k = 1/0.5$) and n is a counter used to consider high order acoustic modes. All other quantities depend on the rotor design ($r_{\text{tip}}, N_{\text{blade}}, f_{\text{blade}}$) and inlet conditions or the specific operating point ($\kappa, R, T_{\text{s,tip}}$). Assuming tip temperatures between 280°K and 350°K, Equation A.10 reveals critical speeds between 13,000 and 17,000 rpm. Higher or lower temperatures did not occur during the measurements and are considered unlikely in general. The 1T mode is used as natural frequency and fundamental acoustic modes ($n = 1$) are studied. For second order acoustic modes ($n = 2$), the model estimates critical speeds above the maximum speed of the rig.

Hence, the results of this thesis indicate that NSV occur apart from the predicted speeds. A jet core feedback mechanism is an unlikely feature for NSV occurrences in case of the investigated setup. Instead, it is likely that NSV appear in the entire operating range of a compressor according to Equation 4.1. In a multi-stage compressor, the critical NSV speed is rather determined by IGV schedule and rotational speeds that encounter front stage stall.